COLD-FORMED STEEL RESEARCH CONSORTIUM

CANTILEVER TESTING OF CONCRETE-FILLED STEEL DECK COMPOSITE DIAPHRAGMS USING VARIOUS TYPES OF STEEL REINFORCING

Raul E. Avellaneda-Ramirez, Matthew R. Eatherton, W. Samuel Easterling, Benjamin Schafer, Jerome F. Hajjar

May 2021

COLD-FORMED STEEL RESEARCH CONSORTIUM
REPORT SERIES
CFSRC R-2021-02

SDII
Steel Diaphragm Innovation Initiative

ABSTRACT

The diaphragm is an integral part of a building's structure and the way buildings resist seismic loads. While the diaphragm is arguably just as important in the load path as the vertical LFRS, the seismic demands and seismic behavior of diaphragms is not as well understood as the vertical LFRS. Full-scale testing of diaphragm assemblies is required to understand their cyclic behavior including strength, stiffness, ductility, strength degradation, hysteretic behavior, and failure modes. A testing program was conducted to fill the gaps in the literature related to concrete-filled steel deck diaphragm behavior with specimens representing current practice (i.e., 2 hour fire rated assemblies), specimens that represent the lower end of thickness, and specimens including reinforcing steel.

Eight cantilever diaphragm specimens were tested with variations in depth of concrete cover, deck depth, perimeter stud anchor configuration, concrete type (normal weight (NW) and lightweight (LW)), and the presence of either welded wire mesh or reinforcing steel. This report summarizes the testing program, test matrix, specimen and reaction frame details, and detailed results and observations for each specimen. This report does not contain comparisons to prediction equations, or detailed synthesis of the results as that is intended for future reports and publications.

TABLE OF CONTENTS

ABSTRACT 2

TABLE OF CONTENTS 3

1 INTRODUCTION 5

2 DESCRIPTION OF THE EXPERIMENTAL PROGRAM 7

2.1 Test Matrix 7

2.2 Test Setup 9

2.3 Materials 17

2.4 Instrumentation 18

2.5 Test Procedure and Loading Protocol 22

2.6 Specimen Shoring 23

3 RESULTS 27

3.1 Overview of Strength and Stiffness Results 27

3.2 Specimen 3/6.25-4-L-NF-DT 29

3.3 Specimen 3/7.5-4-N-NF-DT 36

3.4 Specimen 2/4-4-L-NF-DT 42

3.5 Specimen 3/6.25-4-L-NF-P 48

3.6 Specimen 2/4.5-4-N-RS-DT 56

3.7 Specimen 3/7.5-4-N-NF-P 63

3.8 Specimen 3/6.25-4-L-RS-DT 69

3.9 Specimen 3/7.5-NW-NF-RS 76

4 REFERENCES 82

APPENDIX A: PROCEDURE USED TO CORRECT SHEAR ANGLE OF SPECIMEN 3/7.5-4-N-NF-P 84

APPENDIX B: BAREFRAME TEST RESULTS 88

APPENDIX C: TESTING FRAME DRAWINGS AND DETAILS 90
APPENDIX D: SPECIMEN DETAILS 103
D.1 Specimen 3/6.25-4-L-NF-DT 103
D.2 Specimen 3/7.5-4-N-NF-DT 104
D.3 Specimen 3/7.5-NW-NF-RS 105

1 INTRODUCTION

The diaphragm is an integral part of a building's structure and the way buildings resist seismic loads. The majority of the seismic load originates at the diaphragm and the diaphragm acts to transfer these loads to the vertical elements of the lateral force resisting system (LFRS). While the diaphragm is arguably just as important in the load path as the vertical LFRS, the seismic demands and seismic behavior of diaphragms is not as well understood as the vertical LFRS. For example, it was only recently discovered that US code level forces significantly underpredict the elastic force demands experienced in diaphragms during earthquakes and thus that diaphragms may be subject to inelasticity during design level earthquakes ([1],[2]). Full-scale testing of diaphragm assemblies is required to understand their cyclic behavior including strength, stiffness, ductility, strength degradation, hysteretic behavior, and failure modes.

A recent effort to assemble past diaphragm testing into a database found approximately 750 diaphragm test specimens, but only about 10% of the specimens were concrete-filled steel deck and the majority of those were not representative of typical floor assemblies in North America [3]. An experimental program conducted by Luttrell [4] included nine specimens with insulating concrete, tested monotonically. Davies and Fisher [5] performed four cantilever diaphragm tests with structural concrete fill, but these tests were also monotonic and only failed the structural fasteners. A testing series conducted by ABK [6] included one specimen with structural concrete fill, but it was not loaded to failure. The most comprehensive experimental study on concrete-filled steel deck diaphragms was performed at Iowa State ([7]-[15]) and consisted of 32 cantilever diaphragm specimens subjected to cyclic loading. Of these specimens, only three used shear studs as the only means of perimeter fastening; the majority used arc welds as perimeter fastening.

A testing program was conducted to fill the gaps in the literature related to concrete-filled steel deck diaphragm behavior with specimens representing current practice (i.e., 2 hour fire rated assemblies), specimens that represent the lower end of thickness, and specimens including reinforcing steel. Eight cantilever diaphragm specimens were tested with variations in depth of concrete cover, deck depth, perimeter stud anchor configuration, concrete type (normal weight (NW) and lightweight (LW)), and the presence of either welded wire mesh or reinforcing steel. This report summarizes the testing program, test matrix, specimen and reaction frame details, and detailed results and observations for each specimen. This report does not contain comparisons to

prediction equations, or detailed synthesis of the results as that is intended for future reports and publications.

2 DESCRIPTION OF THE EXPERIMENTAL PROGRAM

The details of the test program are presented in this chapter including a description of the test variables and test matrix, the test setup including reaction frame, materials, and testing procedures.

2.1 Test Matrix

The test matrix is given in Table 2-1. The testing program consisted of 8 specimens with varying geometries and material properties. Two deck heights were used (2 in. and 3 in.) since they are two of the most common heights used in modern construction in the United States. The concrete thickness above the top of the deck flute varied from 2 in. to 4.5 in. The thinnest slabs were intended to investigate the lower limit of concrete-filled steel deck used in practice, while the 6.25 in. and 7.5 in. slabs represent the thickness required for a 2-hour fire rating in the United States using lightweight and normal weight concrete, respectively. The concrete mix was designed to produce a 28-day strength of approximately 4000 psi, with measured concrete strength on the testing day (28 days) given in Table 2-2. Both normal weight and lightweight mixes were used. The majority of the specimens consisted of 17 ft. by 13 ft – 4 in. composite slabs, with a few exceptions detailed below. The 17 ft. dimension was chosen to accommodate five sheets of deck between the centerline of the beams with an edge distance of 12 in. from the centerline of the beam to edge of concrete on each side, while the 13 ft - 4 in. dimension was decided based on space considerations in the testing laboratory. The deck direction was as shown in Figure 2-2 for all specimens, with the exception of specimen 3/6.25-4-L-RS-DT, for which the deck direction was oriented parallel to the direction of loading.

The specimen notation (Figure 2-1) used in the test matrix consists of the deck height, followed by the total slab thickness, the nominal concrete compressive strength at 28 days in ksi, the concrete type (L for lightweight and N for normal weight), the reinforcement present in the specimen (NF for No Reinforcement and RS for Reinforcing Steel), and finally the expected failure mode (DT for Diagonal Tension Cracking and P for Perimeter Fastener Failure). As an example, a specimen with a 3 in. steel deck, 6.25 in. total slab thickness, 4 ksi lightweight concrete mix, with reinforcing steel meant to fail through diagonal tension cracking would have a specimen notation of: 3/6.25-4-L-RS-DT.

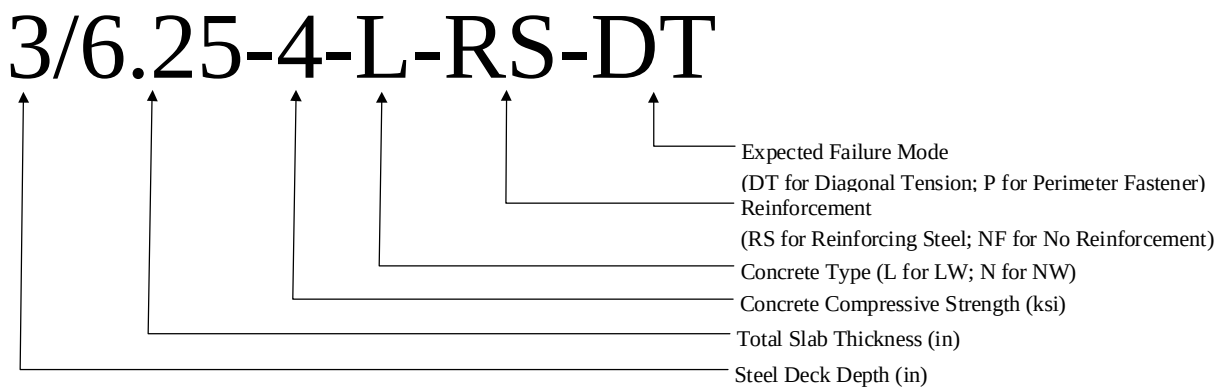

Figure 2-1. Description of Specimen Notation

Table 2-1. Test Matrix

Specimen Type	Test Specimen	Total Slab Depth (mm)	Deck Height, D_d (mm)	Concrete Type	Expected Failure Mode	Reinforcement
Unreinforced	2/4-4-L-NF-DT	4	2	LW	DT	none
	3/6.25-4-L-NF-DT	6.25	3	LW	DT	none
	3/7.5-4-N-NF-DT	7.5	3	NW	DT	none
Reinforcing Bars	2/4.5-4-L-RS-DT	4.5	2	LW	DT	#4 bars at 12 in. spacing
	3/6.25-4-L-RS-DT	6.25	3	LW	DT	6x6 D2.1xD2.1
	3/7.5-4-N-RS-DT	7.5	3	NW	DT	#3 bars at 18 in. spacing
Perimeter Fastener Failure	3/6.25-4-L-NF-P	6.25	3	LW	P	none
	3/7.5-4-N-NF-P	7.5	3	NW	P	none

NW = normal weight concrete
LW = lightweight

The specimens are divided into three groups. The first set of three specimens consisted of unreinforced concrete-filled steel deck diaphragms. The purpose of these three tests was to provide a baseline of comparison for the rest of the specimens, as well as a source of validation for existing strength prediction equations which were used in the development of prediction models for the reinforced specimens. Two of these specimens (3/6.25-4-L-NF-DT and 3/7.5-4-N-NF-DT) were meant to be representative of 2-hour fire rating assemblies using lightweight and normal weight

concrete, respectively. Each of these two specimens have nearly identical corresponding specimens which include reinforcing steel (3/6.25-4-L-RS-DT and 3/7.5-4-N-RS-DT) as well as corresponding specimens meant to fail the perimeter fasteners (3/6.25-4-L-NF-P and 3/7.5-4-N-NF-P).

The second group of specimens contained reinforcing steel. The intended limit state was diagonal tension cracking, which occurs when the applied shear force exceeds the shear capacity of the concrete slab. The purpose of these specimens was to investigate the effect of reinforcement on the strength and behavior of concrete-filled steel deck diaphragms. Specimen 2/4.5-4-L-RS-DT included #4 bars at 12 in. spacing. This specimen was designed to investigate the effect of reinforcement with minimum concrete cover considered to represent one of the thinnest reinforced concrete-filled steel deck diaphragms that may be used in practice. Specimen 3/6.25-4-L-RS-DT included wire mesh (6x6 D2.1xD2.1). This specimen also had the deck sheets spanning perpendicularly to the deck direction shown in Figure 2-2 and instead of the typical slab dimensions, this specimen consisted of an 18 ft. by 15 ft. slab. The modified slab dimensions were chosen to prevent perimeter fastener limit states which may occur for small edge distances perpendicular to the shear load. Specimen 3/7.5-4-N-RS-DT included #3 bars at 18 in. spacing. The purpose of this specimen was to investigate the upper limits of shear capacity of reinforced concrete-filled steel deck diaphragms as well as the effect of larger spacing of reinforcement. Similar to specimen 3/6.25-4-L-RS-DT, the dimensions of this specimen were modified to prevent perimeter fastener limit states. The specimen consisted of a 17 ft. by 14 ft. slab.

The last pair of specimens were designed to fail by exceeding the shear transfer capacity of the perimeter fasteners without reaching the full shear capacity of the concrete, using lightweight and normal weight concrete.

2.2 Test Setup

Figure 2-2 illustrates the experimental setup which consists of a frame using W24x84 beams that are 12 ft. by 15 ft. center to center. The deck sheets are oriented perpendicular to the shear load, except for specimen 3/6.25-4-L-RS-DT, for which the deck sheets were oriented parallel to the shear load. The load is introduced into the specimens through the loading beam which rests on rollers to allow for lateral translation, while constraining out-of-plane movement, as shown in Figure 2-4. Specimens 2/4-4-L-NF-DT, 3/6.25-4-L-NF-DT, and 3/7.5-4-N-NF-DT only included out-of-plane bracing on the loading beam (as shown in Figure 2-4 (b)) while the remaining

specimens also included additional out-of-plane bracing attached to the actuators as (as shown in Figure 2-4 (a)). The loading is transferred from the loading beam, through the shear studs onto the diaphragm and onto the fixed beam, which is in turn connected to supports restraining it from translation and rotation.

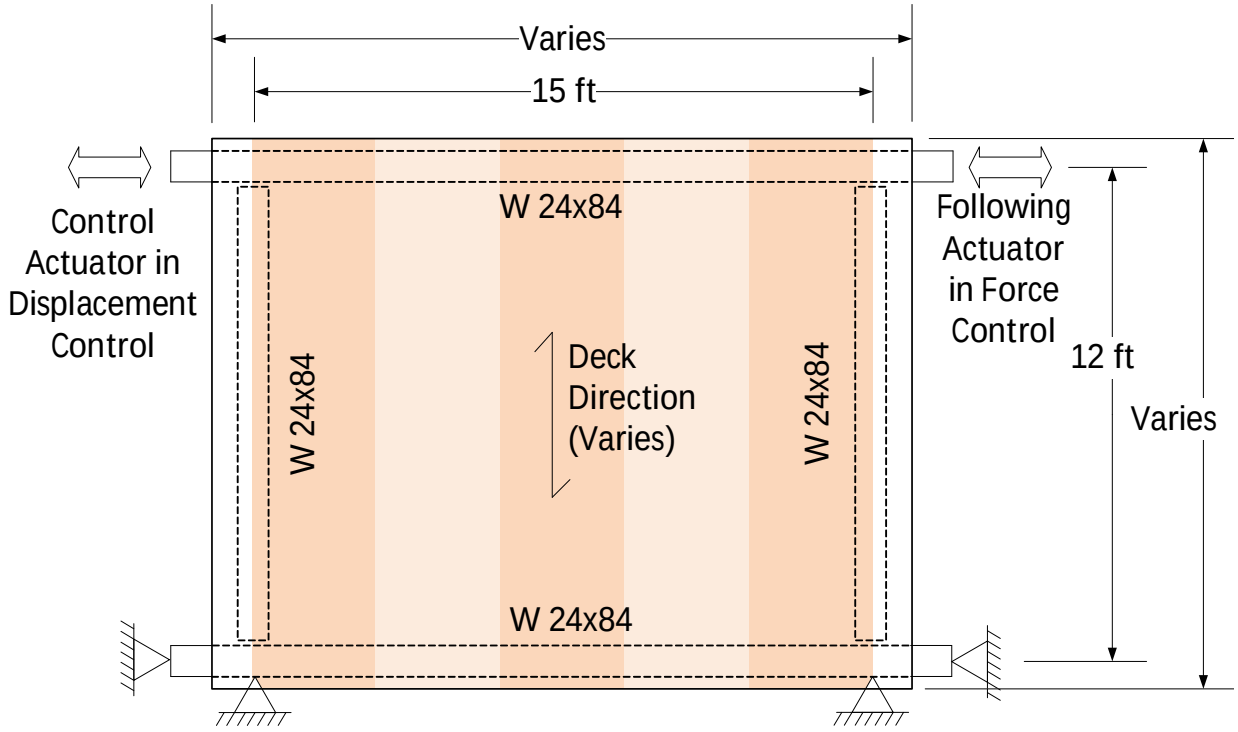

Figure 2-2. Experimental Setup

Figure 2-3. Specimen Prior to Testing

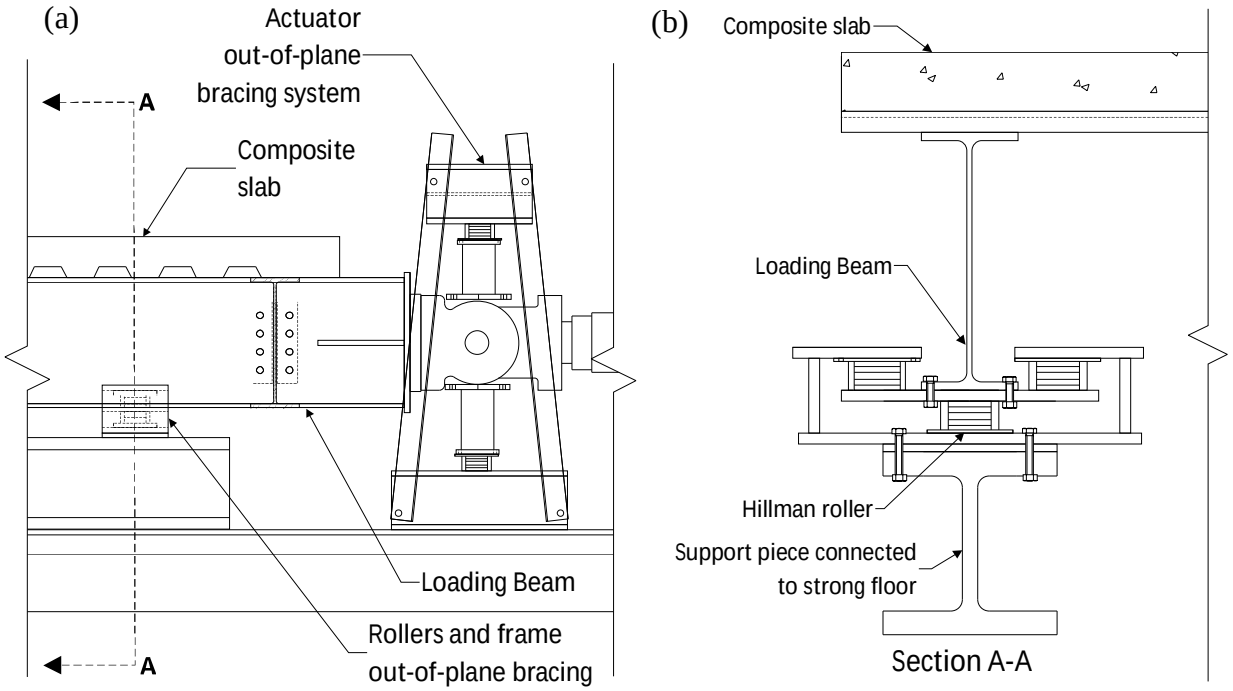

Figure 2-4. Out-of-Plane Bracing: (a) Actuator Out-of-Plane Bracing (b) Loading Beam Out-of-Plane Bracing

The loading beam and fixed beam are also connected through two side beams. The steel beams were connected with double angle connections as shown in Figure 2-5 and Figure 2-6. The connection between the loading beam and the side beams included eight 1.125 in. diameter A490 bolts connecting the angles to the loading beam (Figure 2-5 (b)) and four 1.125 in. diameter A490 bolts connecting the angles to the side beams (Figure 2-5 (a) and (c)). For specimens 2/4-4-L-NF-DT, 3/6.25-4-L-NF-DT, and 3/7.5-4-N-NF-DT the angles used in the connection between the loading beam and the side beams were L4x4x1/4 (Figure 2-5 (c)), while for the remaining specimens the angles used for this connection were L8x8x3/4 (Figure 2-5 (a)). The connection between the side beams and the fixed beam included eight 1.125 in. diameter A490 bolts connecting the angles (L8x8x3/4) to the fixed beam and ten 1.25 in. diameter A490 bolts connecting the angles to the side beams, as shown in Figure 2-6. All connections between the beams were slip-critical and the bolts were pretensioned per requirements of Section 8.2 of the Specification for Structural Joints Using High-Strength Bolts [21]. The fabrication drawings and details are contained in Appendix C.

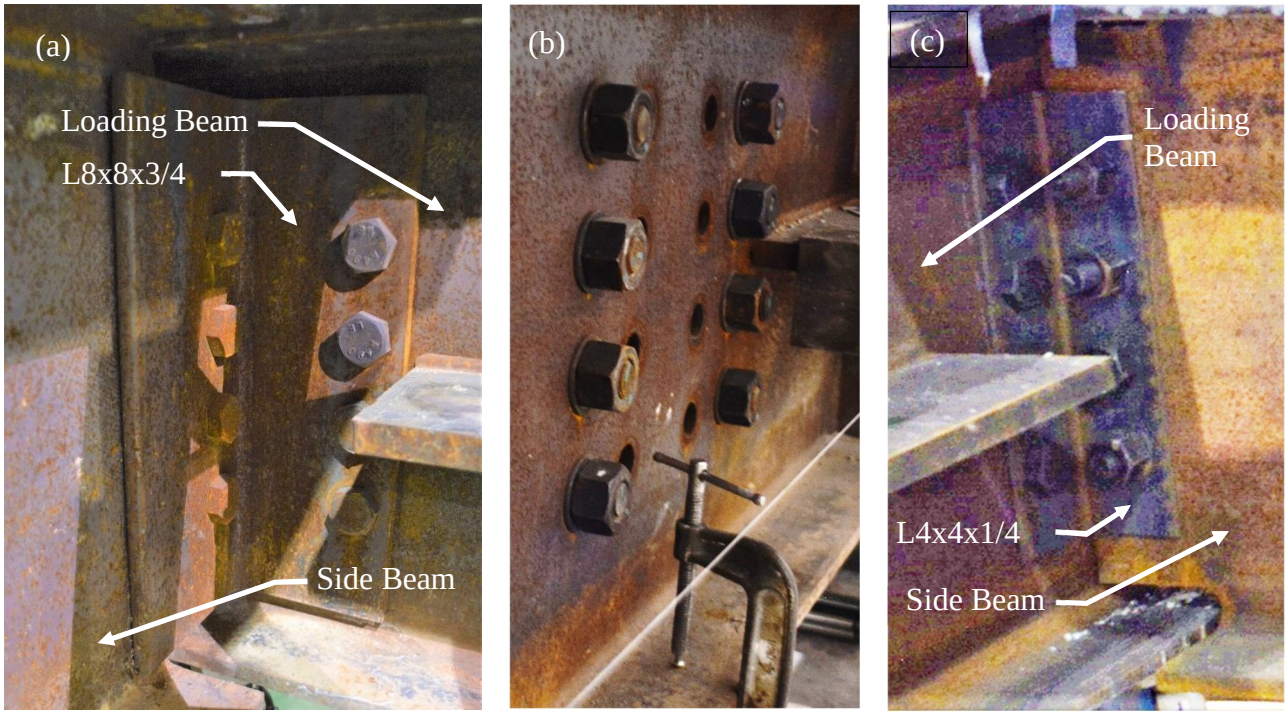

Figure 2-5. Connection between Loading Beam and Side Beams: (a) Angles (8x8x3/4) Used in Reinforced Specimens and Specimens Failing Perimeter Fasteners, (b) Eight Bolts Connecting Loading Beam to Side Beam, (c) Angles (4x4x1/4) Used in Unreinforced Specimens with DT Failure

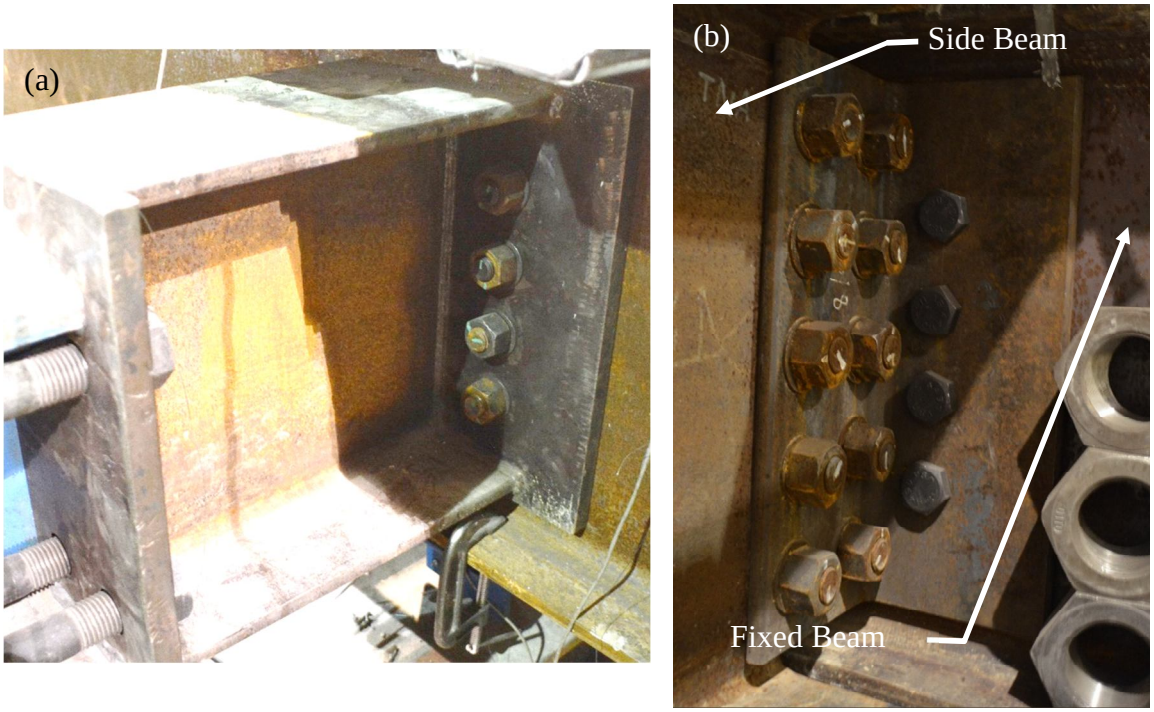

Figure 2-6. Connection between Side Beams and Fixed Beam

The load is introduced into the testing frame using a pair of servo-controlled hydraulic actuators working in tandem. The master actuator (MTS 201.80 Hydraulic Actuator) was displacement-controlled while the following actuator (MTS 201.60 Hydraulic Actuator) was force-controlled to be in the opposite direction with a magnitude equal to the force in the master actuator multiplied by the ratio of following to master actuator force capacities. The capacity of the master actuator in tension and compression was 301 and 446 kips, respectively, while the capacity of the following actuator in tension and compression was 146 and 228 kips, respectively, For the specimens meant to fail the perimeter fasteners, the magnitude of the force in the following actuator was equal to the force in the master actuator.

The shear stud configuration for the specimens meant to fail through diagonal tension cracking was designed to prevent a failure of the perimeter fasteners and included two studs per rib staggered in the direction perpendicular to the deck and stud spacing of 12 in. in the direction parallel to the deck, as shown as Figure 2-7.

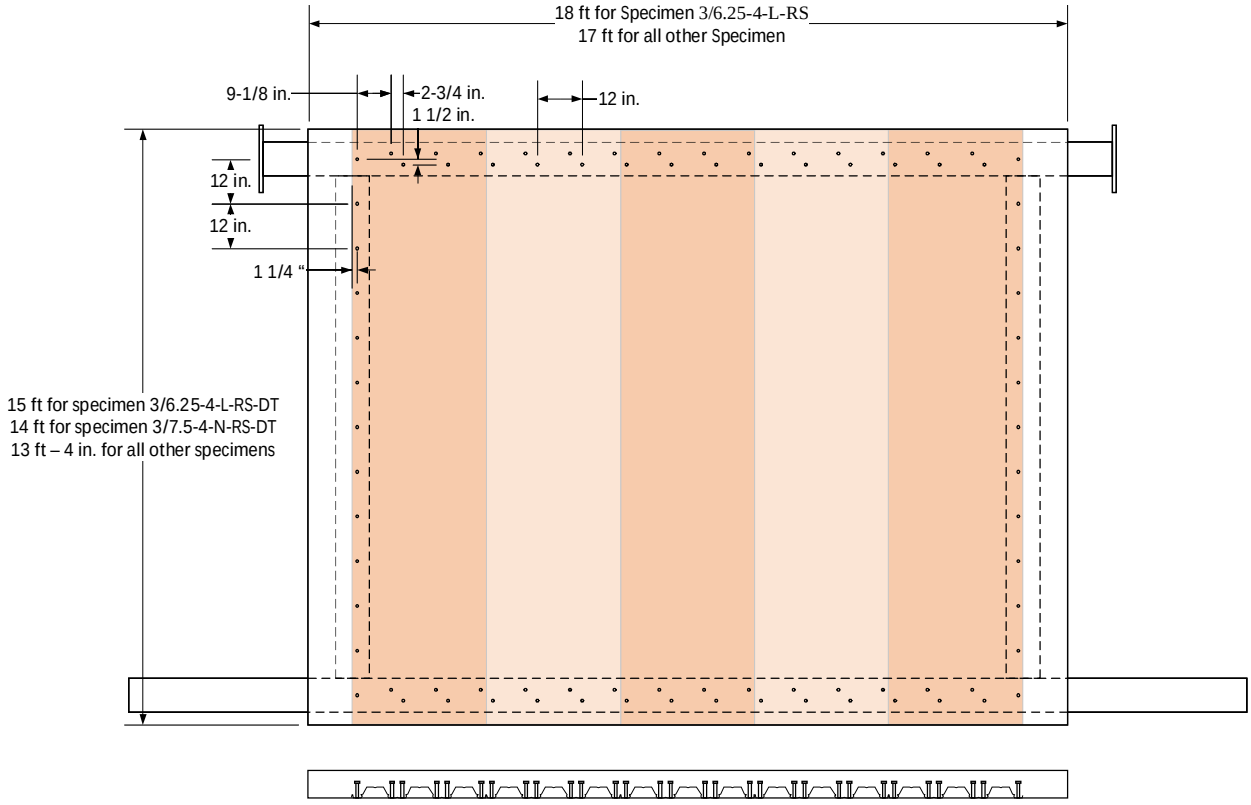

Figure 2-7. Headed Stud Placement for Typical Specimen Designed for Diagonal Tension Failure

For the specimens meant to fail the perimeter fasteners, the shear stud configuration included 1 stud every third rib in the direction perpendicular to the deck and 1 stud every 36 in. in the direction parallel to the deck, as shown in Figure 2-8. The position of the studs within each individual rib in the beams oriented parallel to the direction of loading was chosen such that half of the studs would be in the strong position and the other half would be in the weak position, for both loading directions. For example, the left-most stud in the loading beam in Figure 2-8 was welded so that it would be in the strong position of the rib when the loading was oriented from left to right but would be in the weak position when the loading was reversed. The shear stud height for all specimens satisfied AISC 360-16 [20] requirements (1.5 in. above the deck after welding and at least ½ in. of concrete cover above the head of the stud). The specimens with 3 in. and 2 in. tall deck used shear studs with a height after welding of 4.5 in. and 3.5 in., respectively.

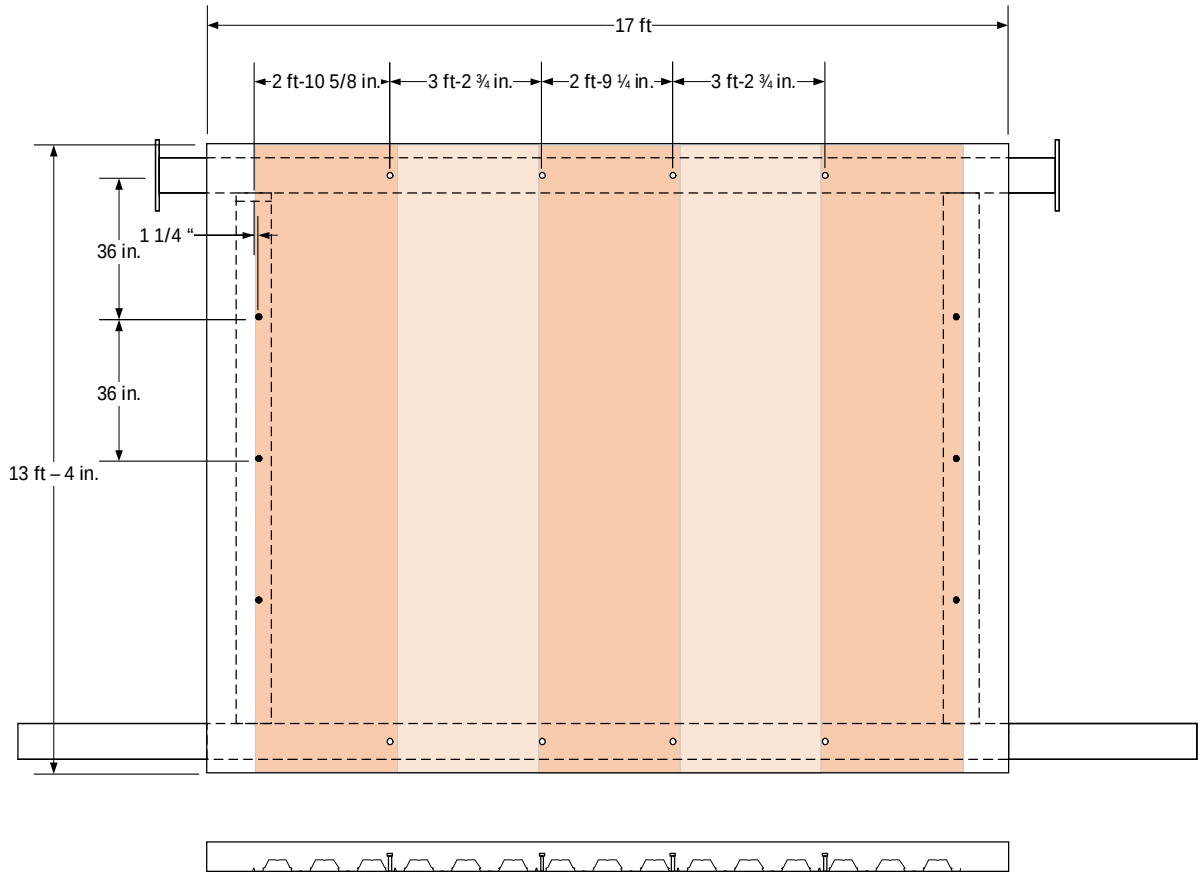

Figure 2-8. Headed Stud Placement in Specimens Designed to Fail Perimeter Fasteners

As discussed in Section 2.1, three of the specimens included steel reinforcement. Specimen 2/4.5-4-L-RS included #4 bars at 12 in. center-to-center spacing, in both directions, as shown in Figure 2-9. The bars were elevated above the top of the deck flutes using plastic rebar chairs so as

to have a clear cover of 0.75 in. from the top of the top-most bar to the top of the slab, and from the bottom of the bottom-most bar to the top of the deck flute.

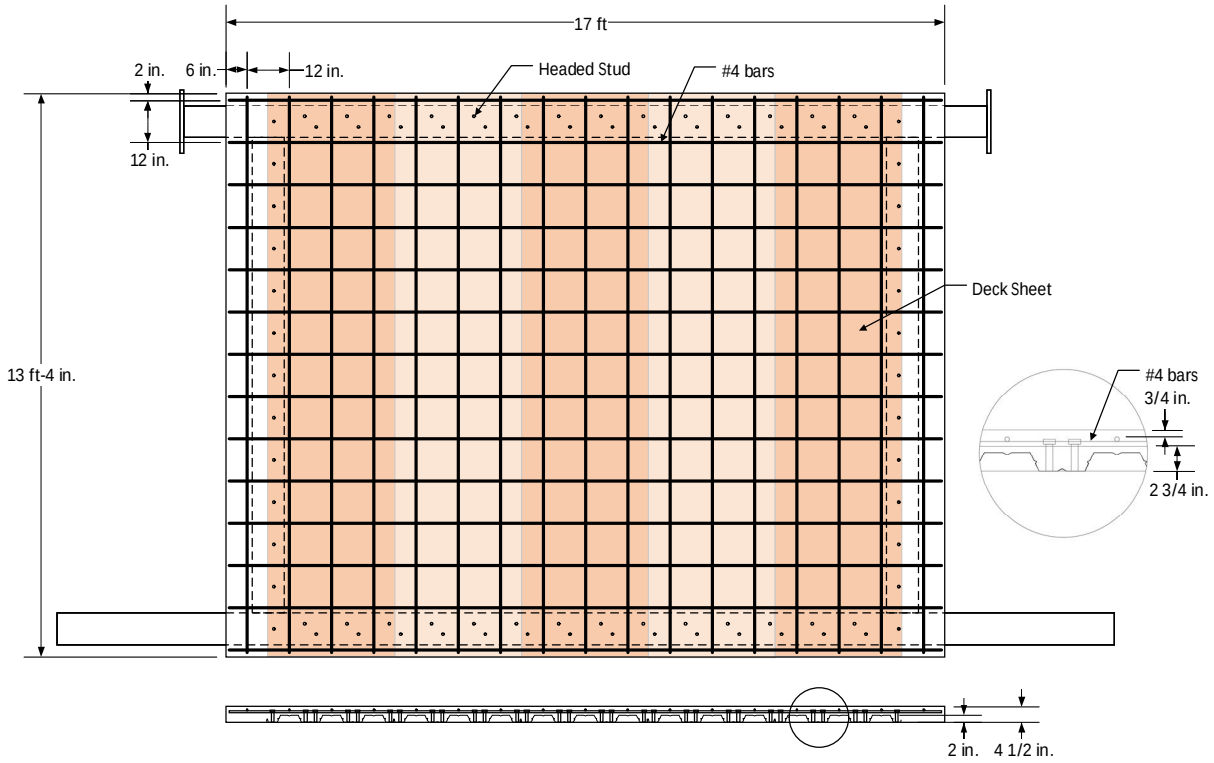

Figure 2-9. Reinforcement Arrangement for Specimen 2/4.5-4-L-RS

Specimen 3/6.25-4-L-RS included 6x6 D2.1xD2.1 wire mesh, as shown in Figure 2-10. The wire mesh was placed directly on top of the deck flutes. The wire mesh panels were 5 ft by 10 ft. The overlap between outermost cross wires of each wire mesh sheet was 2 in. while the lap splice length was 8 in. in accordance with ACI Section 25.5.3 [22]. The deck sheets were oriented parallel to the direction of loading. The shear stud configuration included two studs per rib staggered in the direction perpendicular to the deck and stud spacing of 12 in. in the direction parallel to the deck. The location of the studs is detailed in Figure 2-10. The dimensions of the concrete slab for this specimen were 18 ft. by 15 ft. so as to increase the distance from the centerline of the beams to the edge of the slab in order to prevent failure modes of the shear connection associated with small edge distances perpendicular to the direction of loading.

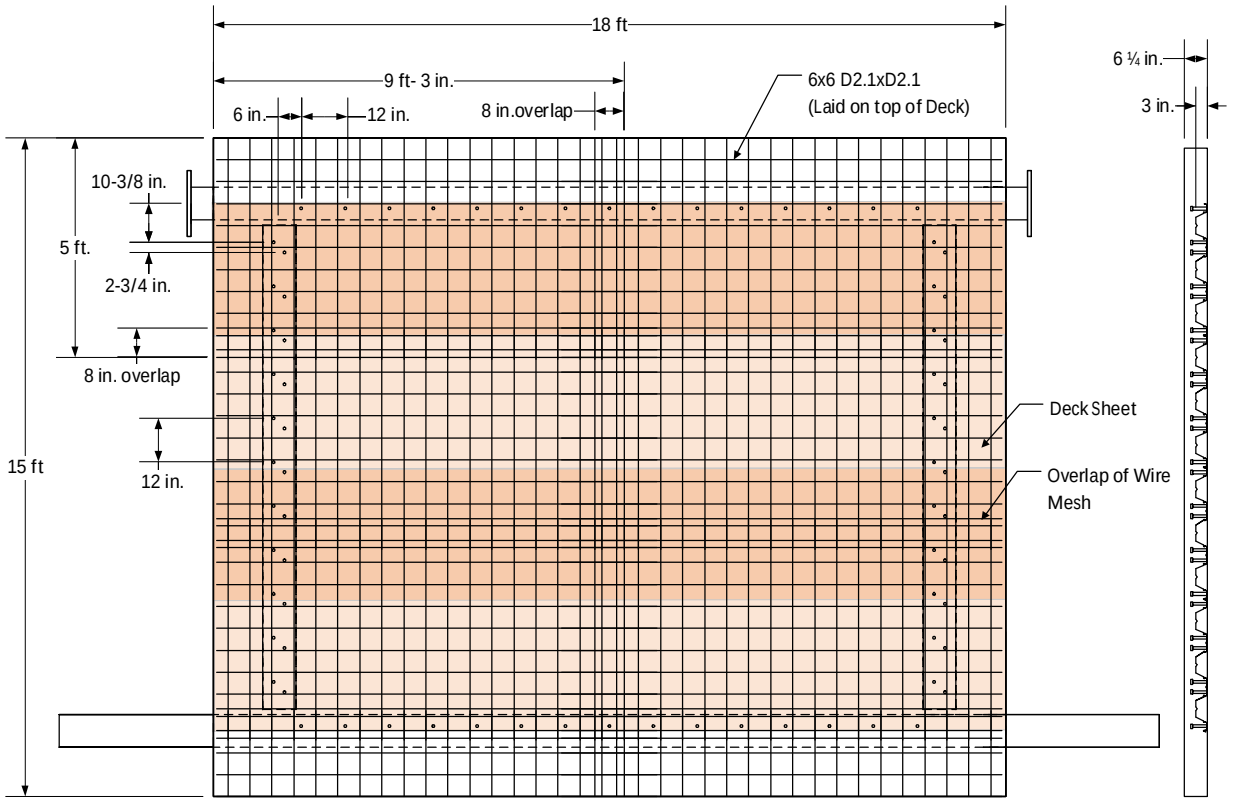

Figure 2-10. Reinforcement and Headed Stud Placement for Specimen 3/6.25-4-L-RS

Specimen 3/7.5-4-N-RS included #3 bars at 18 in. center-to-center spacing, in both directions, as shown in Figure 2-11. The bars were elevated above the top of the deck flutes using plastic rebar chairs so as to center them on the concrete cover above the deck flutes with a clear cover of 1.875 in. from the top of the top-most bar to the top of the slab, and from the bottom of the bottom-most bar to the top of the deck flute. The dimensions of the concrete slab for this specimen were 17 ft. by 14 ft., as opposed to the typical 17 ft. by 13 ft. – 4 in., so as to increase the distance from the centerline of the loading and fixed beams to the edge of the slab from the typical 8 in. to 12 in. This was done to prevent failure modes of the shear connection associated with small edge distances perpendicular to the direction of loading.

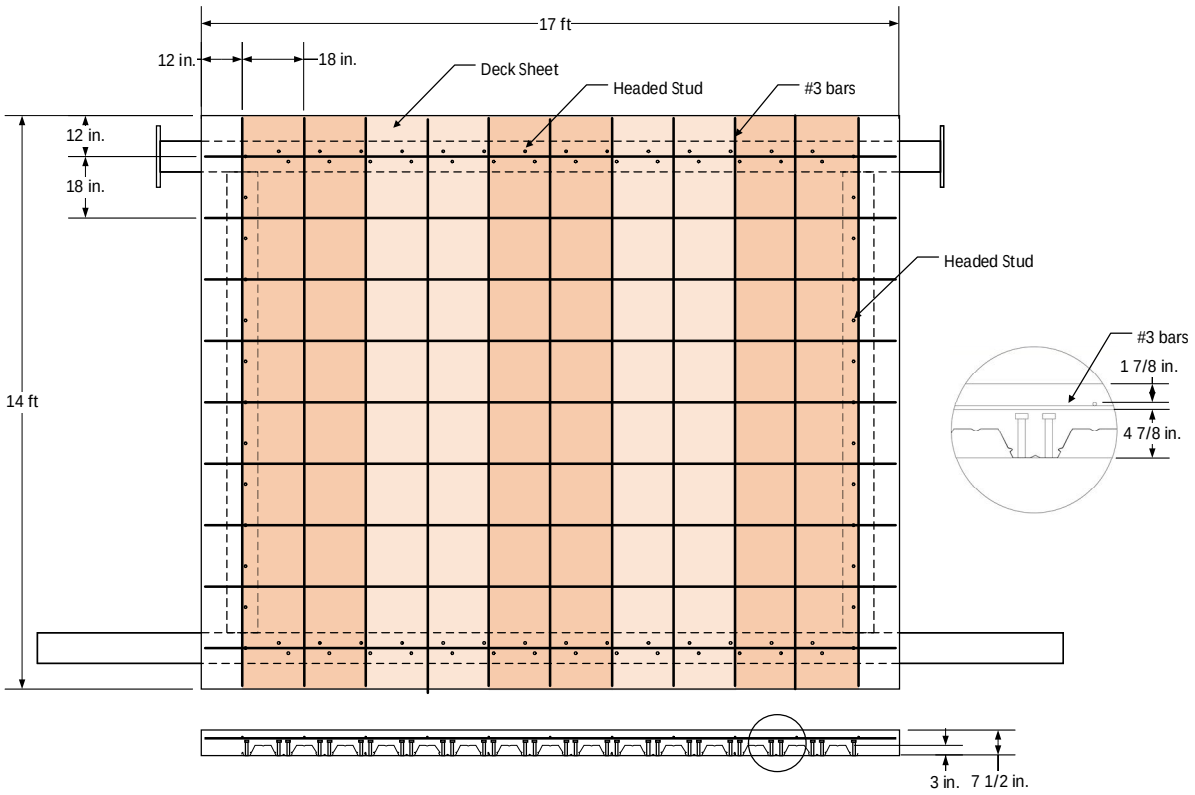

Figure 2-11. Reinforcement Arrangement for Specimen 3/7.5-4-N-RS

2.3 Materials

The steel deck used was gauge 20 (0.0358 in. nominal thickness) Verco W2-36 Formlok™ or W3-36 Formlok™ satisfying ASTM A653. The headed studs were ¾ in. diameter, satisfying ASTM A29 with nominal tensile strength of 65 ksi. Reinforcing steel bars were ASTM A615/A615M and the welded wire mesh was likely ASTM A1064/A1604M although mill certification reports were not available. The material properties of the concrete mixes used are summarized in Table 2-2

Table 2-2. Concrete Compressive Strength

Test Specimen	Concrete Type	Concrete Compressive Strength (psi)
3/6.25-4-L-NF-DT	LW	3990
3/7.5-4-N-NF-DT	NW	3940
2/4-4-L-NF-DT	LW	3800
3/6.25-4-L-NF-P	LW	4490
2/4.5-4-L-RS-DT	LW	3950
3/7.5-4-N-NF-P	NW	4820
3/6.25-4-L-RS-DT	LW	4350
3/7.5-4-N-RS-DT	NW	4070

Table 2-3. Concrete Mixture Proportions

Specimen	3/6.25-4-L-NF-DT	3/7.5-4-N-NF-DT	2/4-4-L-NF-DT	3/6.25-4-L-NF-P	2/4.5-4-L-RS-DT	3/7.5-4-N-NF-P	3/6.25-4-L-RS-DT	3/7.5-4-N-RS-DT
Cast Date	8/16/2018	10/30/2018	2/13/2019	10/7/2019	2/7/2020	7/23/2020	10/6/2020	12/21/2020
Type I/II Portland Cement (lbs)	460	450	460	460	460	450	460	410
Fly Ash (lbs)	120	150	120	120	120	150	120	137
Coarse Aggregate (1/2 in. Stalite) (lbs)	900	-	900	900	900	-	900	-
Coarse Aggregate (#57 Limestone) (lbs)	-	1835	-	-	-	1835	-	1835
Fine Aggregate (Natural Sand) (lbs)	1493	662	1493	1495	1495	662	1495	685
Fine Aggregate (Manuf. Sand) (lbs)	-	706	-	-	-	706	-	729
Water Potable (lbs)	290	292	290	290	290	290	290	292
High Range Water Reducer (oz/cwt)	4	3	4	4	4	3	4	4
Retarder (oz/cwt)	-	-	-	-	-	0.5	-	-
Water-to-Cement Ratio	0.5	0.48	0.5	0.5	0.5	0.48	0.5	0.53

2.4 Instrumentation

An array of string potentiometers (Figure 2-12) was used to collect displacement data from the specimens. Shear angle was calculated per AISI S907-13 [17]. AISI S907 provides two different methods for calculating shear angle. The first method (Eq. 1) utilizes lateral displacement sensors (SP2 and SP4 in Figure 2-12) and perpendicular sensors (SP3 and SP7 in Figure 2-12) capturing the rotation of the fixed beam. The second method (Eq. 2) utilizes diagonal displacement sensors (SP1 and SP5 in Figure 2-12). In order to account for the flexibility of the frame for some of the specimens, three layers of diagonal sensor pairs (SP1 and SP5 for the bottom layer, SP10 and SP11 for the top layer, and SP12 and SP13 for the mid layer) were placed along the height of the specimen, as shown in Figure 2-13. Uplift sensors (US1 and US2 in Figure 2-12) were included in some of the specimens to measure the uplift of the corners of the free end.

$$\gamma = \left(\Delta_{SP2} - \left(\Delta_{SP4} + (\Delta_{SP3} + \Delta_{SP7})\left(\frac{a}{b}\right)\right)\right)/a \quad (1)$$

$$\gamma = \left(\frac{(|\Delta_{SP1}| + |\Delta_{SP5}|)\sqrt{a^2 + b^2}}{2b}\right)/a \quad (2)$$

Where,

γ = shear angle of the specimen based on linear displacement sensors

Δ_{SPi} = linear displacement of ith sensor. Sensor location and numbering is illustrated in Figure 2-12.

a = center-to-center spacing between loading beam and fixed beam (12 ft.)

b = center-to-center spacing between side beams(15 ft.)

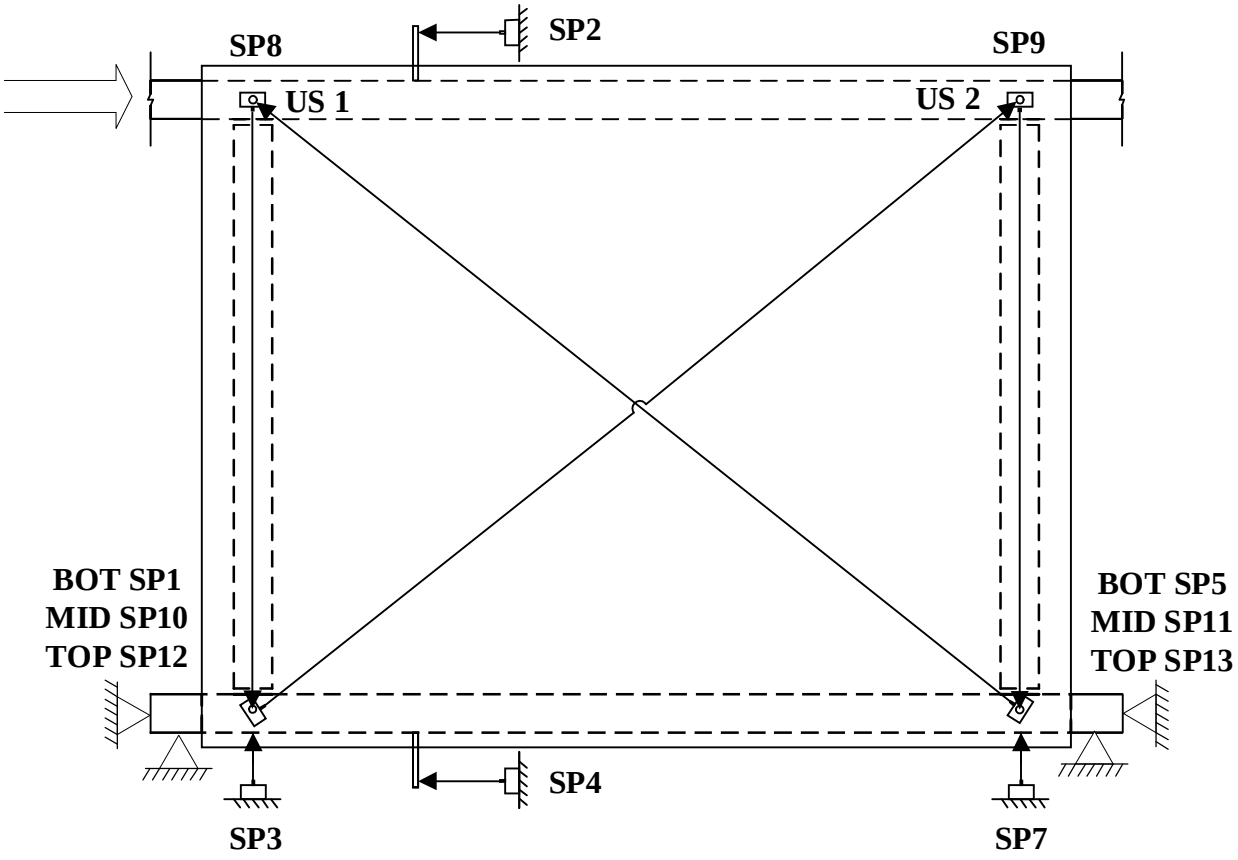

Figure 2-12. Instrumentation Setup

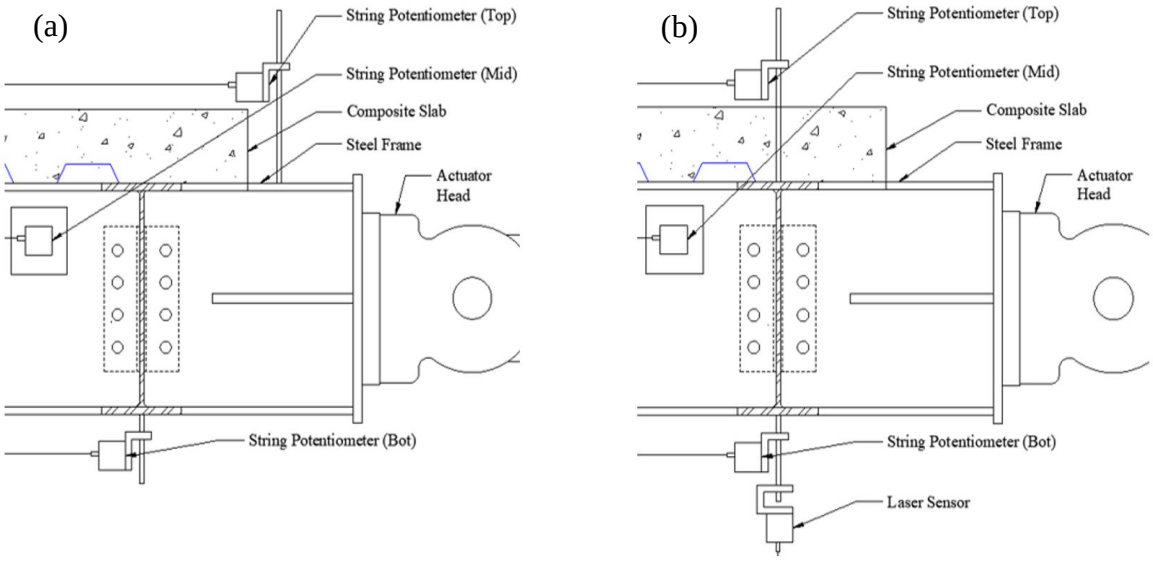

Figure 2-13. Instrumentation Detail: Specimens 3/7.5-4-N-NF-DT, 3/6.25-4-L-NF-DT, and 2/4-4-L-NF-DT (a). Typical configuration (b)

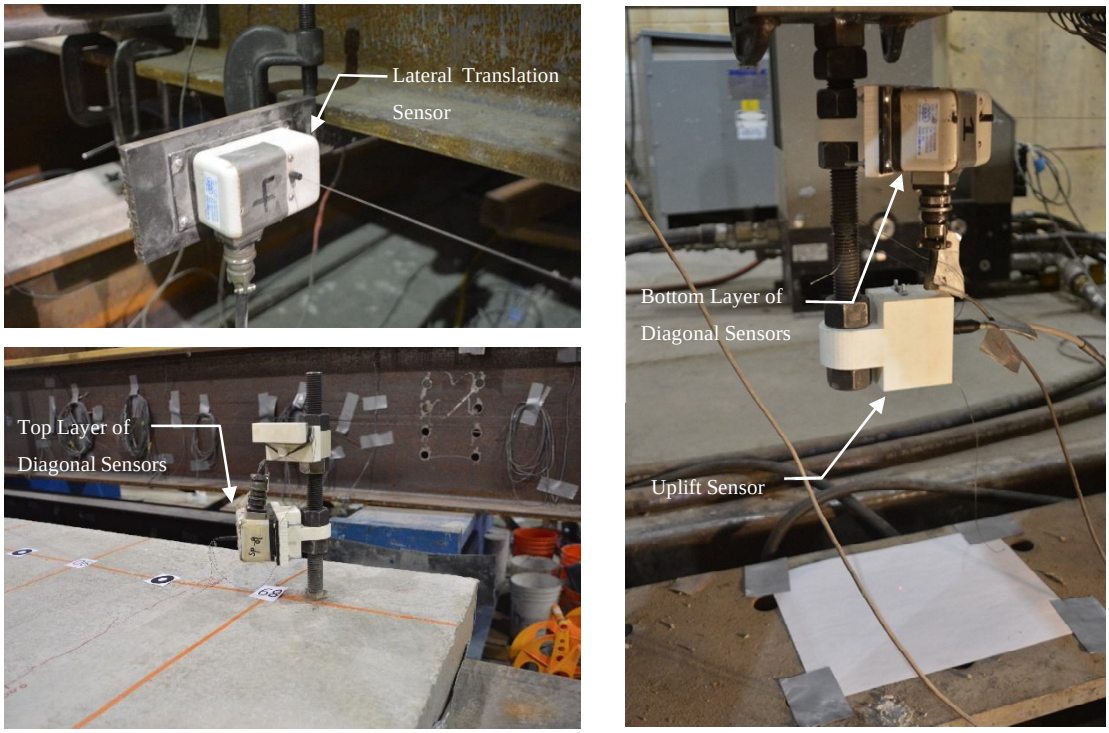

Figure 2-14. Instrumentation Pictures

A grid was painted on all of the specimens with 18 in. by 18 in. squares. At each intersection between the lines in the grid, numbers were placed in ascending order from left to right, starting on the top left corner of the specimen (with an orientation as shown in Figure 2-12)

and ending on the bottom right corner. One of the grids is shown in Figure 2-15. Another purpose of the grid was to facilitate photo stitching used to produce high-resolution pictures of the entire slab at several points during the test. This is done by taking pictures of each individual square in the grid and using software to overlap the individual images into a large high resolution composite image of the entire specimen. The grid provides easily identifiable overlap between the images which aids with the process. An example of an image used as part of a larger composite image is shown in Figure 2-16.

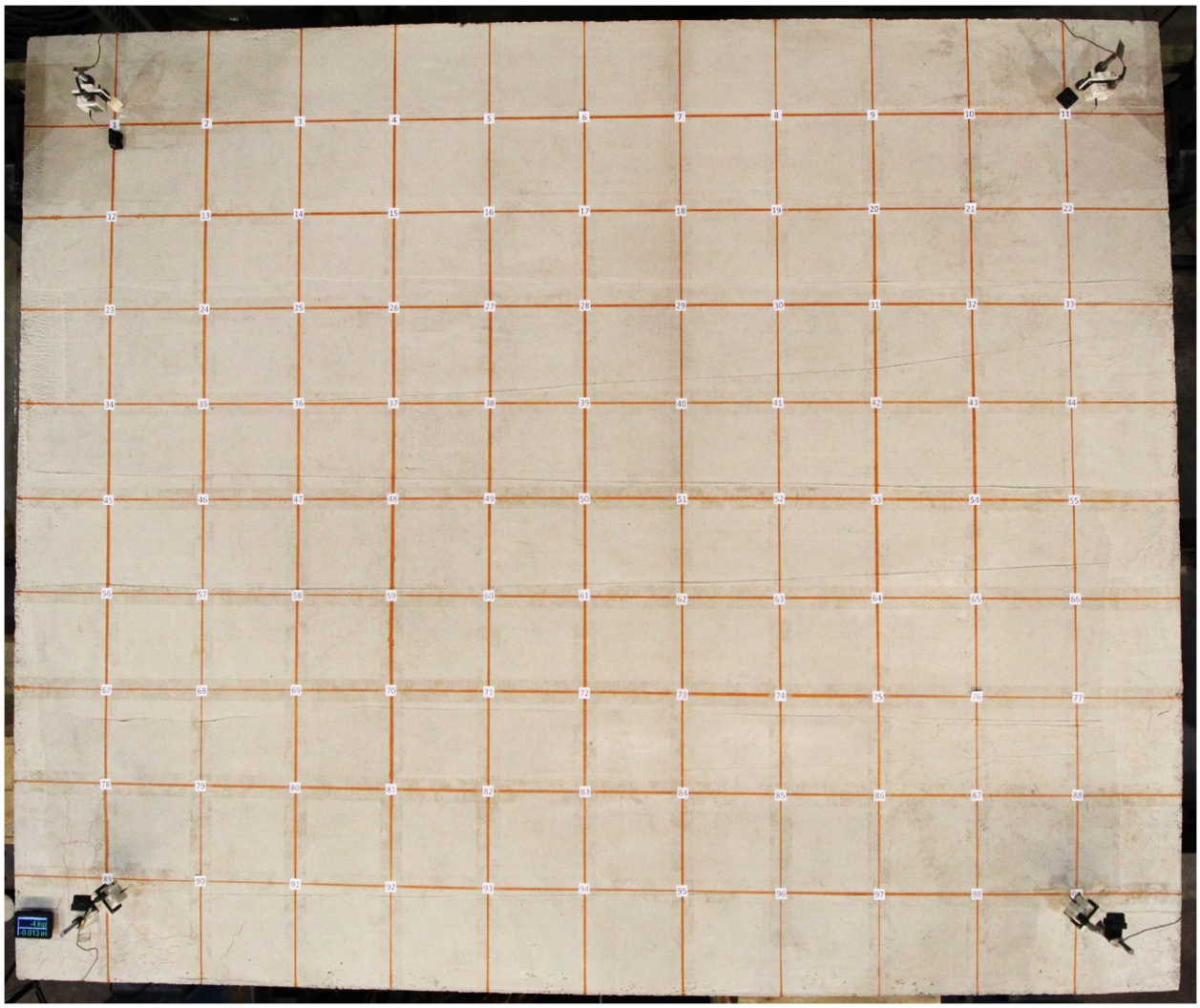

Figure 2-15. Painted Grid used for Crack Documentation

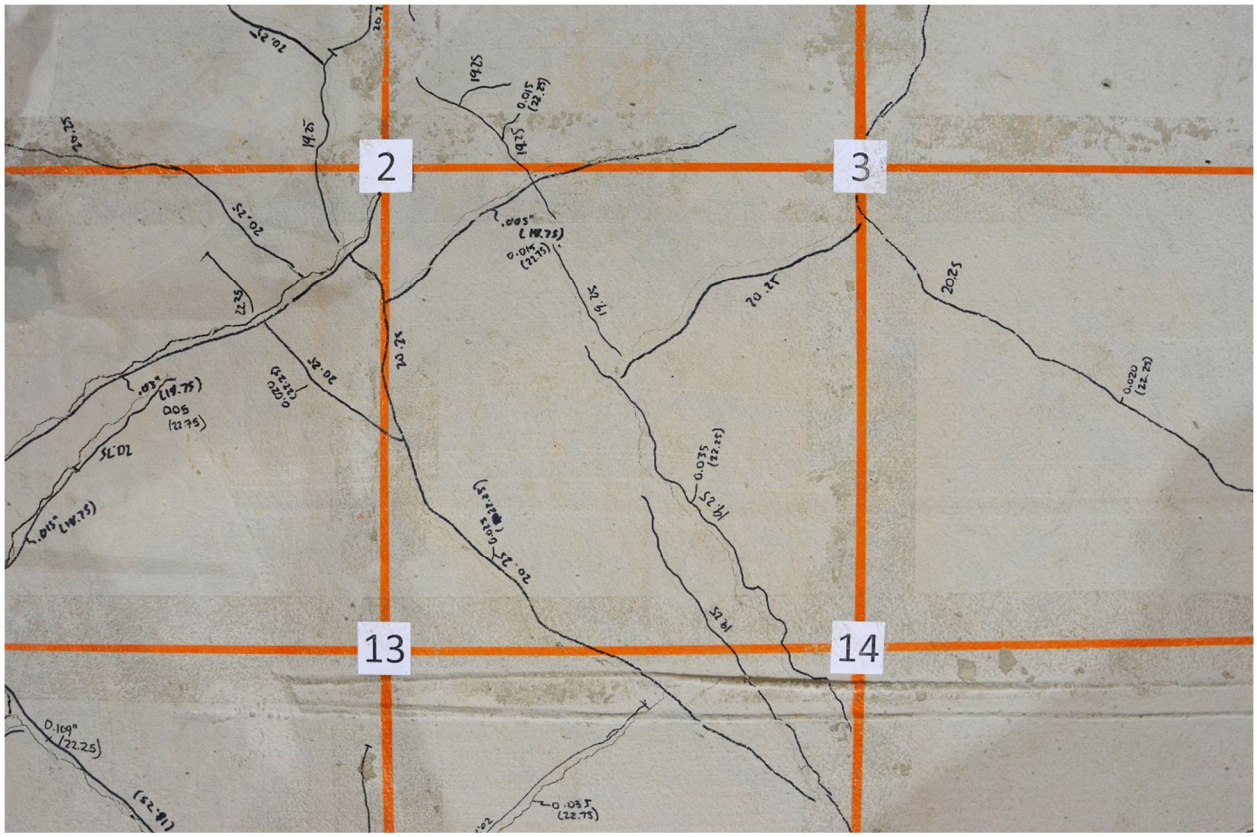

Figure 2-16. Sample Image used in Photo-Stitching

2.5 Test Procedure and Loading Protocol

AISI S310 [19] specifies that the nominal diaphragm shear strength and the diaphragm stiffness are permitted to be determined by tests in accordance with AISI S907 [17]. AISI S907 was used to formulate the test procedure. Per this standard, a bare frame test was performed to show that a negligible amount of shear was being resisted by the frame. AISI S907 [17] states that if the load from a bare frame test is less than 2% of the maximum load from the diaphragm test (measured at the same displacement), then the shear load from the diaphragm test need not be corrected for bare frame resistance. For all specimens, the bare frame resistance was less than 0.02 times the shear strength of the specimen, and therefore bare frame resistance was neglected. The results of the bare frame test are included in Appendix B.

For each specimen, the following test procedure was followed:

1. Search for and mark visible pre-existing cracks on the concrete slab
2. Remove the initial offset in the readings for all displacement sensors
3. Initiate loading protocol
4. Pause loading protocol at predicted elastic limit (both positive and negative cycle amplitudes) to assess the condition of the slab. Mark cracks if observed

5. Continue the loading protocol until diagonal tension cracking is reached
6. Pause loading protocol at first occurrence of diagonal tension cracking (both positive and negative cycle amplitudes) to mark cracks
7. Continue with loading protocol until considerable degradation of strength is reached (Load < 80% of maximum load)
8. Note and record the mode of failure

The cyclic loading protocol was based on FEMA 461 [16], Section 2.9.1, and includes at least six cycles before reaching the elastic limit. The elastic limit was calculated as a ratio of the predicted ultimate strength to the predicted stiffness. It was verified afterwards that this approach resulted in more than six cycles of loading before reaching the elastic limit. The loading protocol includes two cycles for every displacement step with a 40% increase in amplitude between displacement steps. The loading was implemented using two actuators working in tandem. An example of a loading protocol is shown in Figure 2-17.

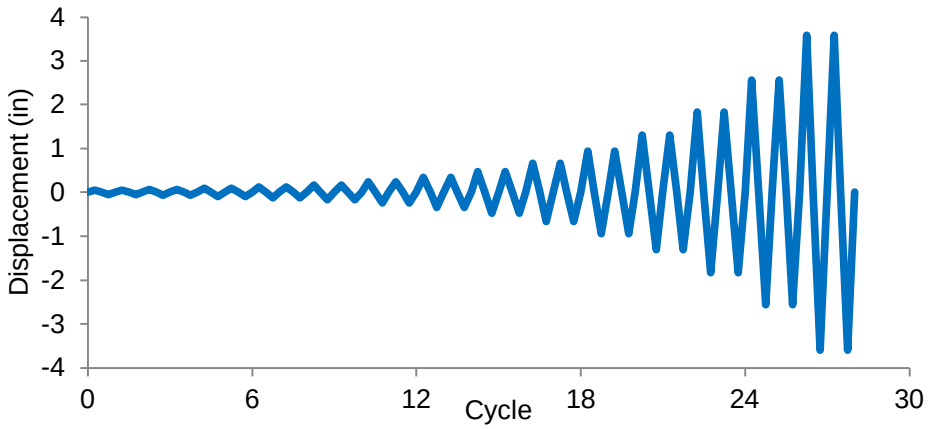

Figure 2-17. Sample Loading Protocol

2.6 Specimen Shoring

In order to prevent sagging of slab during concrete curing, intermediate shoring was placed below the specimens, as shown in Figure 2-18. The shoring consisted of 4x4 wooden beams oriented perpendicular to the deck span direction with 4 ft spacing. The beams were supported by 4x4 wooden columns, resting on the strong floor. The shoring was kept in place for 7 days while the concrete moist cured. Cold-formed pour stops were used along the edges of the specimens. In the direction perpendicular to the deck span direction, where the deck extended past the edge of the supporting frame, the pour stop was fastened to the deck using self-tapping screws. In the direction parallel to the deck span direction, where the steel deck sheets stopped at the centerline of the steel beams, the pour stop was supported continuously by a steel angle (L4x4x1/4). The pour

stop was placed below the top flange of the steel beams, with ¾ in. plywood used to fill the gap between the pour stop and the top of the flange, as shown in Figure 2-19. A piece of 2x4 was fitted snugly every 24 in. approximately, between the bottom of the pour stop and the top of the bottom flange to prevent movement of the pour stop during concrete placement. After moist curing, the pour stop was removed so that the edges of the specimen could be observed during the test, as shown in Figure 2-20.

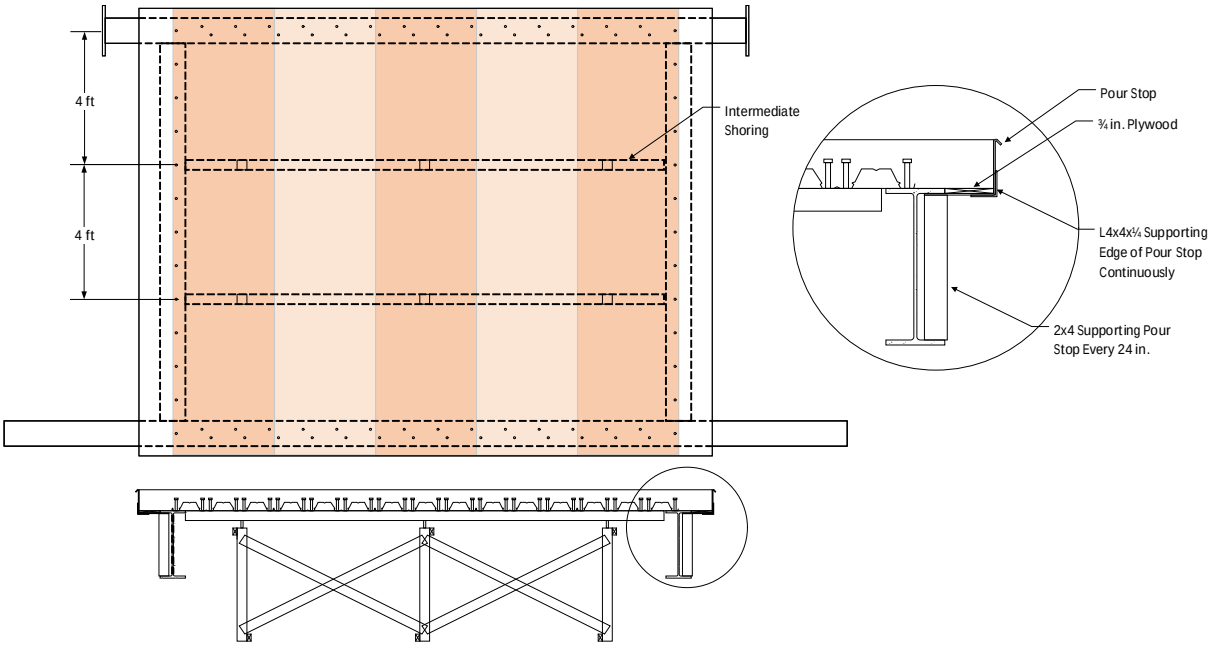

Figure 2-18. Shoring for Typical Specimen

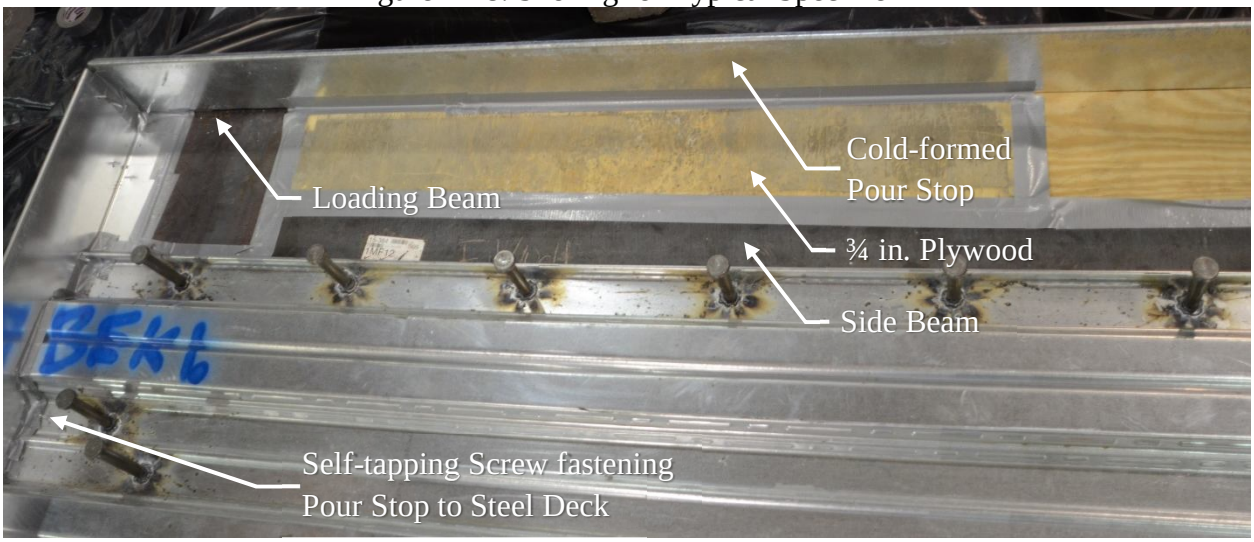

Figure 2-19. Pour Stop Along Edge Parallel to Deck Span Direction

Figure 2-20. Specimen After Removal of Pour Stop

As shown in Figure 2-10, the deck sheets in Specimen 3/6.25-4-L-RS-DT were oriented parallel to the loading direction. This specimen also had larger external slab dimensions than typical, with an edge distance measured from the centerline of the steel beam of 18 in. in each direction. The shoring for this specimen was oriented as shown in Figure 2-21. Due to the larger-than-usual distance from the centerline of the beams to the edge of the concrete slab, continuous 4x4 wooden beams were placed along the edges of the concrete slab, supported by wooden brackets connected to the steel frame. This was done to support the weight of the concrete along the edges of the specimen during concrete curing.

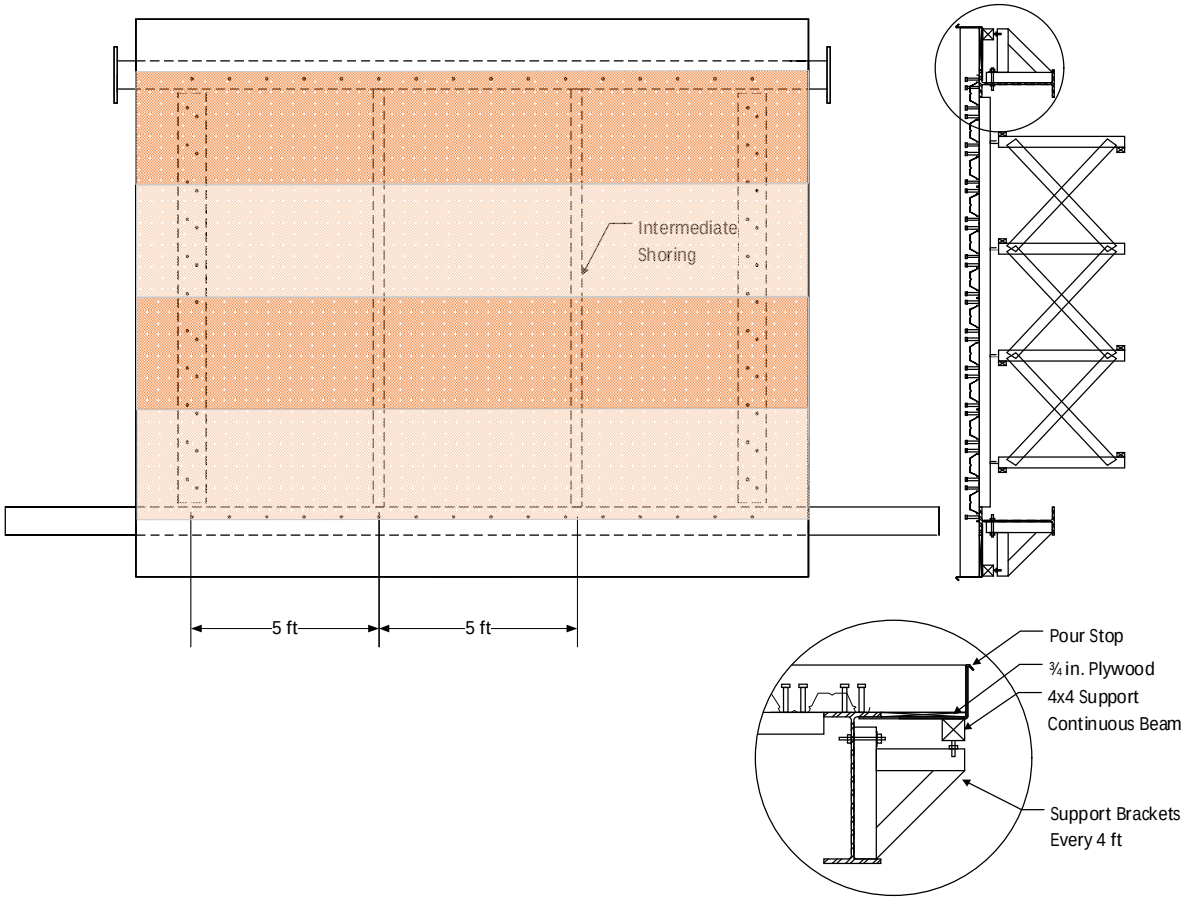

Figure 2-21. Shoring for Specimen 3/6.25-4-L-RS-DT

3 RESULTS

This chapter includes a summary of the experimental result for all the specimens. Shear strength is calculated as the force measured by the actuator load cells divided by the 15 ft. length of the diaphragm to obtain a strength per foot of diaphragm. Shear angle is calculated using the mid layer of diagonal string potentiometers (Eq. 2 in Section 2.4) unless otherwise stated.

The load-deformation behavior of the individual specimens is also described in this chapter. Each specimen summary includes a load-deformation plot in which shear angle is calculated using the mid layer of diagonal sensors unless otherwise specified, as well as observations of the behavior of each specimen at different stages during the test.

3.1 Overview of Strength and Stiffness Results

A tabulated summary of the peak strength results as well as shear angle at relevant points in the test, and residual strength for each specimen is provided in Table 3-1

Table 3-1. Summary of Experimental Results

Specimen	Ultimate Experimental Shear Strength (kip/ft)	Shear Angle at Ultimate Strength (rad)	Shear Angle at 80% of Ultimate Strength (rad)	Residual Shear Strength (kip/ft)
3/6.25-4-L-NF-DT	9.6	0.0015	0.0049	3.4
3/7.5-4-N-NF-DT	15.4	0.0013	0.0023	4.3
2/4-4-L-NF-DT	8.9	0.0031	0.0069	3.4
3/6.25-4-L-NF-P	4.0	0.0011	0.0013	1.3
2/4.5-4-L-RS-DT	17.6	0.0041	0.0059	3.2
3/7.5-4-N-NF-P	5.6	0.0037	0.0039	0.9
3/6.25-4-L-RS-DT	13.3	0.0024	0.0055	4.2
3/7.5-4-N-RS-DT	21.6	0.0012	0.0030	4.2

A summary of the initial stiffness measurements is provided in Table 3-2. Stiffness is calculated as the shear load at 40% of the peak load divided by the shear angle at that point. Shear angle can be calculated using diagonal sensors (Eq. 2 in Section 2.4) connected to opposing corners of the specimens (such as SP12 and SP13 in Figure 2-12) as well as using the lateral translation sensors (SP2 and SP4 in Figure 2-12) and sensors SP3 and SP7 in Figure 2-12 to correct for rotation of the fixed end (Eq. 1 in Section 2.4). Table 3-2 summarizes stiffness calculated using these two configurations. The large initial stiffness of the diaphragm can cause twisting of the supporting frame which results in different values of shear angle depending on the location of the diagonal

sensors used. For this reason, the stiffness is reported using different sets of diagonal sensors. The top layer of diagonal sensors were not used to compute initial stiffness since they consistently measured little-to-none displacement during the initial stages of loading, resulting in initial load deformation behavior as shown in Figure 3-1. This was likely due to the large in-plane stiffness of the specimens, which causes twisting of the testing frame preventing the top layer of sensors from being engaged during the initial loading cycles. The mid layer of diagonal sensors was placed on the upper portion of the web of the supporting beams, closest to the interface between the beams and the composite slabs. This layer is used herein to calculate shear angle since due to its location is deemed to provide the most accurate measurement of deformation for the specimens.

Table 3-2. Summary of Initial Shear Stiffness Measurements

Specimen	Experimental Stiffness Using Mid Diagonal Sensors (kip/in)	Experimental Stiffness Using Bottom Diagonal Sensors (kip/ft)	Experimental Stiffness Using Lateral Translation Sensors (kip/ft)
3/6.25-4-L-NF-DT	1276	602	575
3/7.5-4-N-NF-DT	1305	555	765
2/4-4-L-NF-DT	2116	710	923
3/6.25-4-L-NF-P	1265	771	772
2/4.5-4-L-RS-DT	2433	933	1632
3/7.5-4-N-NF-P	1110*	-	-
3/6.25-4-L-RS-DT	3349	1121	1313
3/7.5-4-N-RS-DT	3557	1256	1974

* Initial stiffness calculated from actuator shear angle modified as described in Appendix A

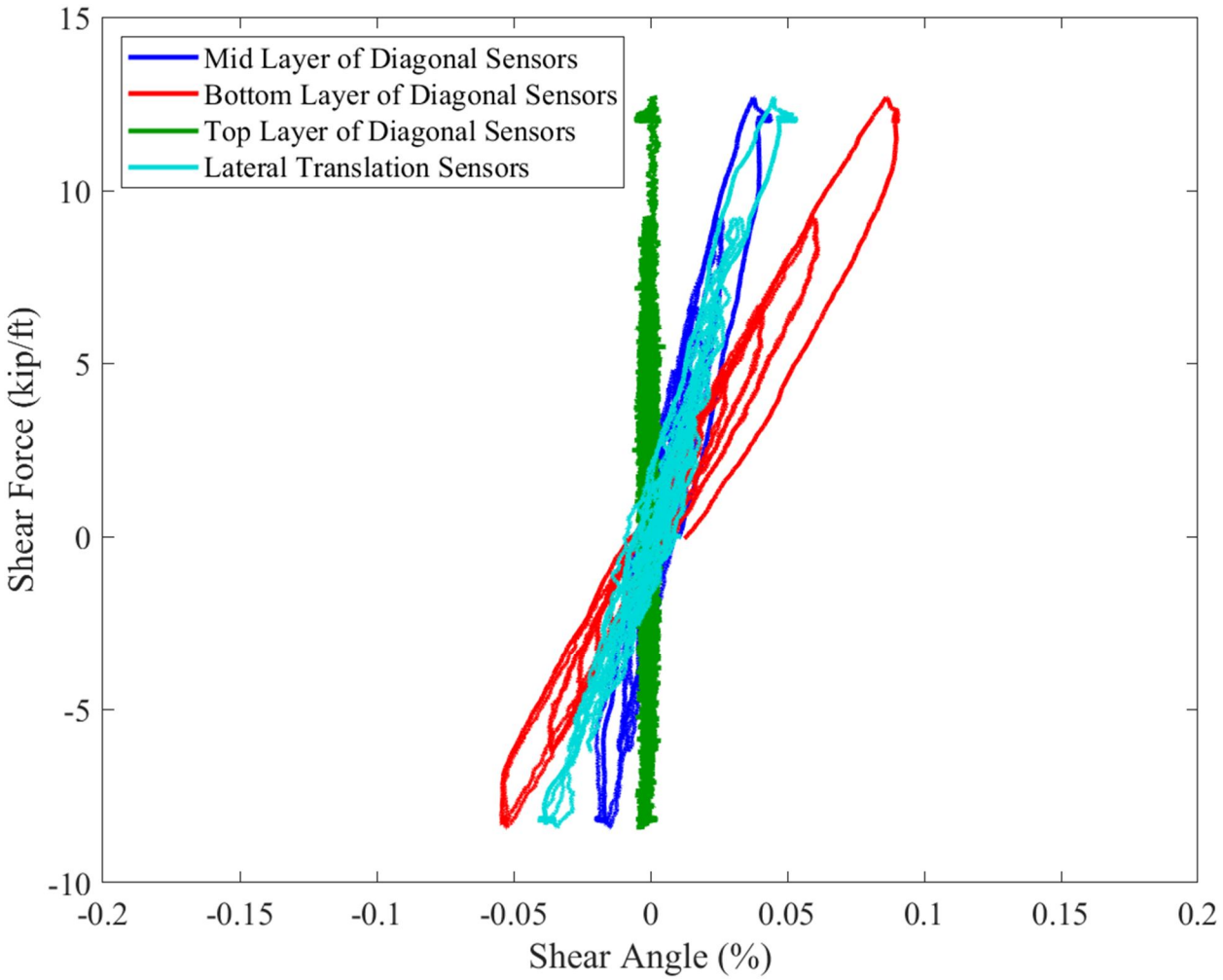

Figure 3-1. Comparison of Initial Load-Deformation Cycles Using Different Displacement Sensors for Specimen 3/7.5-4-N-NF-RS

3.2 Specimen 3/6.25-4-L-NF-DT

The test specimen before and after concrete placement is shown in Figure 3-2. The deformation behavior of the specimen during early loading cycles used to calculate initial stiffness

is shown in Figure 3-3. The measured stiffness using the mid layer of string potentiometers was 1276 kip/in.

Figure 3-2. Specimen 3/6.25-4-L-NF-DT Before and After Concrete Placement

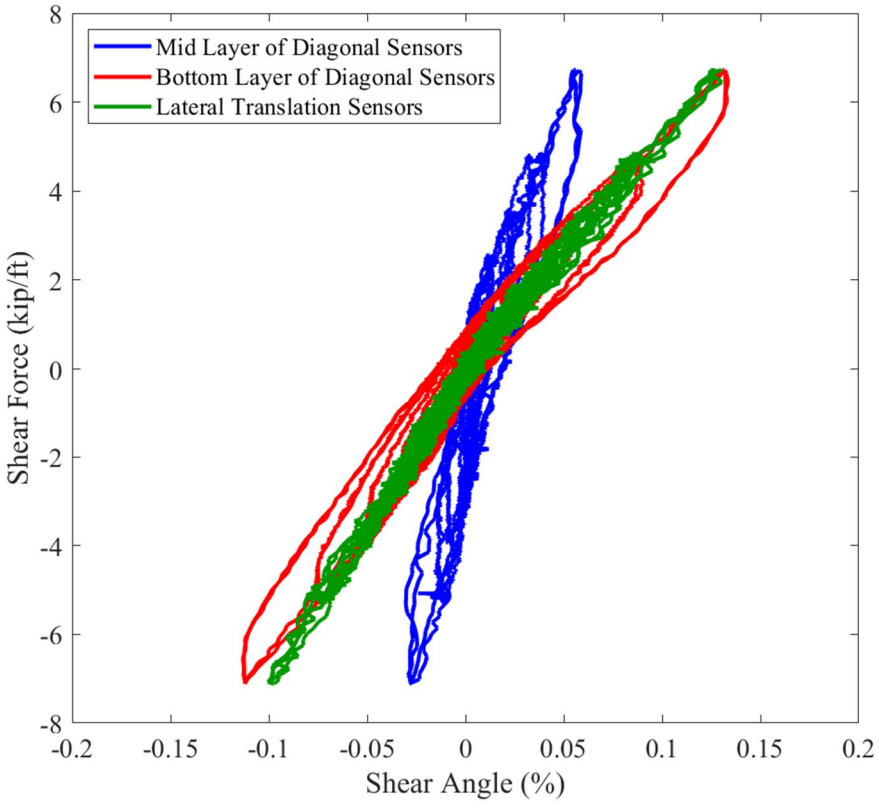

Figure 3-3. Comparison of Initial Load-Deformation Cycles Using Different Displacement Sensors for Specimen 3/6.25-4-L-NF-DT

A load deformation plot used to describe the progression of failure for this specimen is shown in Figure 3-4. The peak strength was 9.6 kip per foot of diaphragm, with a shear angle at peak strength of 0.0015 radians. The shear angle at 80% of peak strength was 0.0049 radians and

the residual strength measured at 0.02 radians of 3.4 kips per foot of diaphragm. Before the test started (Figure 3-4 Point A), some shrinkage cracking was observed and marked on the specimen (Figure 3-5). The first occurrence of diagonal tension cracking was observed at Point B in Figure 3-4. The diagonal cracks were observed to merge with existing shrinking cracking at this point (Figure 3-6).

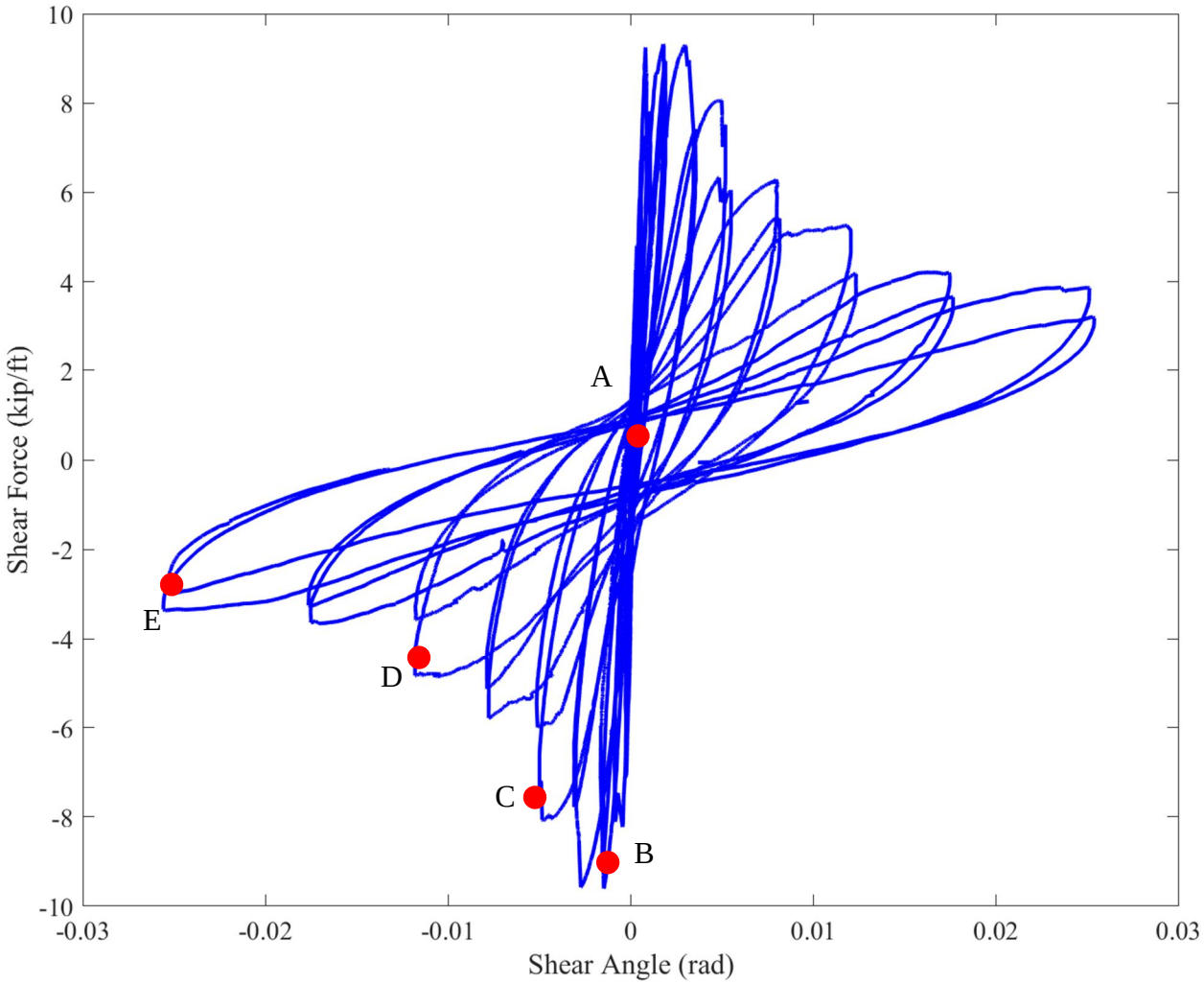

Figure 3-4. Load-Deformation Plot for Specimen 3/6.25-4-L-NF-DT

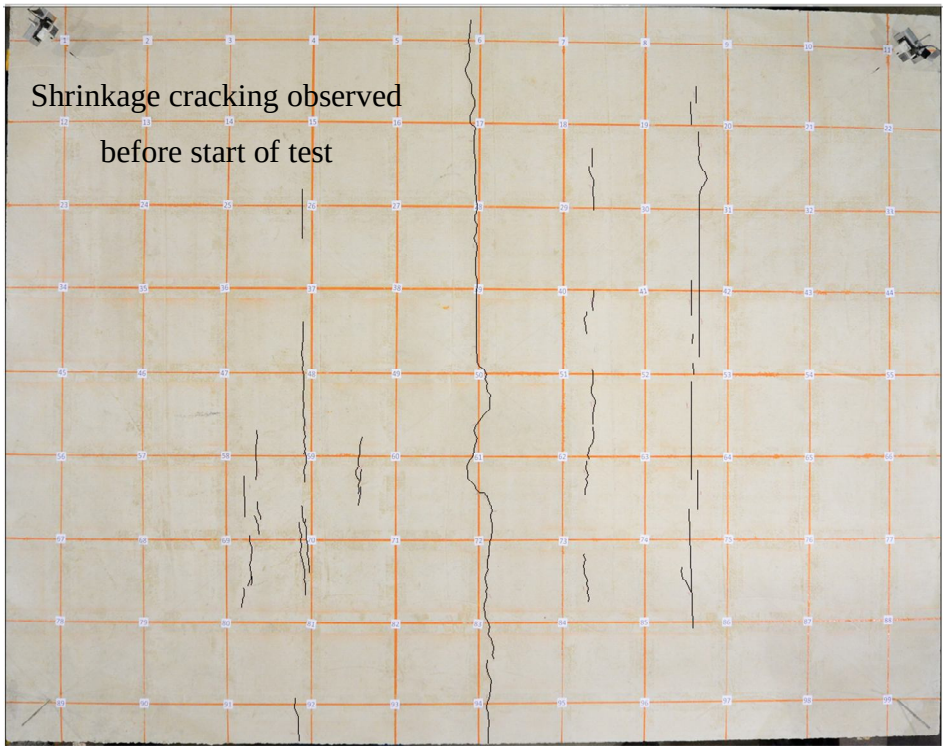

Figure 3-5. Crack Distribution of Specimen 3/6.25-4-L-NF-DT Before Testing (Point A in Figure 3-4)

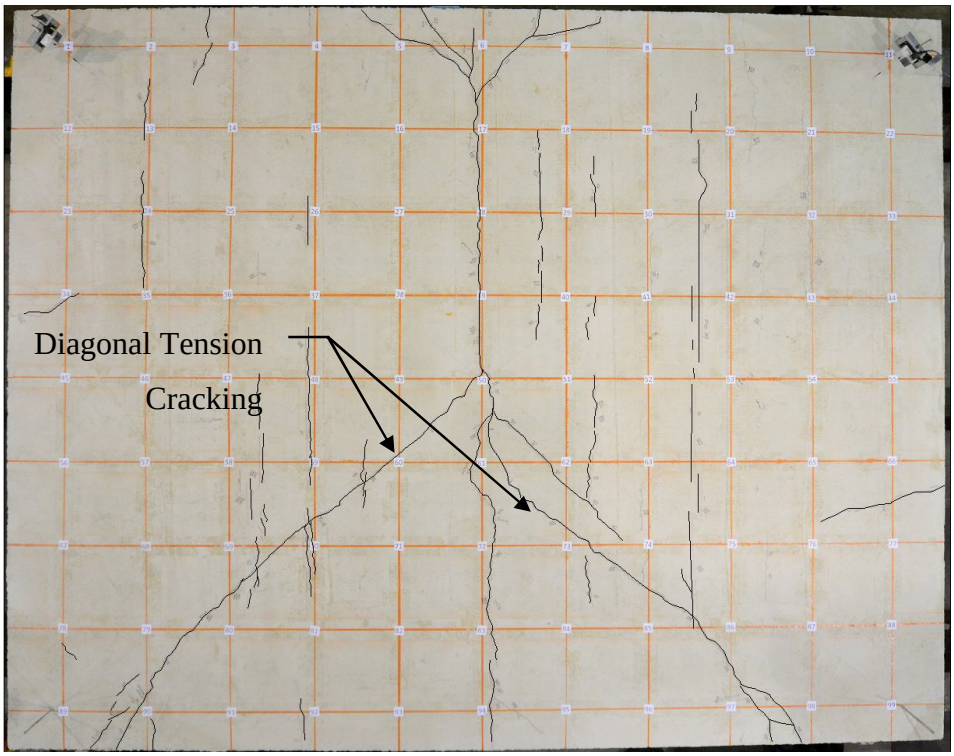

Figure 3-6. Crack Distribution of Specimen 3/6.25-4-L-NF-DT First Occurrence of Diagonal Tension Cracking (Point B in Figure 3-4)

While not visually evident, crackling noises consistent with deck debonding were heard before peak load was reached. A subsequent increase in strength was observed with additional cracking until Point C in Figure 3-4, the diagonal tension cracking was observed to extend the full width of the specimen (Figure 3-7). The shear strength of the specimen then decreased with each displacement step with subsequent crack formation as well as deformation of the steel deck and buckling of the slab. Steel deck deformation and debonding (Figure 3-8) near the edges of the specimen was observed near Point D in Figure 3-4 as well as buckling of the slab (Figure 3-9).

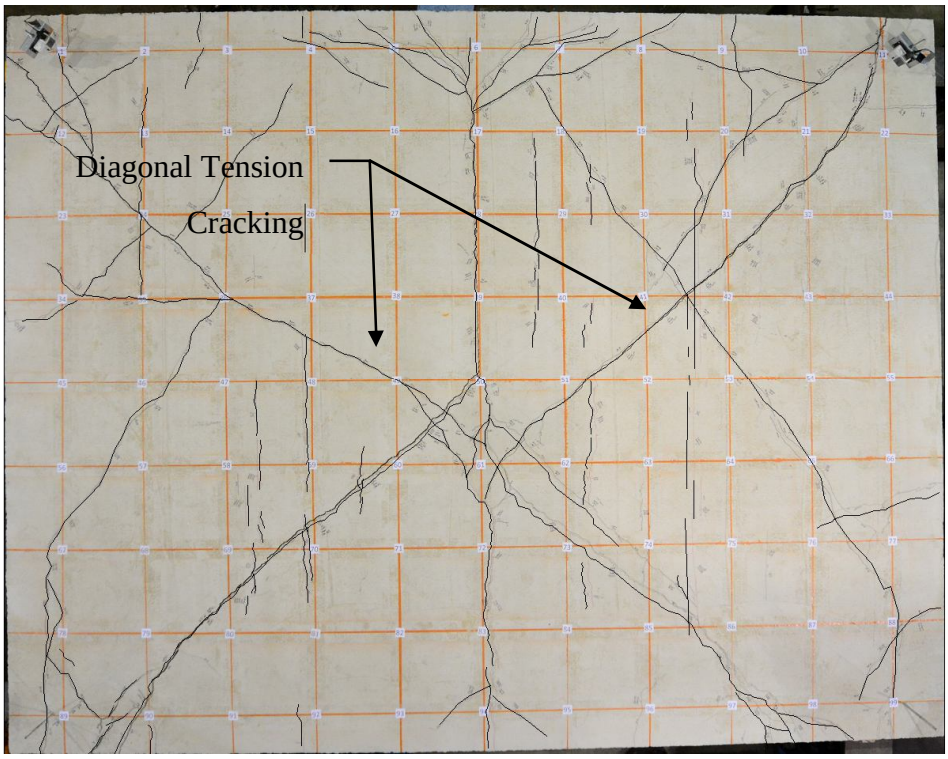

Figure 3-7. Crack Distribution of Specimen 3/6.25-4-L-NF-DT Further Cracking After Strength Decrease (Point C in Figure 3-4)

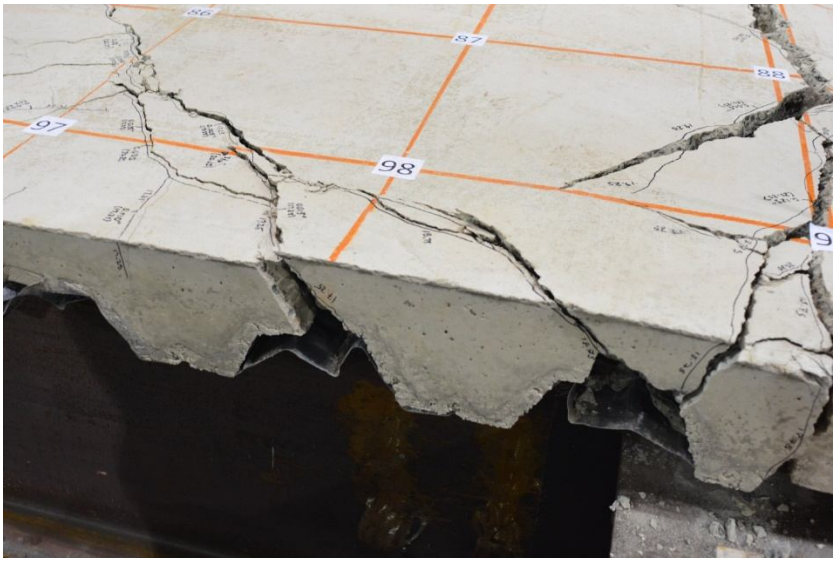

Figure 3-8. Deck Deformation and Overhang Cracking (Point D in Figure 3-4)

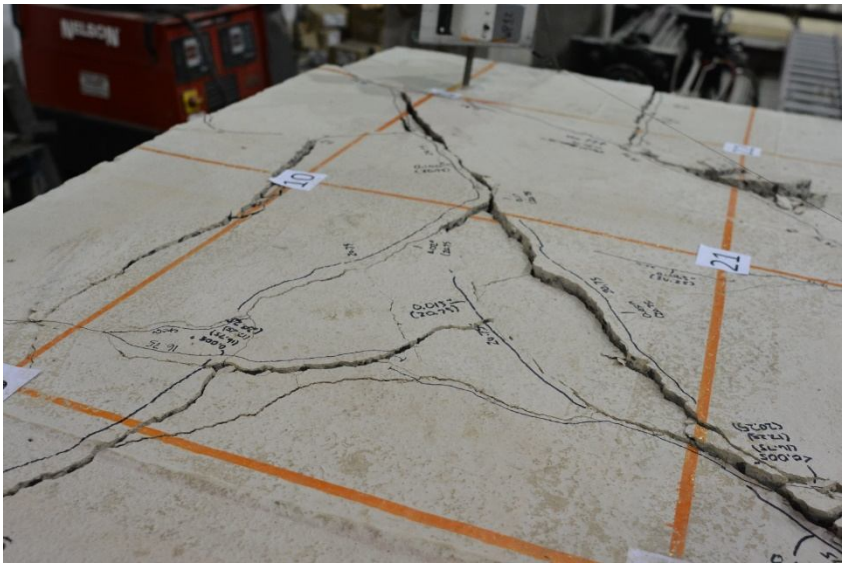

Figure 3-9. Slab Buckling (Point D in Figure 3-4)

The state of the specimen after testing is show in Figure 3-10. At this point, new crack formation was not observed across the field of the diaphragm. Instead, existing cracks opened and extensive cracking of the overhangs was observed.

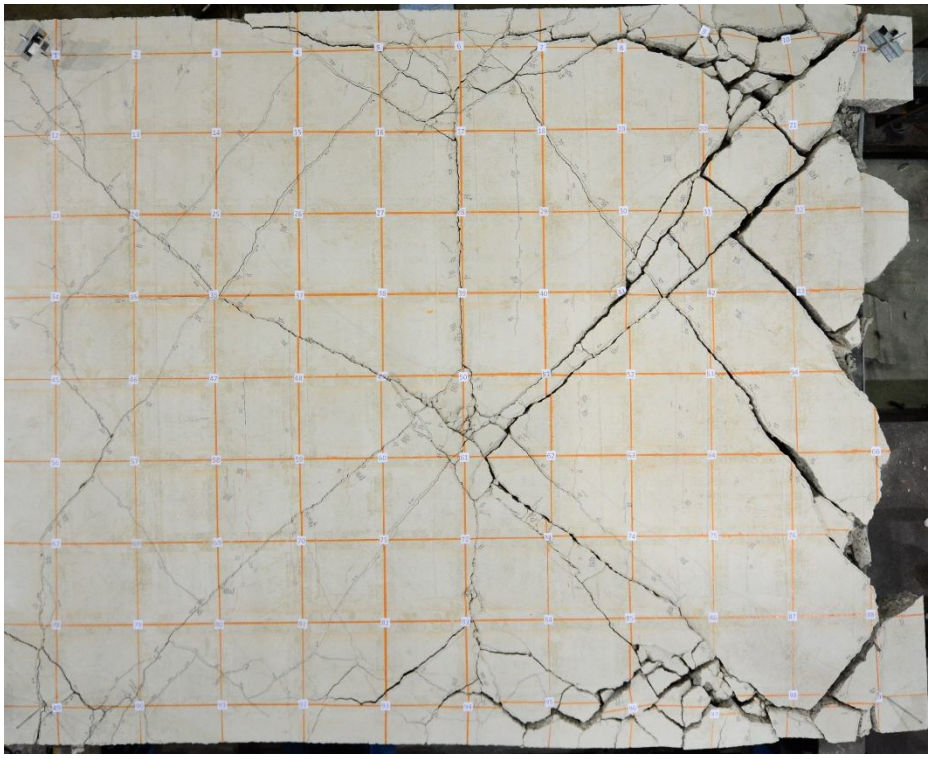

Figure 3-10. Crack Distribution of Specimen 3/6.25-4-L-NF-DT End of Test (Point E in Figure 3-4)

3.3 Specimen 3/7.5-4-N-NF-DT

The test specimen before and after concrete placement is shown in Figure 3-11. The deformation behavior of the specimen during early loading cycles used to calculate initial stiffness is shown in Figure 3-12.

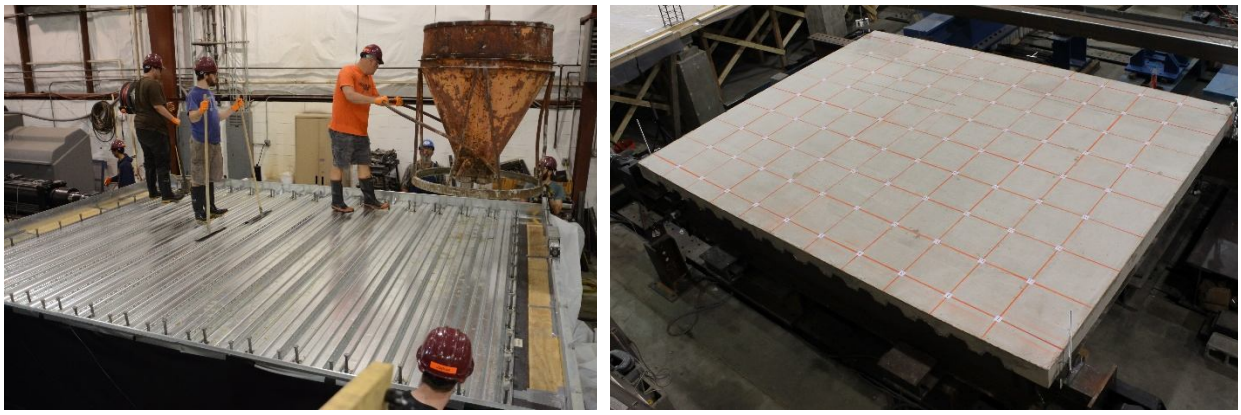

Figure 3-11. Specimen 3/7.5-4-N-NF-DT Before and After Concrete Placement

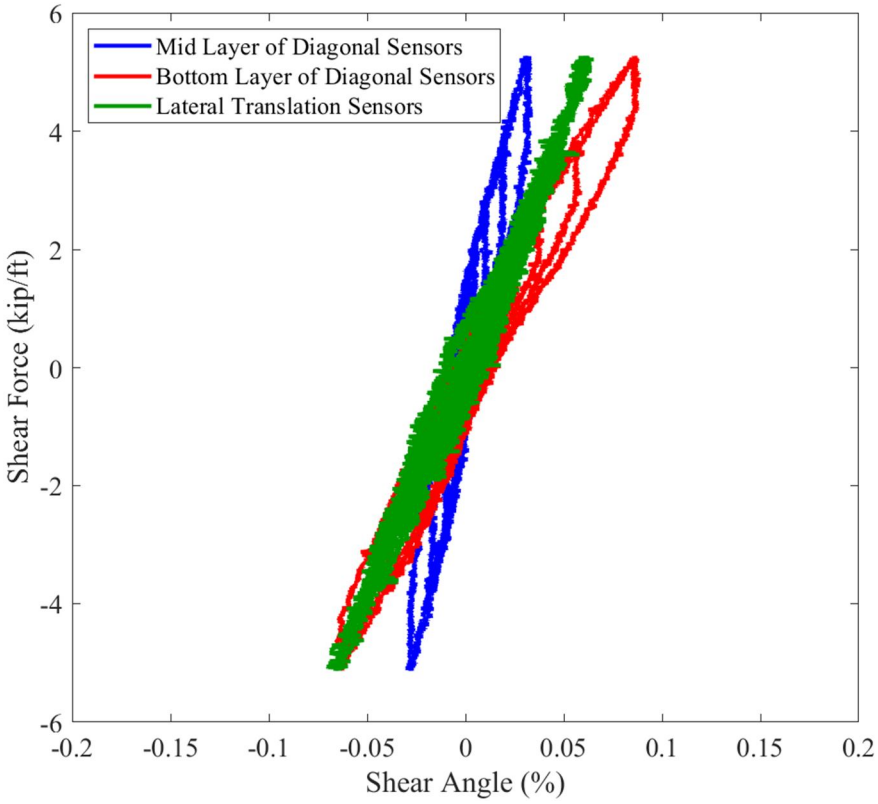

Figure 3-12. Comparison of Initial Load-Deformation Cycles Using Different Displacement Sensors for Specimen 3/7.5-4-N-NF-DT

A load deformation plot used to describe the progression of failure for this specimen is shown in Figure 3-13. The peak strength was 15.4 kip per foot of diaphragm, with a shear angle at peak strength of 0.0013 radians. The shear angle at 80% of peak strength was 0.0023 radians and the residual strength measured at 0.02 radians of 4.3 kips per foot of diaphragm. Before the test started (Figure 3-13 Point A), the specimen was searched for existing cracks, but none were found (Figure 3-14). Some cracking was observed at Point B in Figure 3-13 (See Figure 3-15).

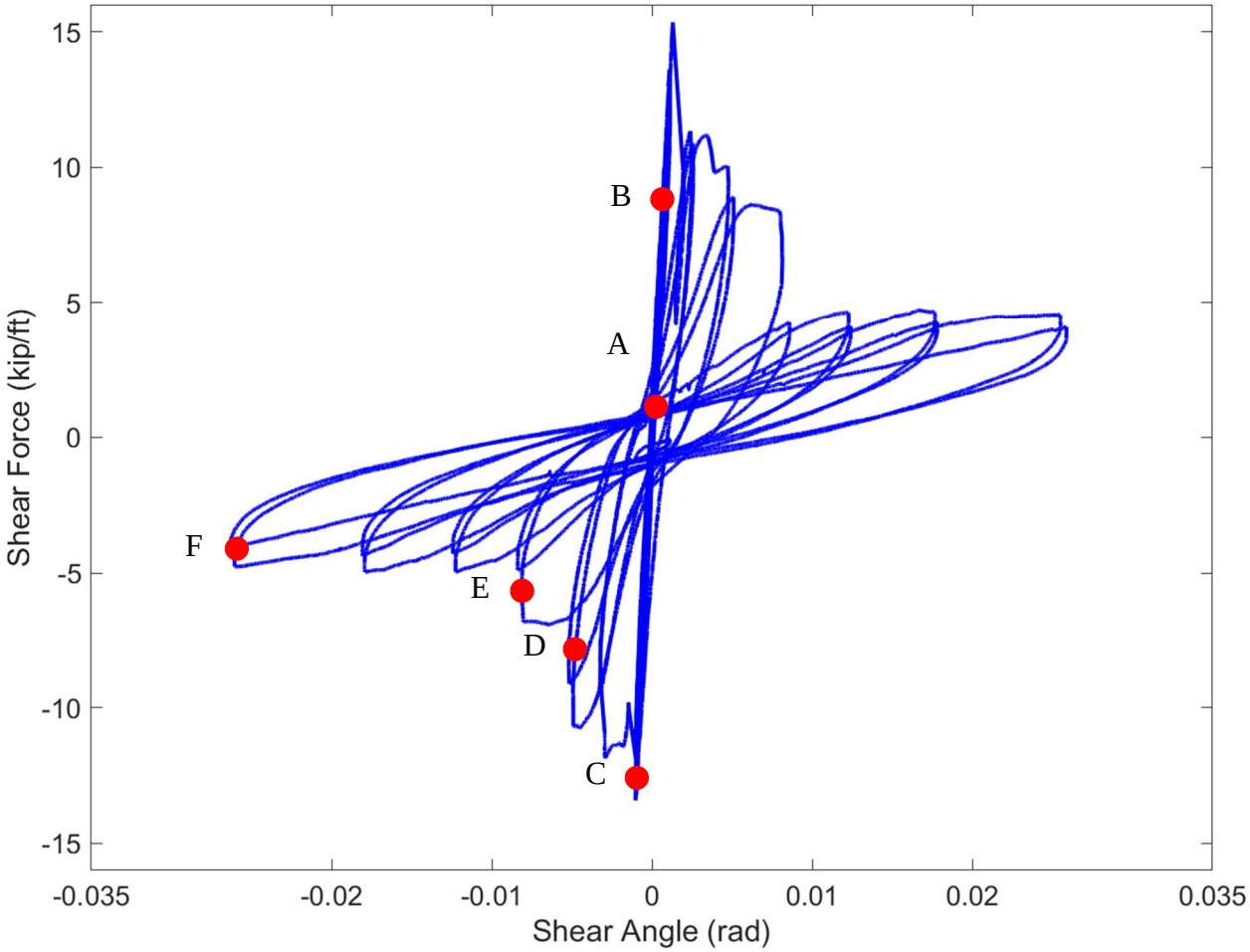

Figure 3-13. Load-Deformation Plot for Specimen 3/7.5-4-N-NF-DT

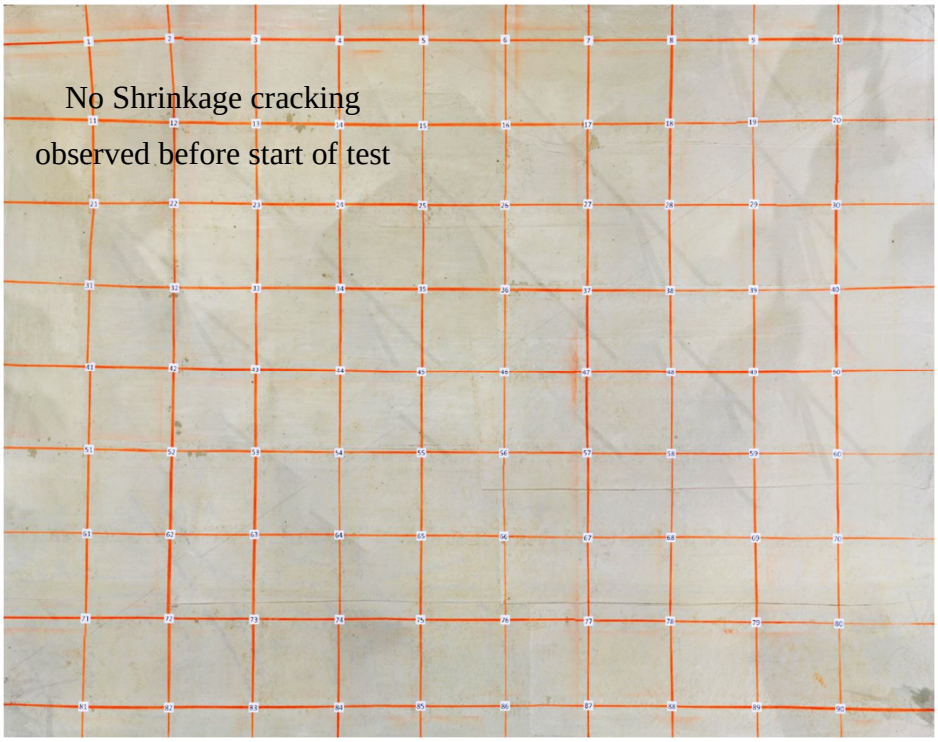

Figure 3-14. Crack Distribution of Specimen 3/7.5-4-N-NF-DT Before Testing (Point A in Figure 3-13)

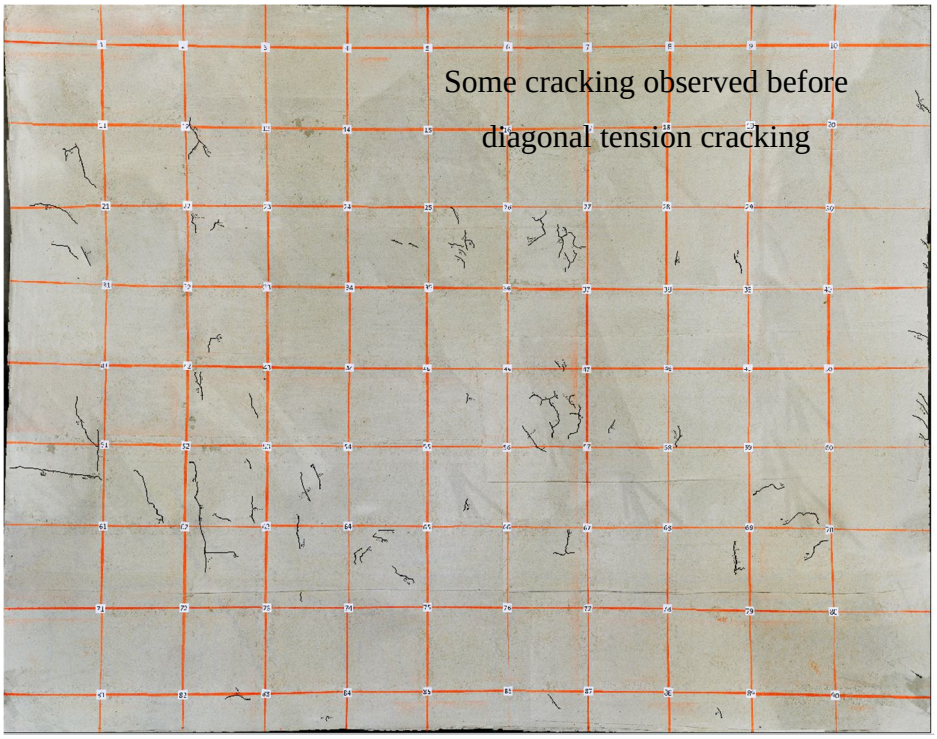

Figure 3-15. Crack Distribution of Specimen 3/7.5-4-N-NF-DT Before Diagonal Tension Cracking (Point B in Figure 3-13)

The first occurrence of diagonal tension cracking in both directions of loading was observed at Point C in Figure 3-13. This coincided with the peak load in both directions and subsequently from this point, the load-carrying capacity of the specimen dropped gradually until the end of the test.

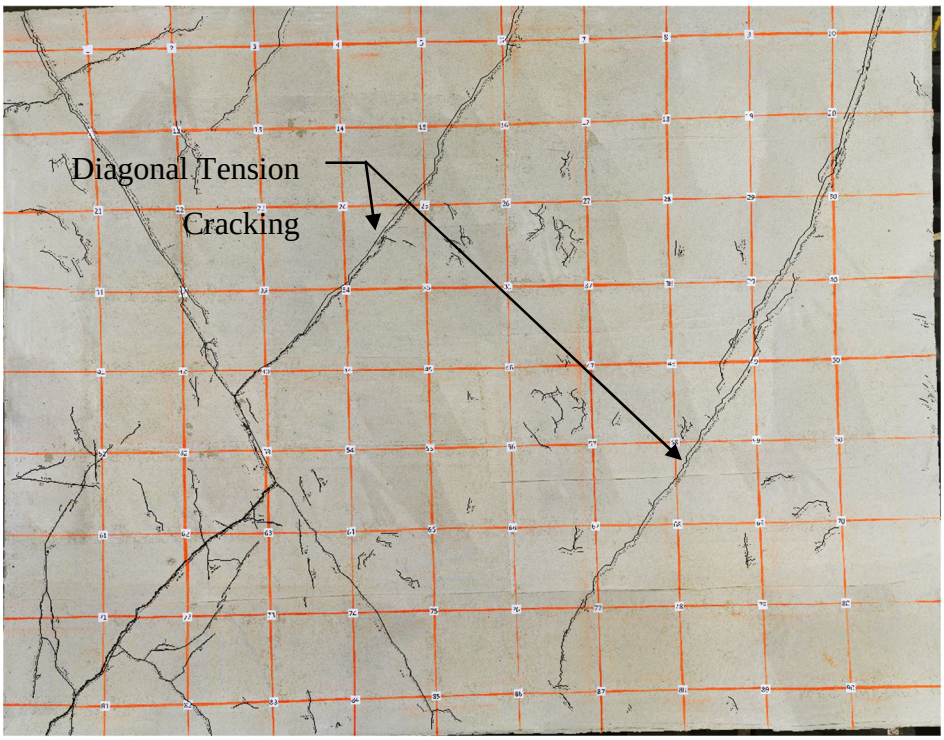

Figure 3-16. Crack Distribution of Specimen 3/7.5-4-N-NF-DT Diagonal Tension Cracking (Point C in Figure 3-13)

Distortions of the deck as well as cracking near the shear connectors was observed past this stage of the test, as shown in Figure 3-17. The specimen continued to develop cracking and opening existing cracks as shown in Figure 3-18 until the test was concluded. The final state of the specimen towards the end of the test is shown in Figure 3-19.

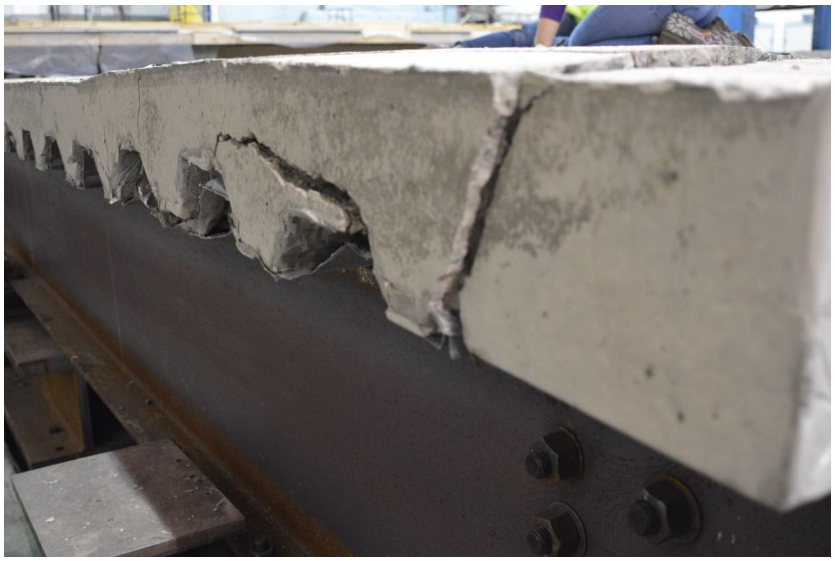

Figure 3-17. Deck Debonding and Overhang Cracking (Point D in Figure 3-13)

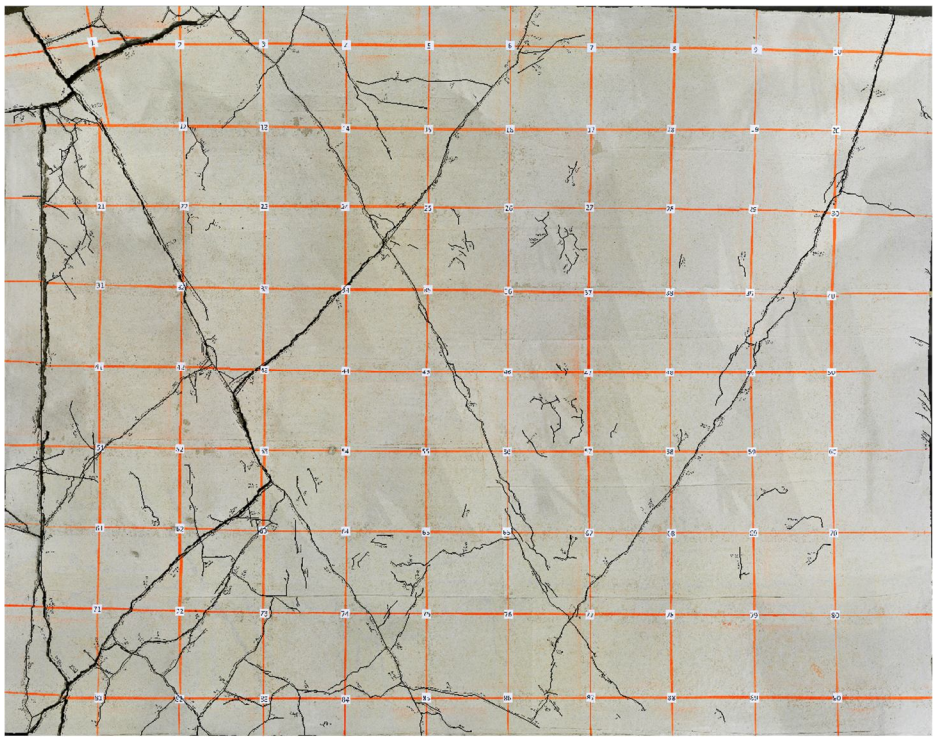

Figure 3-18. Crack Distribution of Specimen 3/7.5-4-N-NF-DT Further Cracking After Strength Decrease (Point E in Figure 3-13)

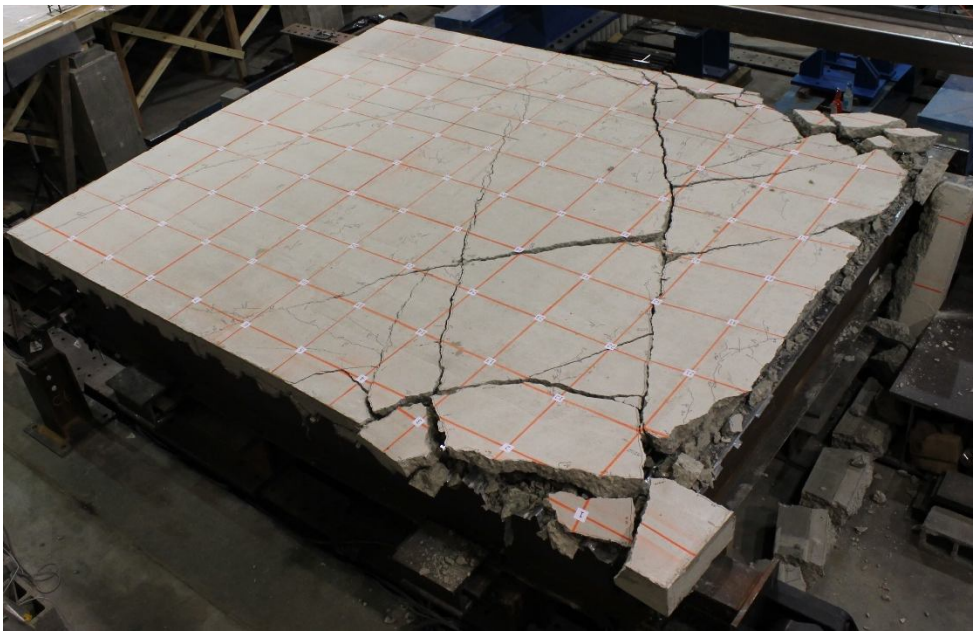

Figure 3-19. Specimen 3/7.5-4-N-NF-DT End of Test (Point F in Figure 3-13)

3.4 Specimen 2/4-4-L-NF-DT

The test specimen before and after concrete placement is shown in Figure 3-20. The deformation behavior of the specimen during early loading cycles used to calculate initial stiffness is shown in Figure 3-21.

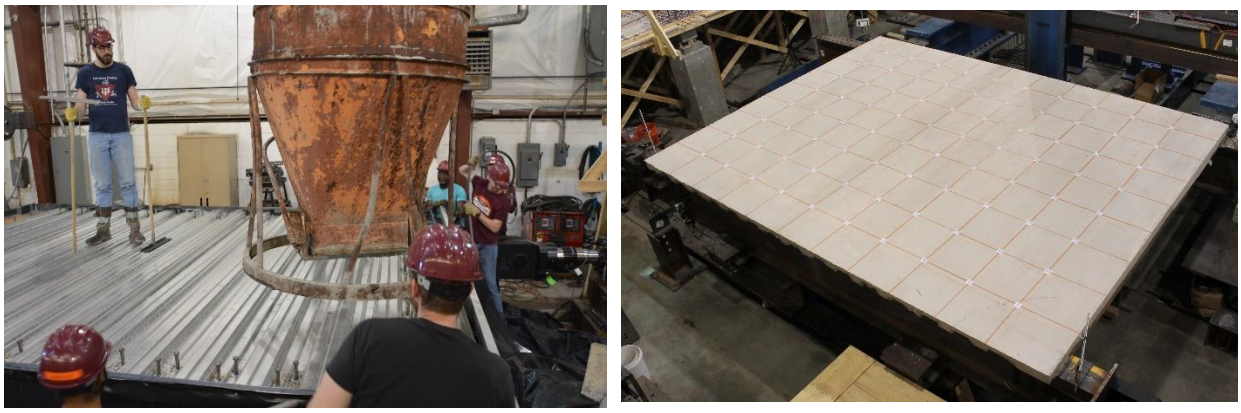

Figure 3-20. Specimen 2/4-4-L-NF-DT Before and After Concrete Placement

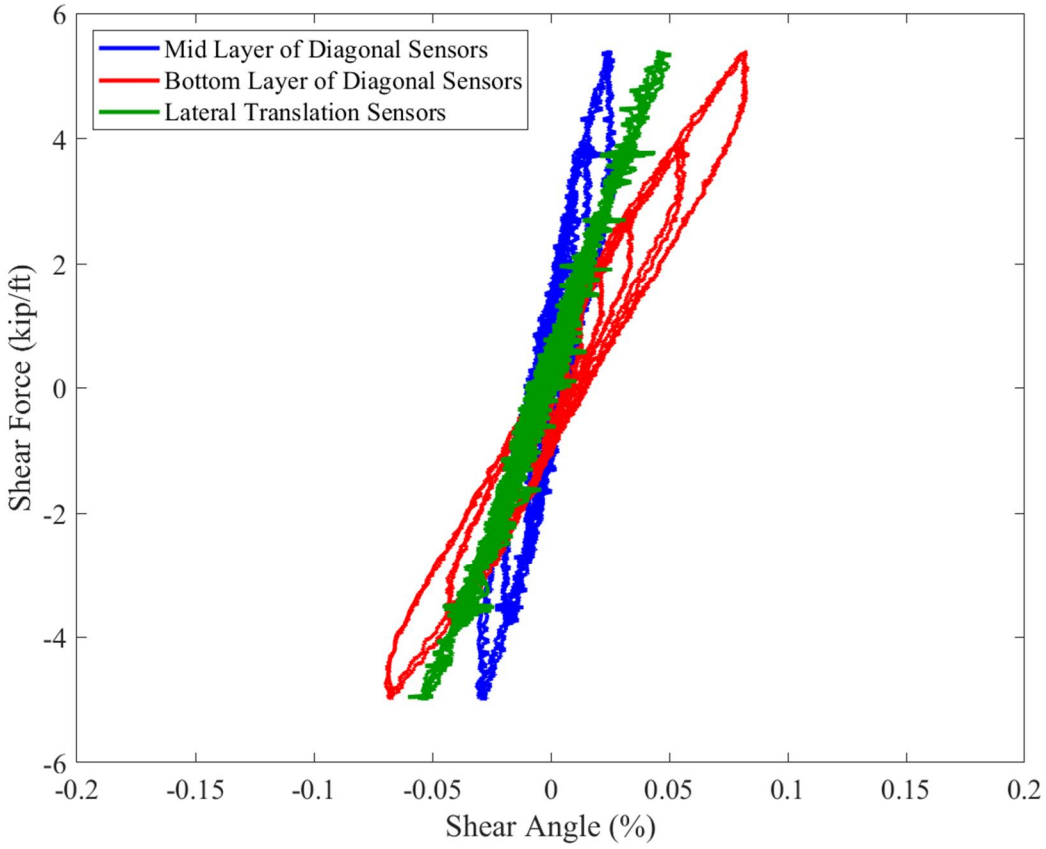

Figure 3-21. Comparison of Initial Load-Deformation Cycles Using Different Displacement Sensors for Specimen 2/4-4-L-NF-DT

A load deformation plot used to describe the progression of failure for this specimen is shown in Figure 3-22. The peak strength was 8.9 kip per foot of diaphragm, with a shear angle at peak strength of 0.0031 radians. The shear angle at 80% of peak strength was 0.0069 radians and the residual strength measured at 0.02 radians of 3.4 kips per foot of diaphragm. Before the test started (Figure 3-22 Point A), some shrinkage cracking was observed and marked on the specimen (Figure 3-23). Some additional cracking was observed at Point B in Figure 3-13 (See Figure 3-24) prior to peak load.

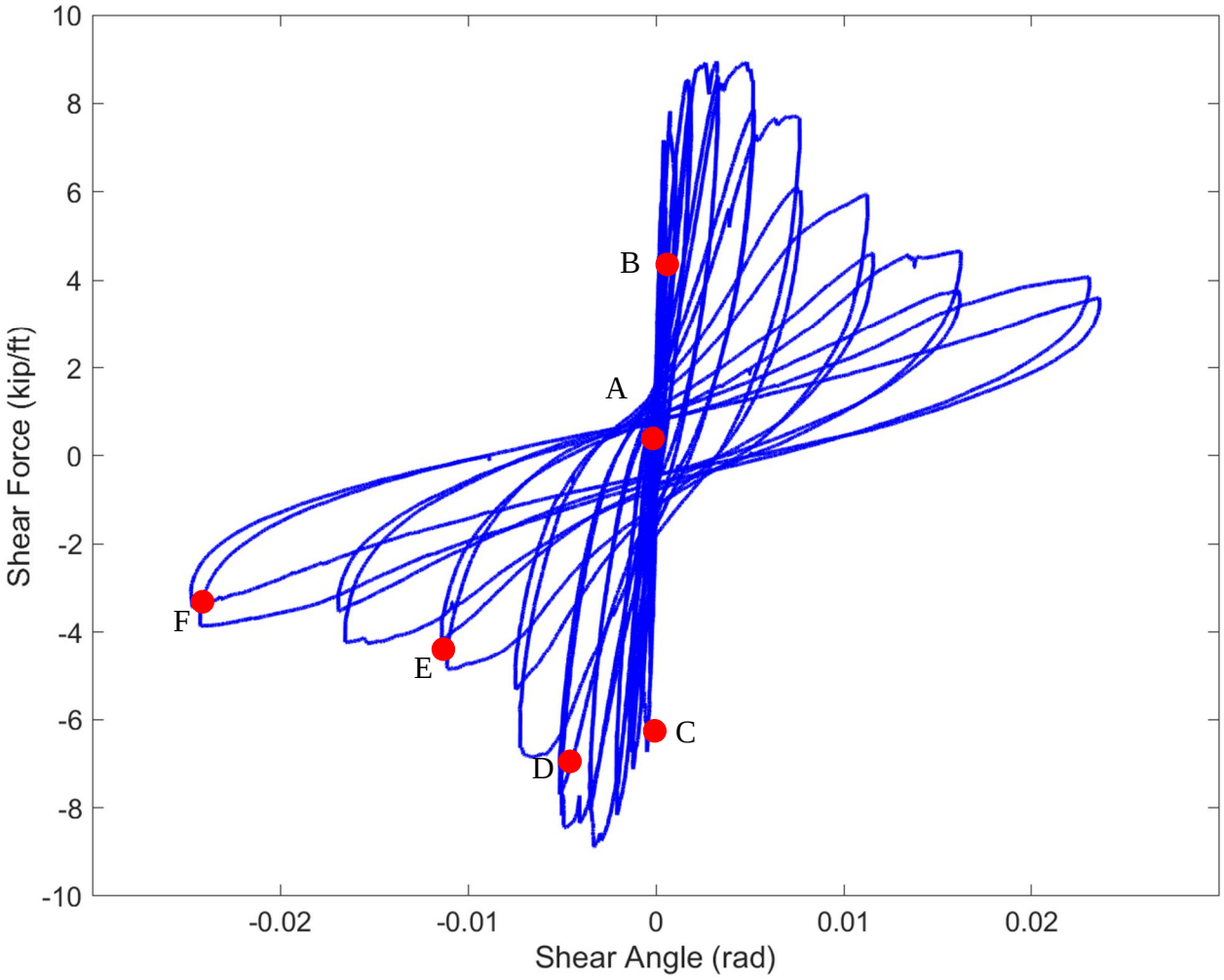

Figure 3-22. Load-Deformation Plot for Specimen 2/4-4-L-NF-DT

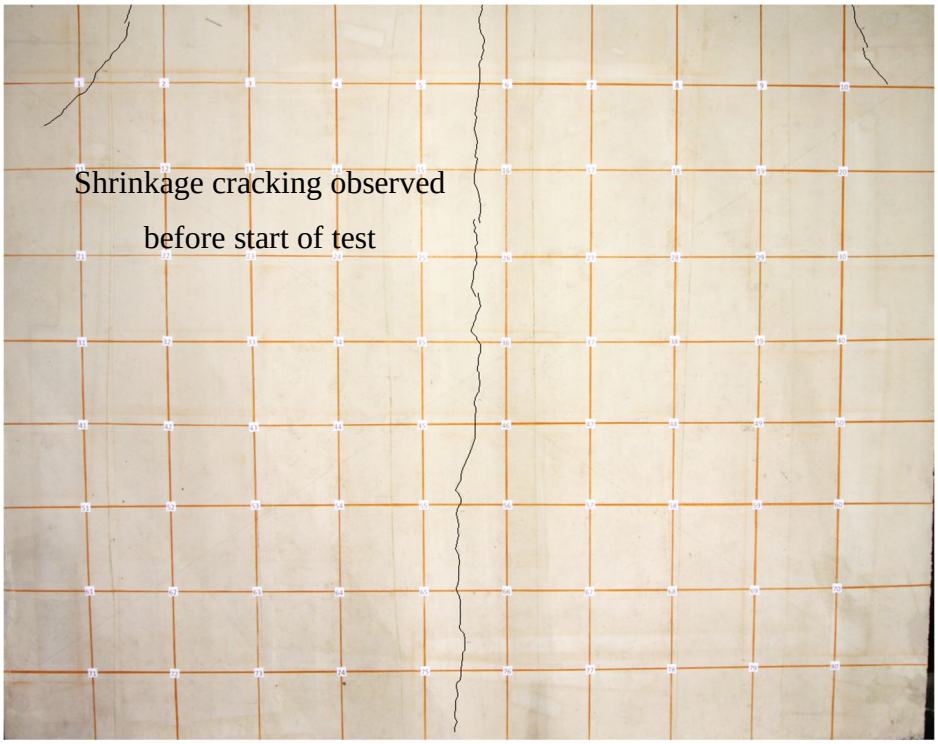

Figure 3-23. Crack Distribution of Specimen 2/4-4-L-NF-DT Before Testing (Point A in Figure 3-22)

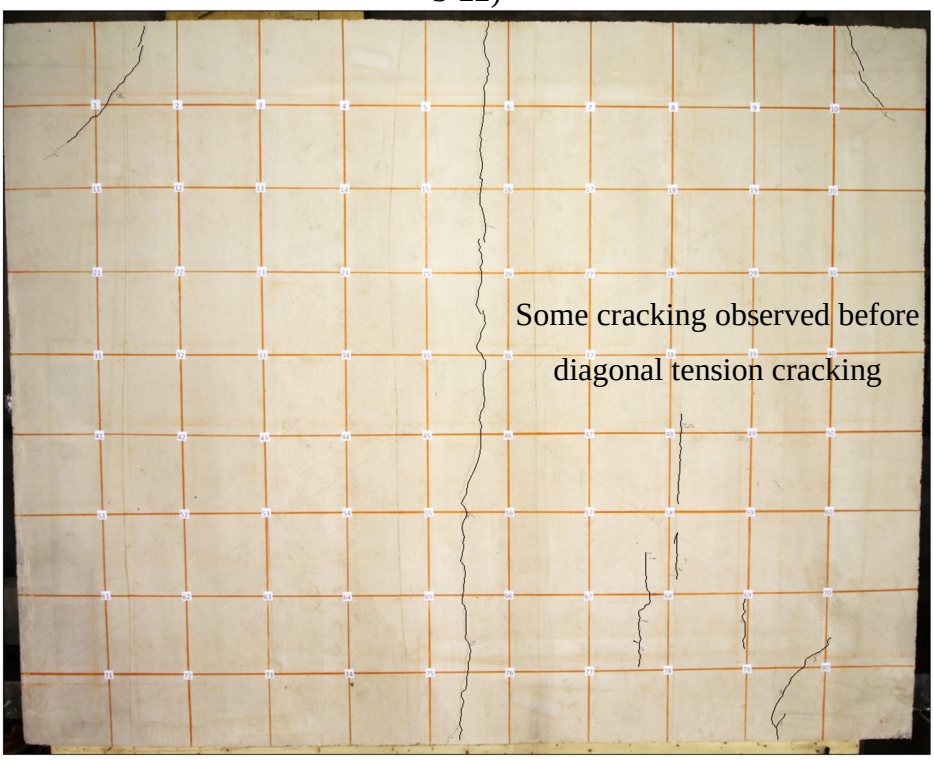

Figure 3-24. Crack Distribution of Specimen 2/4-4-L-NF-DT Before Diagonal Tension Cracking (Point B in Figure 3-22)

The first occurrence of diagonal tension cracking in both directions of loading was observed at Point C in Figure 3-22. This did not coincide with the peak load in both directions. Additional cracking formed at peak load the load-carrying capacity of the specimen dropped, as shown in Figure 3-26 which coincides with Point D in Figure 3-22.

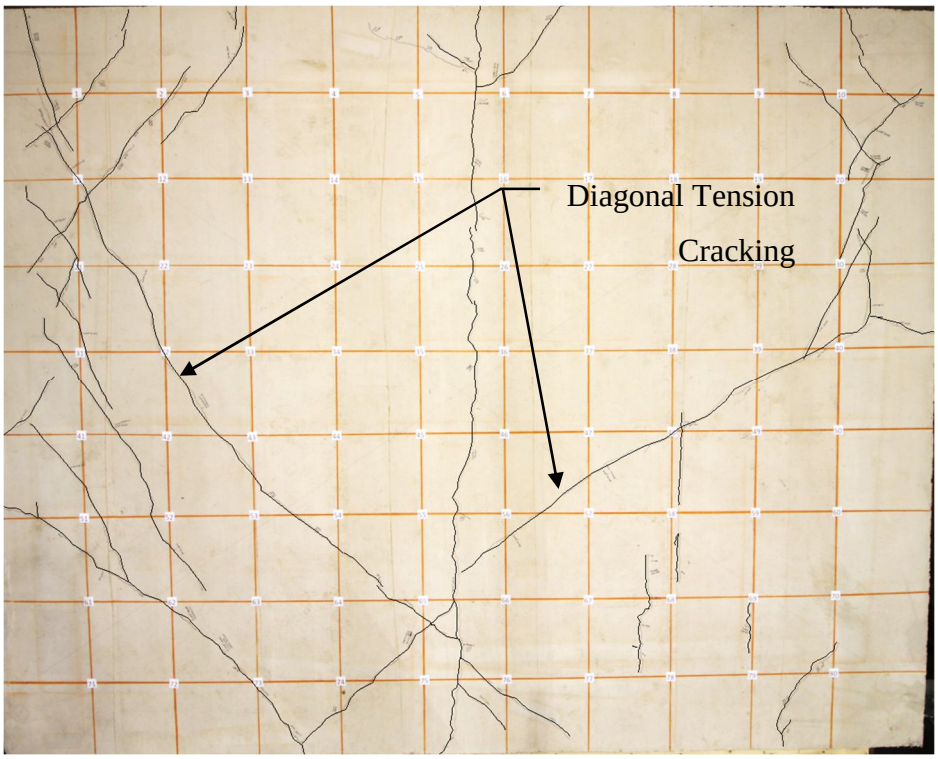

Figure 3-25. Crack Distribution of Specimen 2/4-4-L-NF-DT Diagonal Tension Cracking (Point C in Figure 3-22)

Distortions of the deck as well as cracking near the shear connectors was observed past this stage of the test, as shown in Figure 3-27. As shown in Figure 3-28, the damage of the specimen in the last cycles of the test concentrated along the left edge of the slab. The deck along this damage plane was seen to distort as loading continued, contributing largely to the deformation of the specimen during this stage.

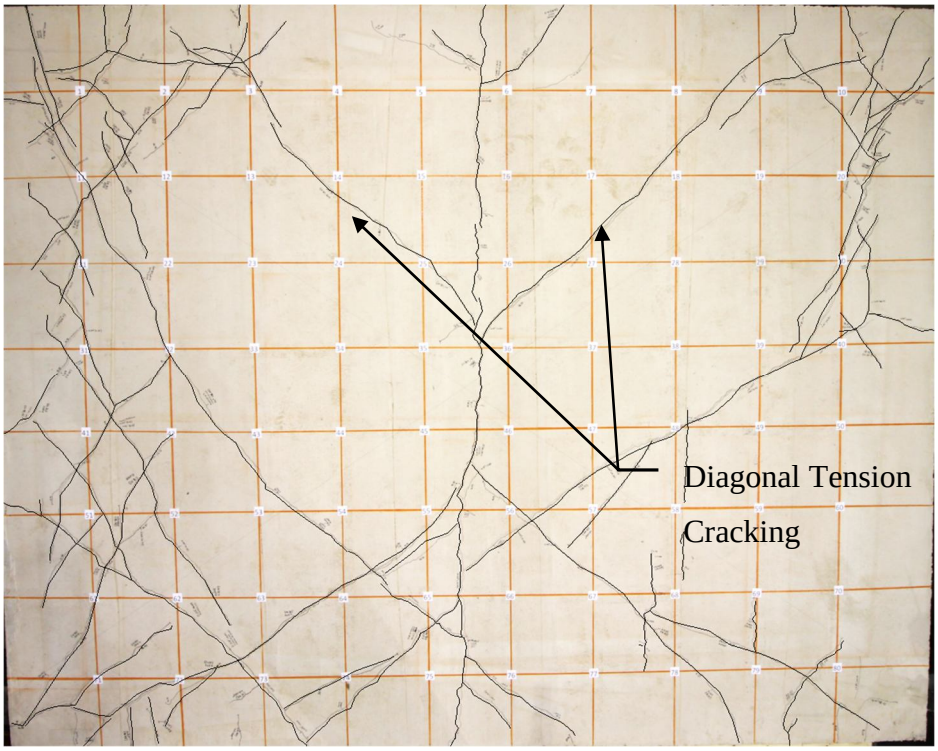

Figure 3-26. Crack Distribution of Specimen 2/4-4-L-NF-DT Further Cracking After Strength Decrease (Point D in Figure 3-22)

Figure 3-27. Deck Debonding and Overhang Cracking (Point E in Figure 3-22)

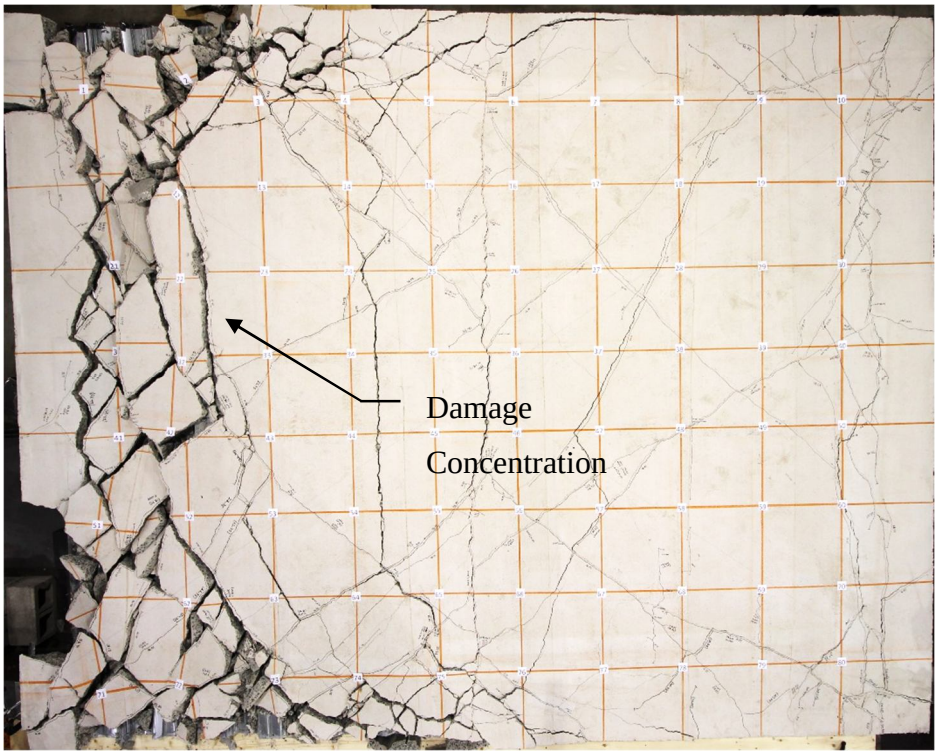

Figure 3-28. Specimen 2/4-4-L-NF-DT End of Test (Point F in Figure 3-22)

3.5 Specimen 3/6.25-4-L-NF-P

The test specimen before and after concrete placement is shown in Figure 3-29. The deformation behavior of the specimen during early loading cycles used to calculate initial stiffness is shown in Figure 3-30.

Figure 3-29. Specimen 3/6.25-4-L-NF-P Before and After Concrete Placement

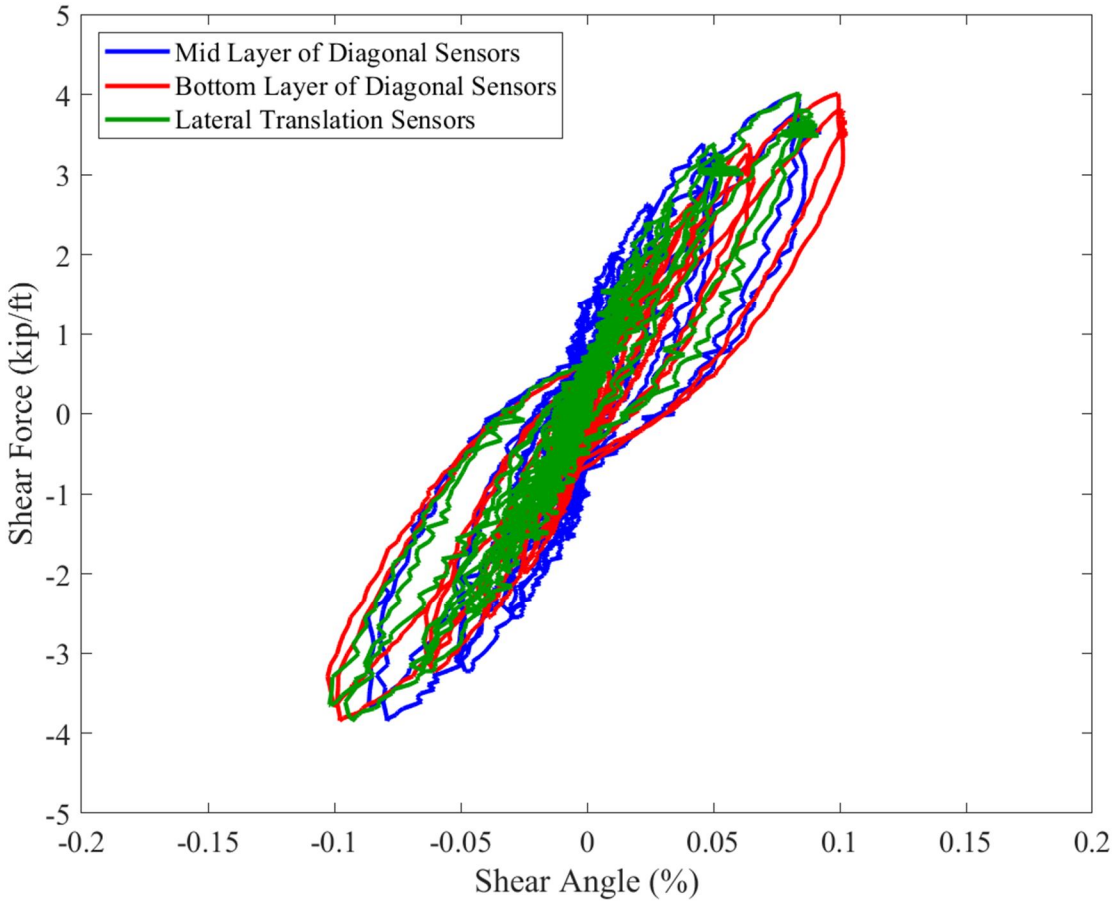

Figure 3-30. Comparison of Initial Load-Deformation Cycles Using Different Displacement Sensors for Specimen 3/6.25-4-L-NF-P

A load deformation plot used to describe the progression of failure for this specimen is shown in Figure 3-31. The peak strength was 4.0 kip per foot of diaphragm, with a shear angle at peak strength of 0.0011 radians. The shear angle at 80% of peak strength was 0.0069 radians and the residual strength measured at 0.02 radians of 3.4 kips per foot of diaphragm. Before the test started (Figure 3-31 Point A), the specimen was searched for existing cracks, but none were found (Figure 3-32). The approximate location of the headed studs is also shown in Figure 3-32.

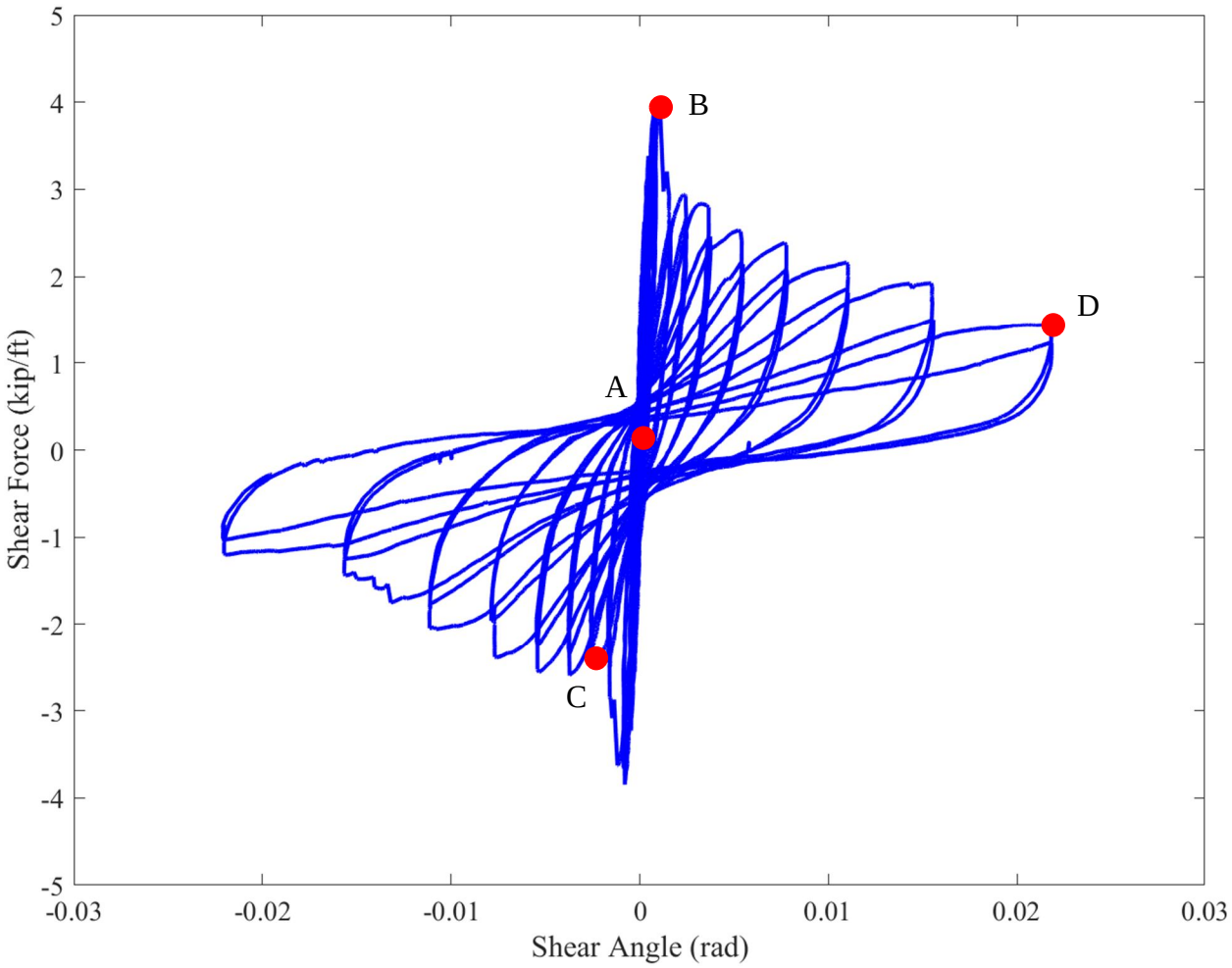

Figure 3-31. Load-Deformation Plot for Specimen 3/6.25-4-L-NF-P

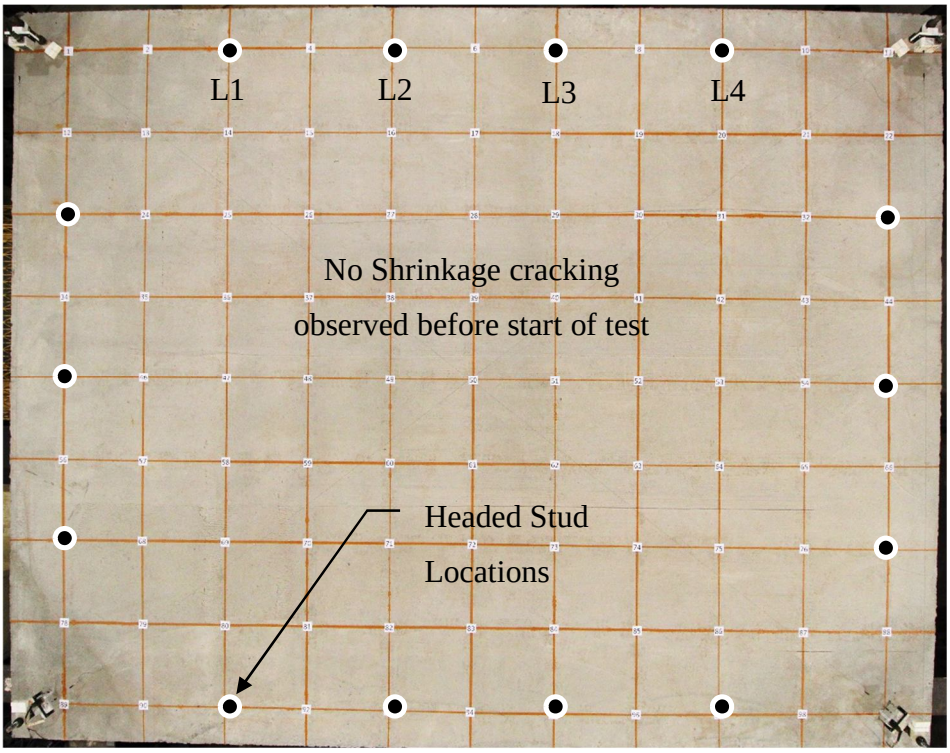

Figure 3-32. Crack Distribution of Specimen 3/6.25-4-L-NF-P Before Testing (Point A in Figure 3-31)

At peak load (Figure 3-31 Point B), cracks formed on the slab between the location of two studs. Strain gauge data showed a drop in the difference in axial strains of the beam on either side of L3 at peak load, which indicates failure of the shear connection. This is supported by strain gauge observations for later cycles which show constant axial strains in the beam segment between L2 and L4 at subsequent peaks. As shown in Figure 3-34, at peak load, evidence of shear transfer failure can be observed on the edges of the specimen.

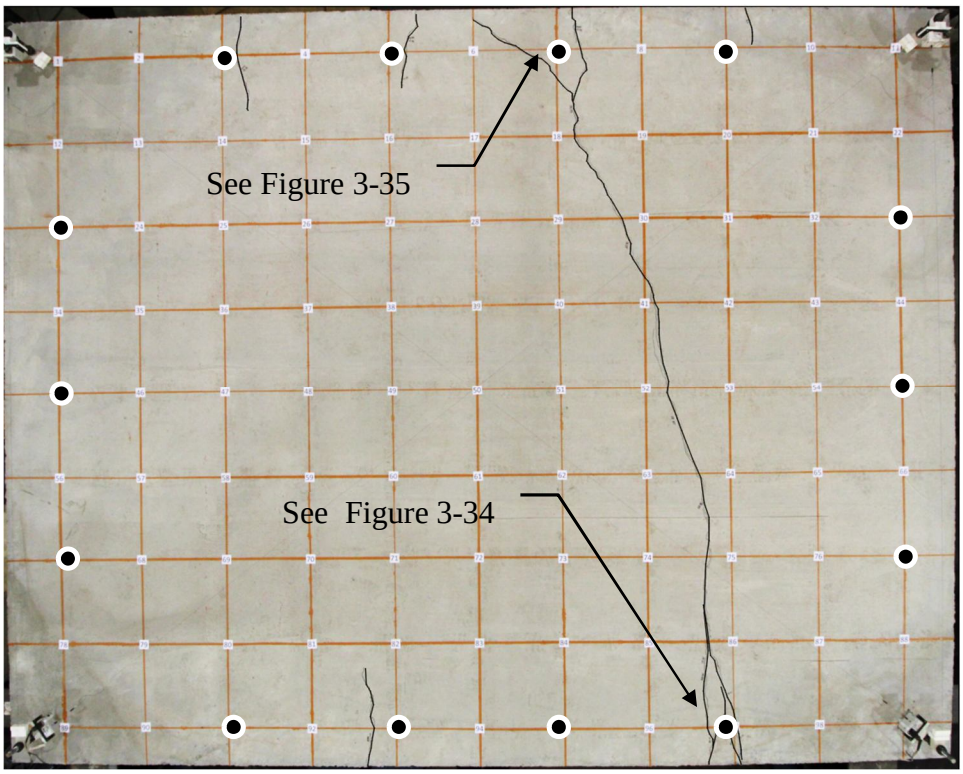

Figure 3-33. Crack Distribution of Specimen 3/6.25-4-L-NF-P at Peak Load (Point B in Figure 3-31)

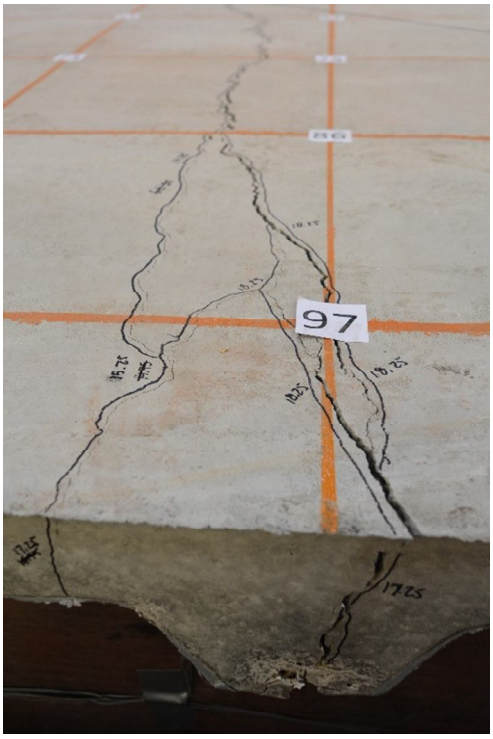

Figure 3-34. Shear Transfer Damage at Peak Load

Figure 3-35. Shear Transfer Damage at Peak Load

Further cracking of the specimen was observed at Point C in Figure 3-31, as shown in Figure 3-36. Evidence of rib shear was found on all the ribs of both the loading beam and the fixed beam by the time the test ended, as shown in Figure 3-37. The state of the specimen after the test was concluded is shown in Figure 3-38. The shear transfer failure was confirmed after the test as evidence by failure surfaces such as the one shown in Figure 3-39.

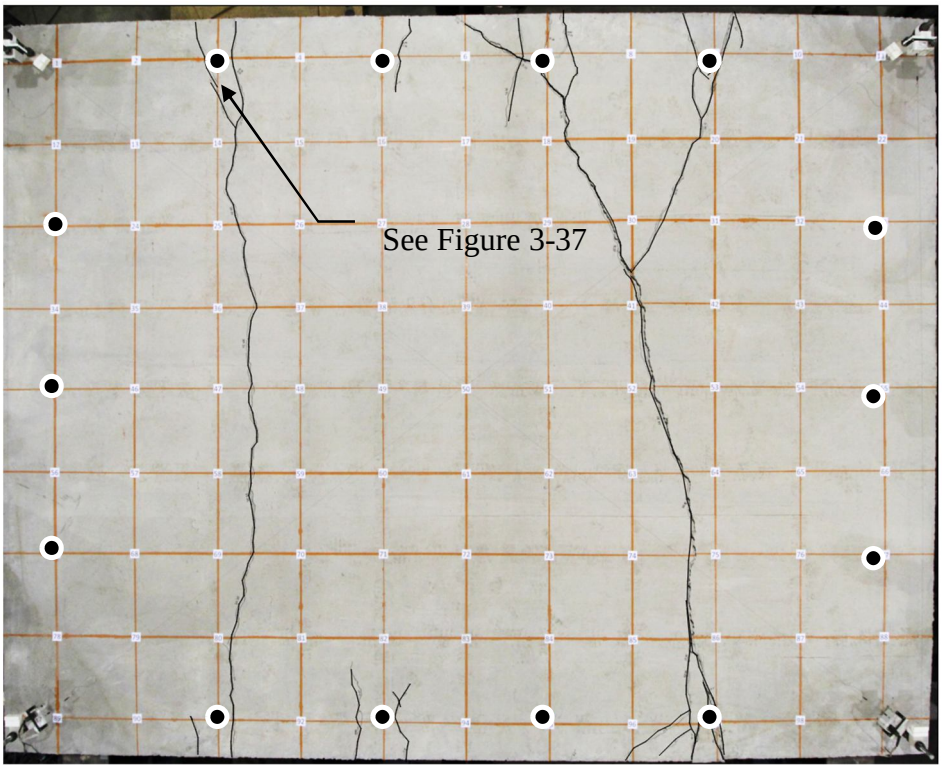

Figure 3-36. Crack Distribution of Specimen 3/6.25-4-L-NF-P (Point C in Figure 3-22)

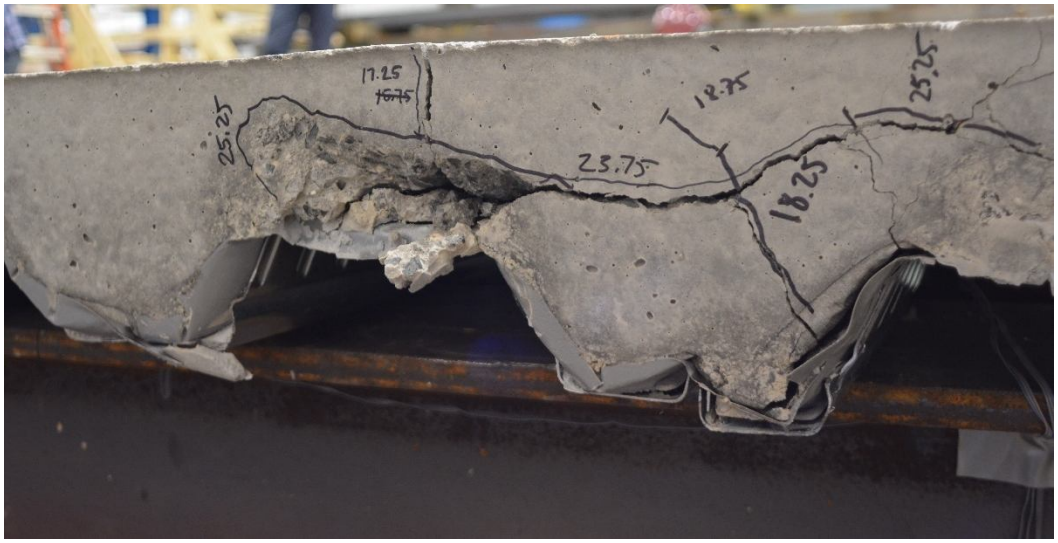

Figure 3-37. Evidence of Rib Shear Failure

Figure 3-38. Crack Distribution of Specimen 3/6.25-4-L-NF-P End of Test (Point E in Figure 3-22)

Figure 3-39. Evidence of Concrete Pullout Failure After Test

3.6 Specimen 2/4.5-4-N-RS-DT

The test specimen before and after concrete placement is shown in Figure 3-40. The deformation behavior of the specimen during early loading cycles used to calculate initial stiffness is shown in Figure 3-41.

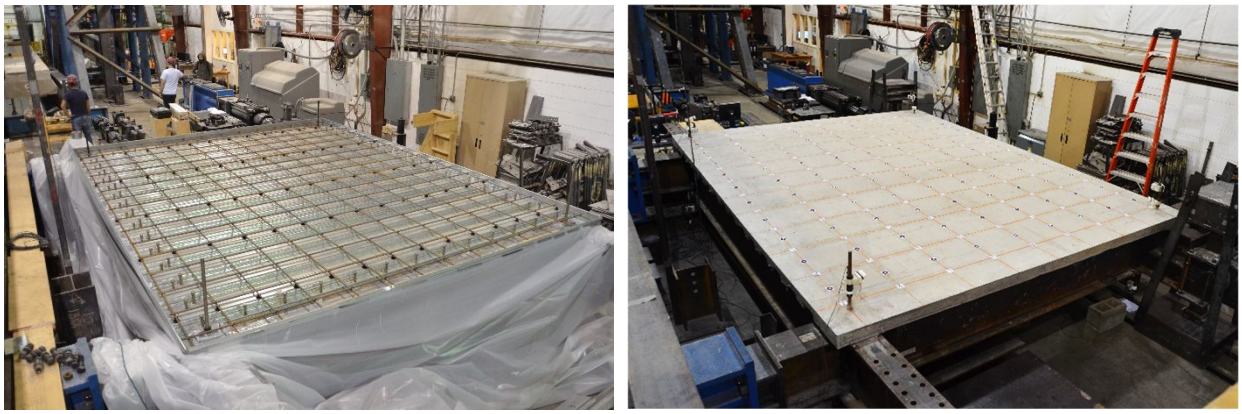

Figure 3-40. Specimen 2/4.5-4-N-RS-DT Before and After Concrete Placement

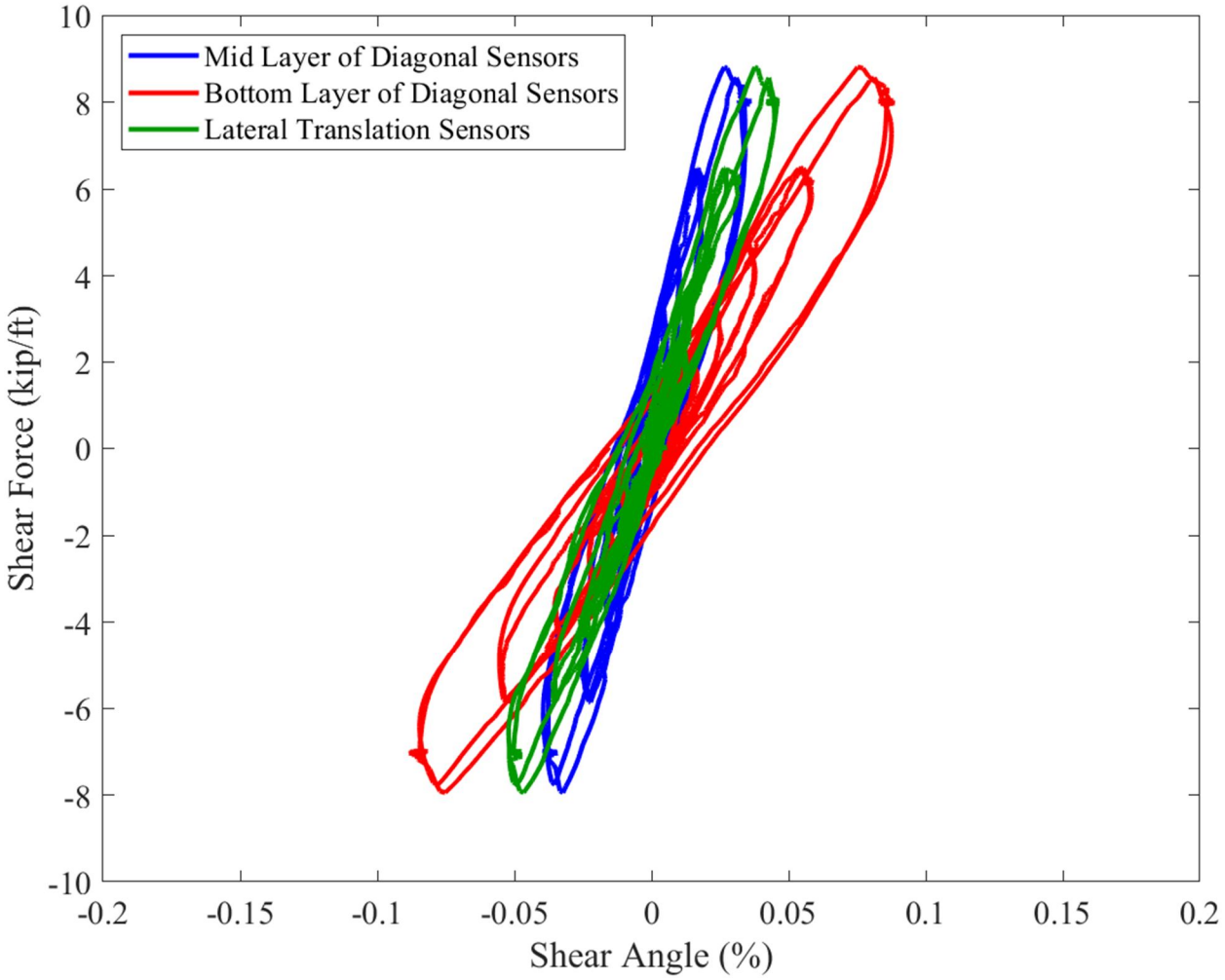

Figure 3-41. Comparison of Initial Load-Deformation Cycles Using Different Displacement Sensors for Specimen 2/4.5-4-N-RS-DT

A load deformation plot used to describe the progression of failure for this specimen is shown in Figure 3-42. The peak strength was 17.6 kip per foot of diaphragm, with a shear angle at peak strength of 0.0041 radians. The shear angle at 80% of peak strength was 0.0059 radians and the residual strength measured at 0.02 radians of 3.2 kips per foot of diaphragm. Before the test started (Figure 3-42 Point A), the specimen was searched for existing cracks, but none were found (Figure 3-43). The first occurrence of diagonal tension cracking in both directions of loading was observed at Point B in Figure 3-42. This did not coincide with the peak load in both directions but it did coincide with a change in slope of the load-deformation plot between Points B and D of Figure 3-42.

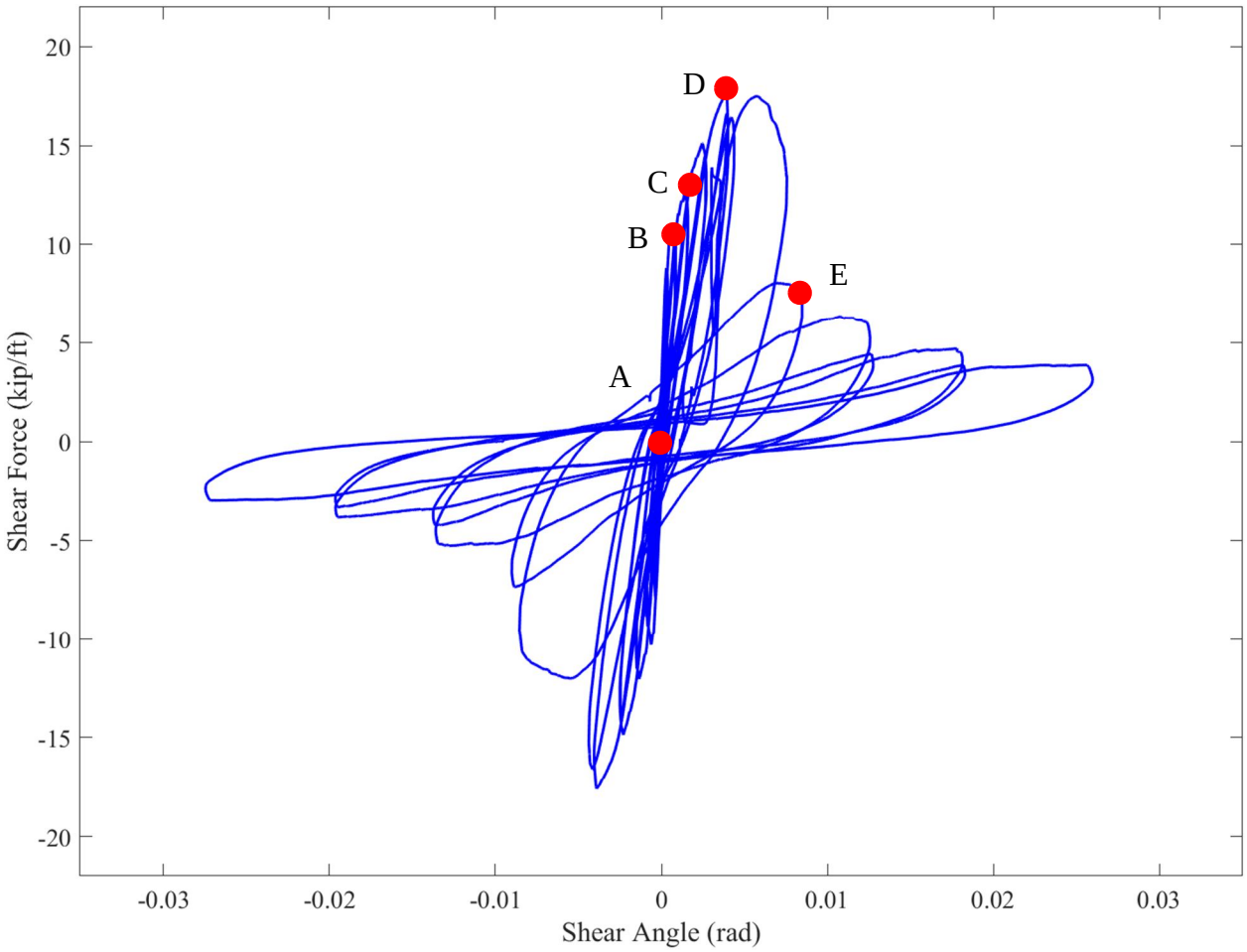

Figure 3-42. Load-Deformation Plot for Specimen 2/4.5-4-N-RS-DT

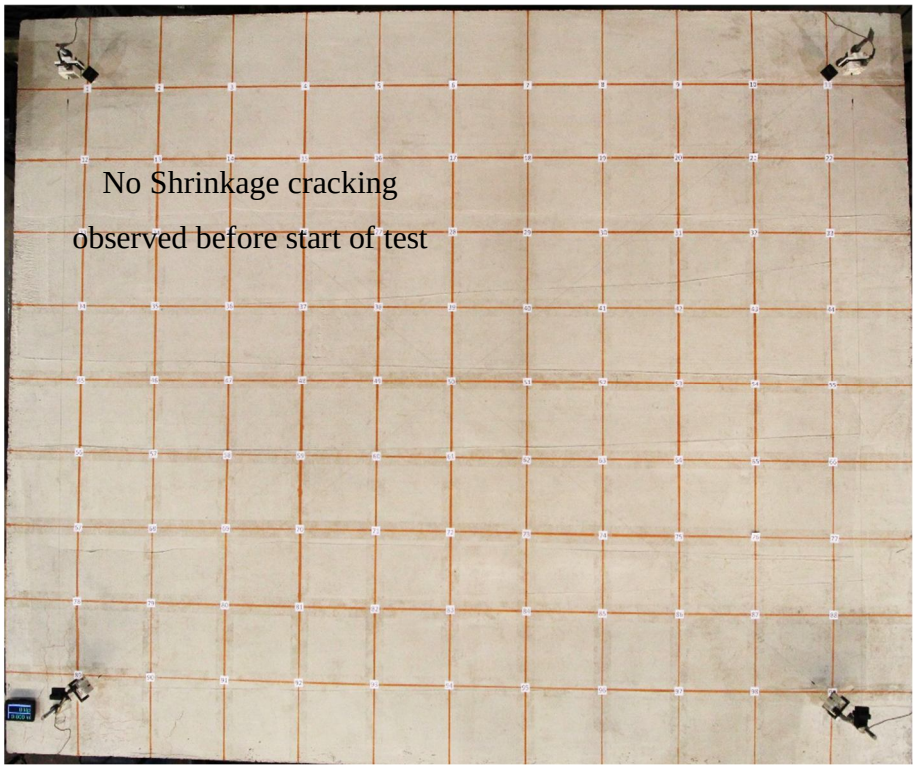

Figure 3-43. Crack Distribution of Specimen 2/4.5-4-N-RS-DT Before Testing (Point A in Figure 3-42)

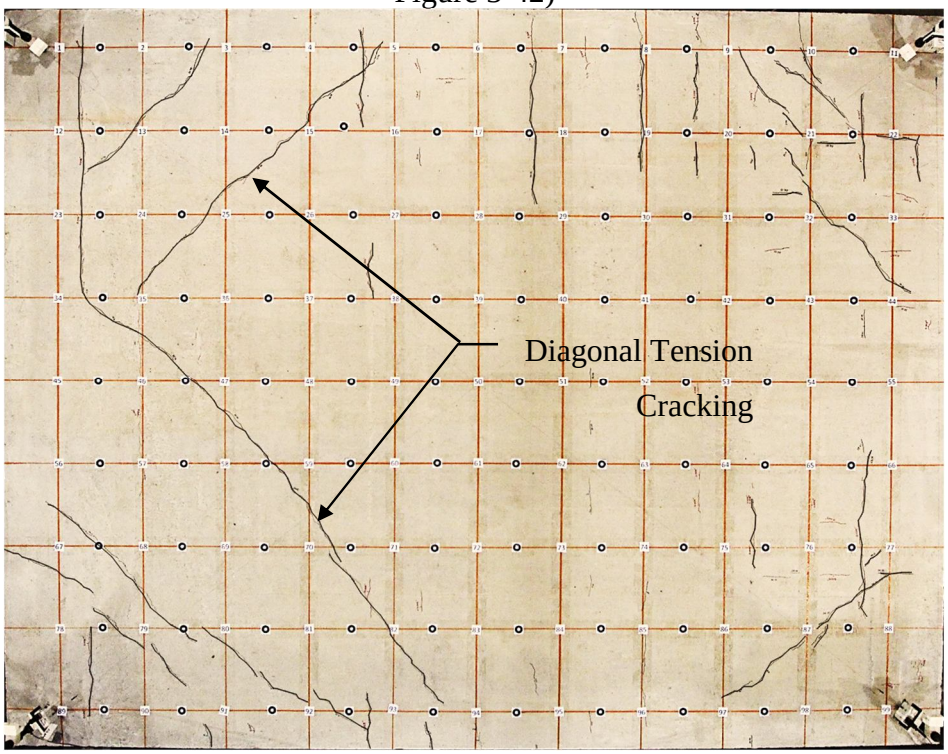

Figure 3-44. Crack Distribution of Specimen 2/4.5-4-N-RS-DT First Occurrence of Diagonal Tension Cracking (Point B in Figure 3-42)

At Point C of Figure 3-42, additional diagonal tension cracks appeared on the specimen, extending nearly across the full width of the specimen, as shown in Figure 3-45.

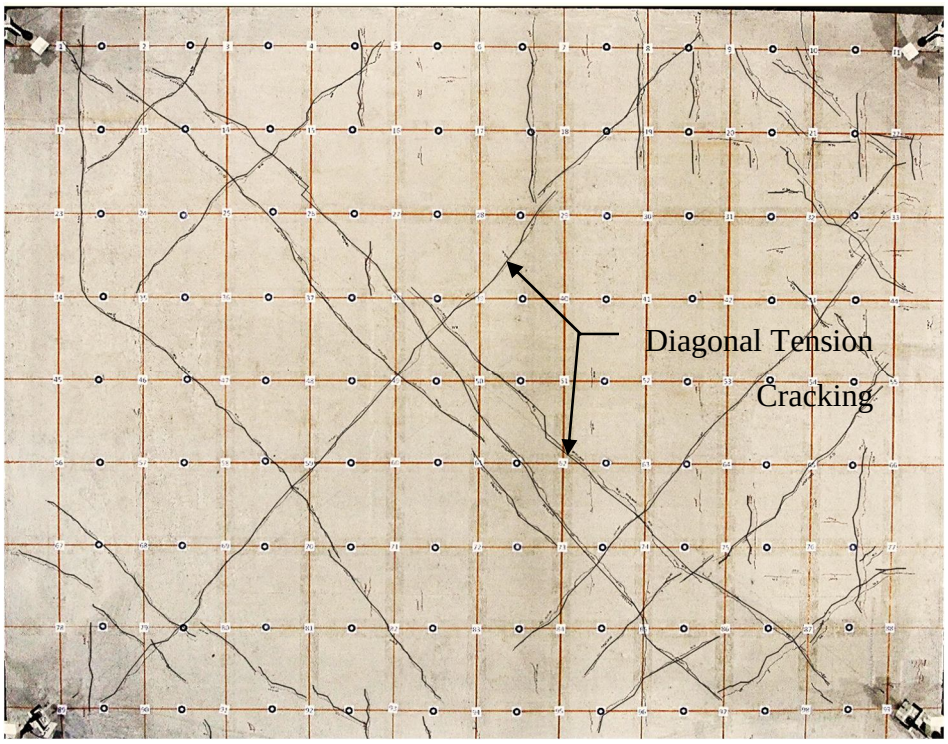

Figure 3-45. Crack Distribution of Specimen 2/4.5-4-N-RS-DT Further Diagonal Tension Cracking (Point C in Figure 3-42)

More cracks appeared on the specimen as the load continued to increase until reaching Point D of Figure 3-42. At this point, the cracking pattern exhibited by the specimen up until this point was extensive as shown in Figure 3-46. The load-carrying capacity of the specimen dropped as the test continued and damage was observed on the edge of the slab closest to the loading beam, that indicated a failure of the perimeter fasteners, as shown from above in Figure 3-47 and on the ribs of the specimen as shown in Figure 3-48.

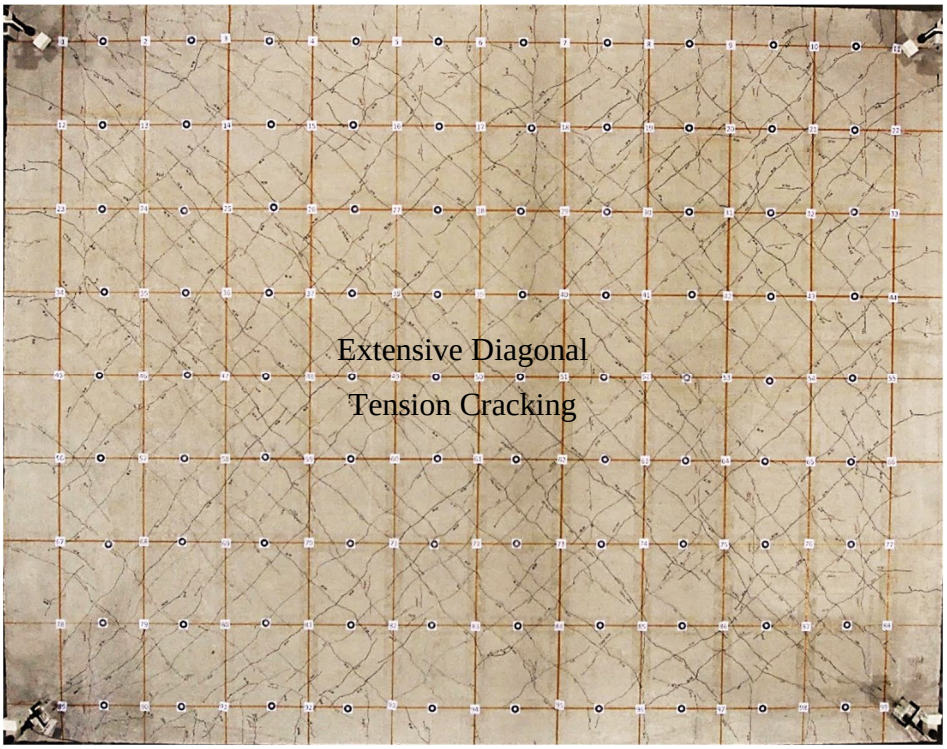

Figure 3-46. Crack Distribution of Specimen 2/4.5-4-N-RS-DT Extensive Cracking Near Peak Load (Point D in Figure 3-42)

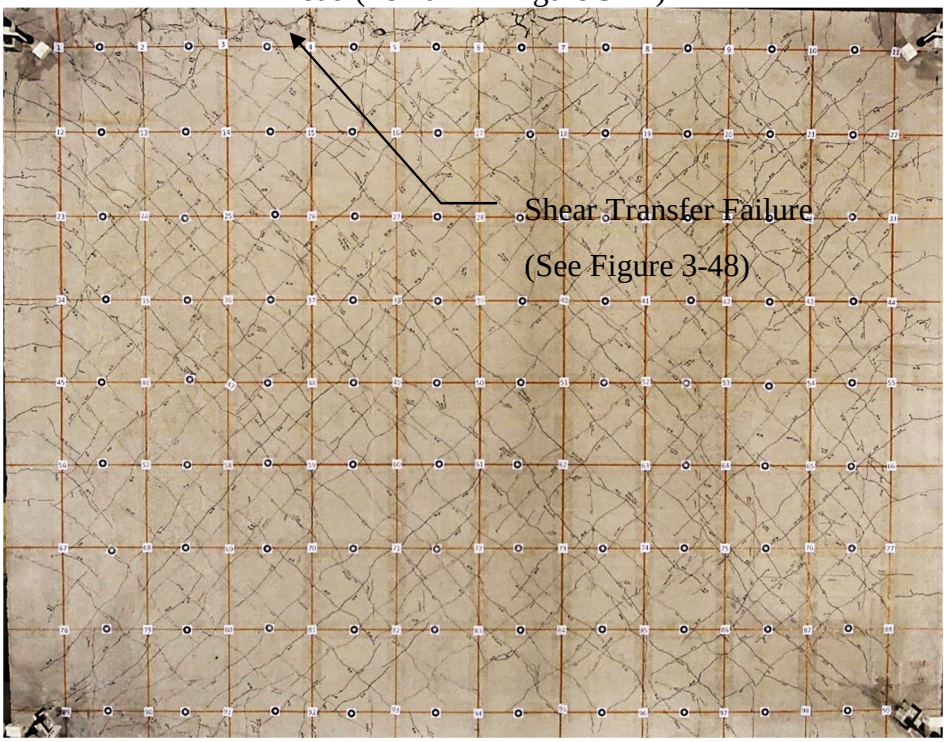

Figure 3-47. Crack Distribution of Specimen 2/4.5-4-N-RS-DT: Perimeter Fastener Failure (Point E in Figure 3-42)

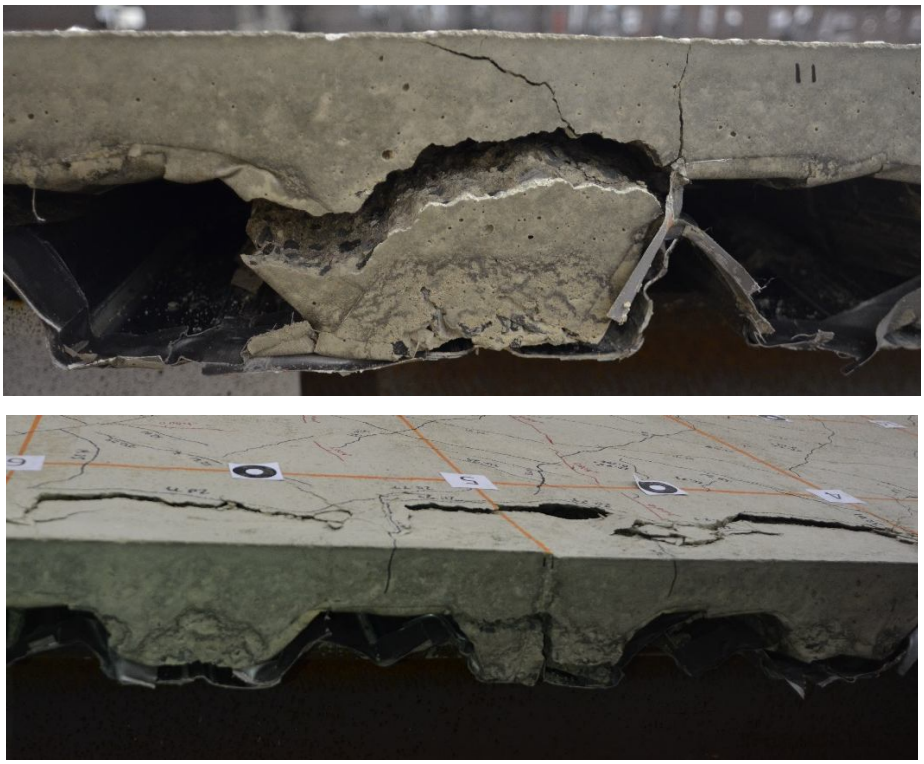

Figure 3-48. Rib Shear Failure of Perimeter Shear Transfer

3.7 Specimen 3/7.5-4-N-NF-P

The test specimen before and after concrete placement is shown in Figure 3-49. A load deformation plot used to describe the progression of failure for this specimen is shown in Figure 3-50. A plot comparing the initial stiffness of the specimen using different sets of sensors is not presented for this specimen since the data acquisition malfunctioned during the test, resulting in the loss of data for the sensors used to obtain the load-deformation behavior. Shear angle for this specimen was calculated using the corrected displacement data obtained from the actuator, as described in Appendix A.

The peak strength was 5.6 kip per foot of diaphragm, with a shear angle at peak strength of 0.0037 radians. The shear angle at 80% of peak strength was 0.0039 radians and the residual strength measured at 0.02 radians of 0.9 kips per foot of diaphragm. Before the test started (Figure 3-50 Point A), the specimen was searched for existing cracks, but none were found (Figure 3-51). The approximate location of the headed studs is also shown in Figure 3-51.

Figure 3-49. Specimen 3/7.5-4-N-NF-P Before and After Concrete Placement

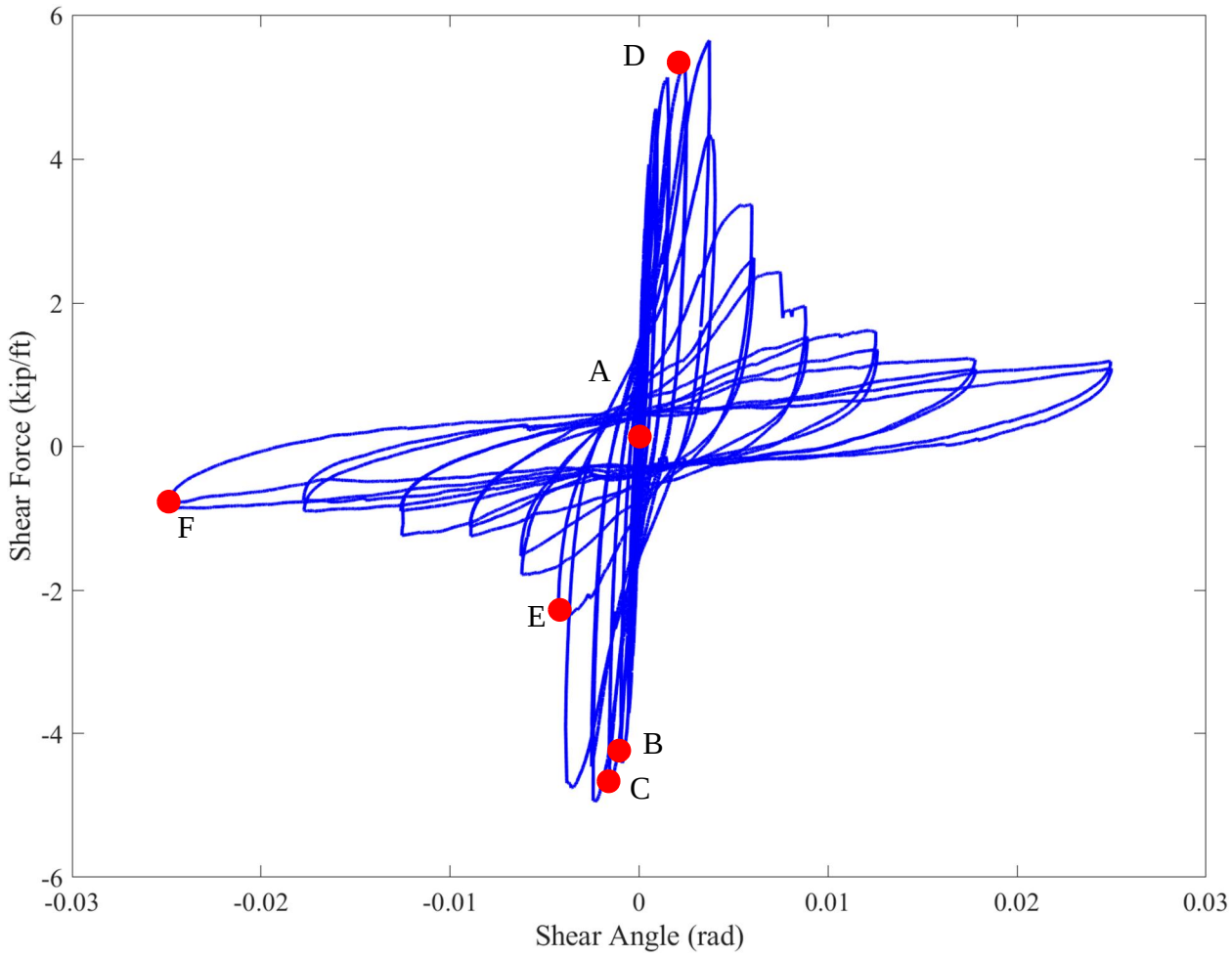

Figure 3-50. Load-Deformation Plot for Specimen 3/7.5-4-N-NF-P (Shear Angle Calculated by Modifying Shear Angle Obtained from Actuator Data as described in Appendix A)

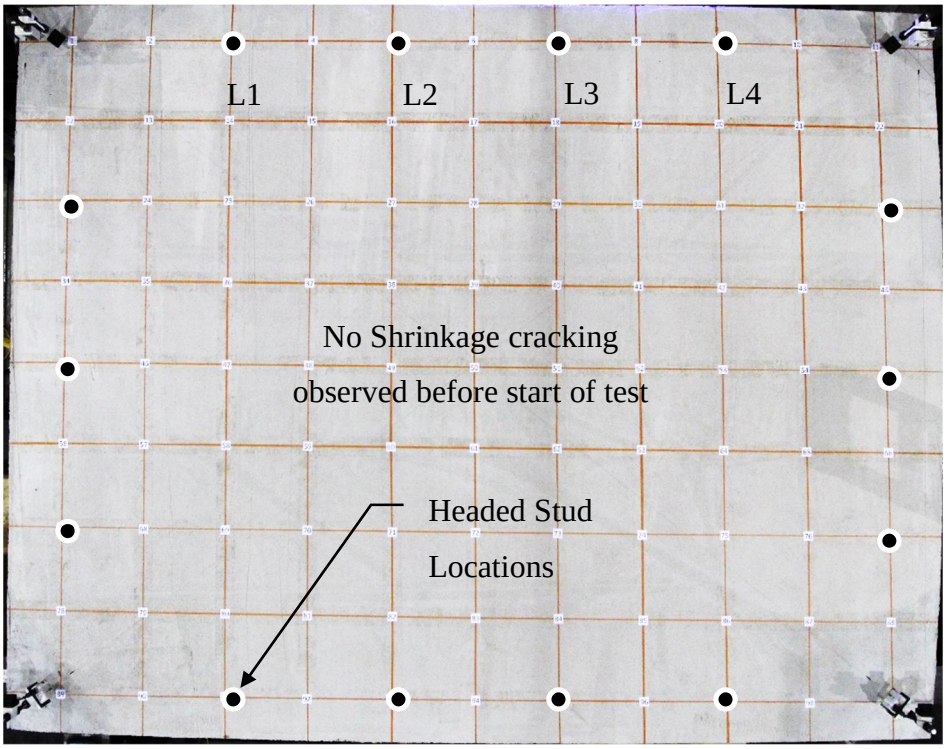

Figure 3-51. Crack Distribution of Specimen 3/7.5-4-N-NF-P Before Testing (Point A in Figure 3-50)

At peak load (Figure 3-50 Point B), evidence of shear transfer failure was observed on the rib in which stud L1 was located, as shown in Figure 3-52. At Point C of Figure 3-50, additional damage appeared on the same rib consistent with rib shear failure, as shown in Figure 3-53. At Point D of Figure 3-50, damage consistent with a concrete pullout failure mode appeared on the ribs in which stud L3 and L4 were located, as shown in Figure 3-54. At Point E in Figure 3-50, all four ribs of the loading beam containing studs exhibited some amount of damage consisting with a shear transfer failure, similar to that seen in Figure 3-55. Past this point in the test, the deck deformed and the damage of the ribs became more extensive, as shown in Figure 3-56.

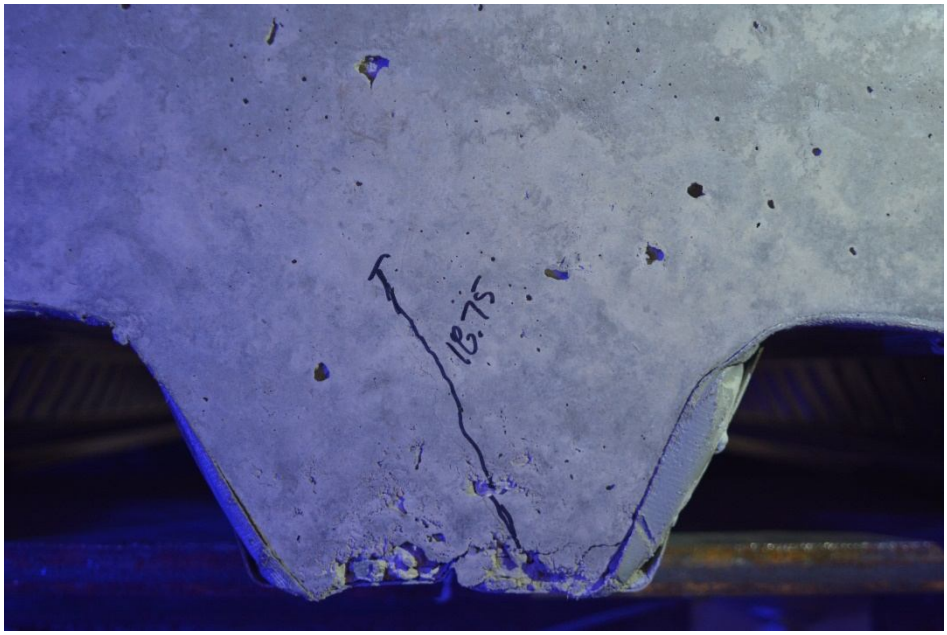

Figure 3-52. First Appearance of Cracks Along Shear Connection (Stud L1) in Specimen 3/7.5-4-N-NF-P (Point B in Figure 3-50)

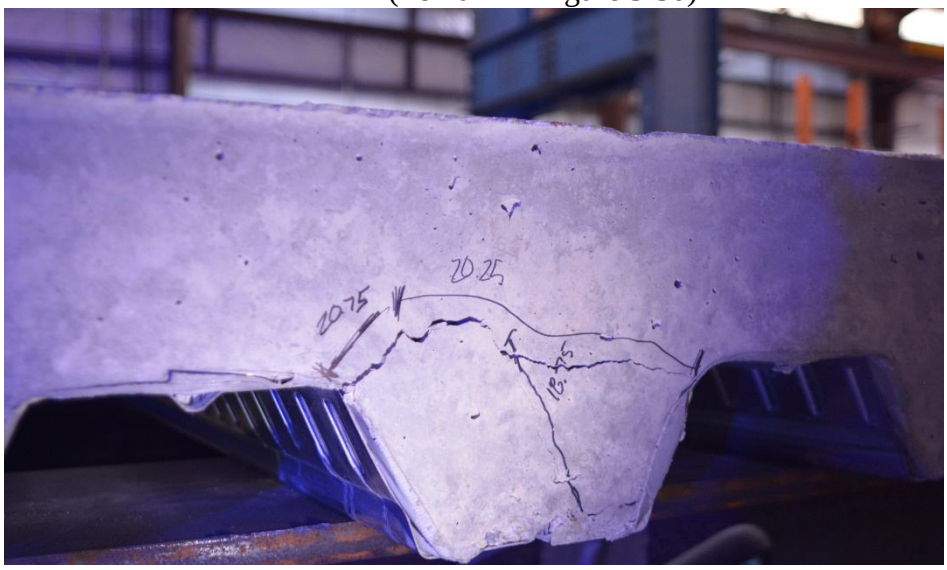

Figure 3-53. Rib Shear Cracks Along Shear Connection (Stud L1) in Specimen 3/7.5-4-N-NF-P (Point C in Figure 3-50)

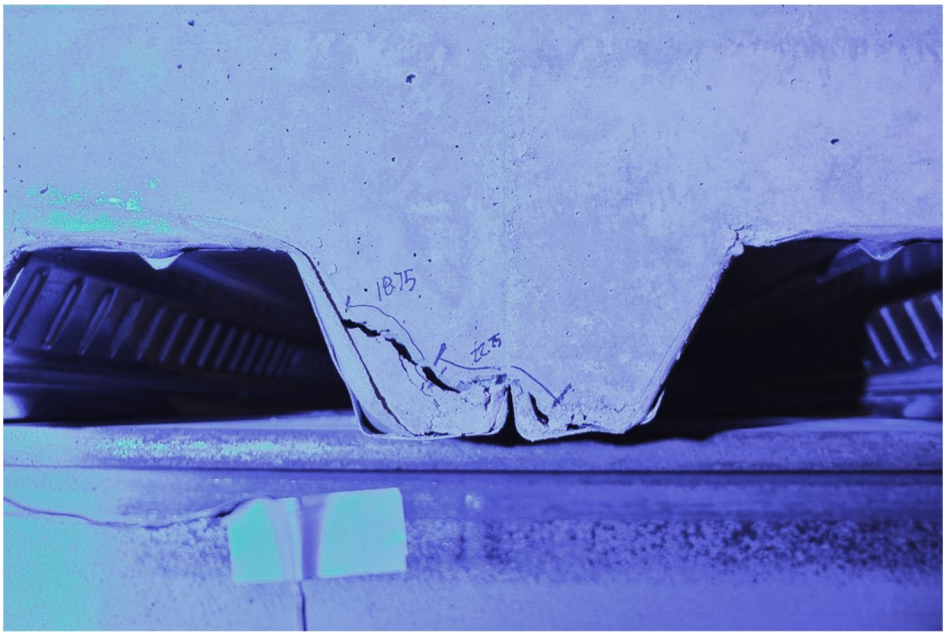

Figure 3-54. Concrete Pullout Cracks Along Shear Connection (Stud L3) of Specimen 3/7.5-4-N-NF-P (Point D in Figure 3-50)

Figure 3-55. Rib Shear Cracks Along Shear Connection (Stud L1) Specimen 3/7.5-4-N-NF-P (Point E in Figure 3-50)

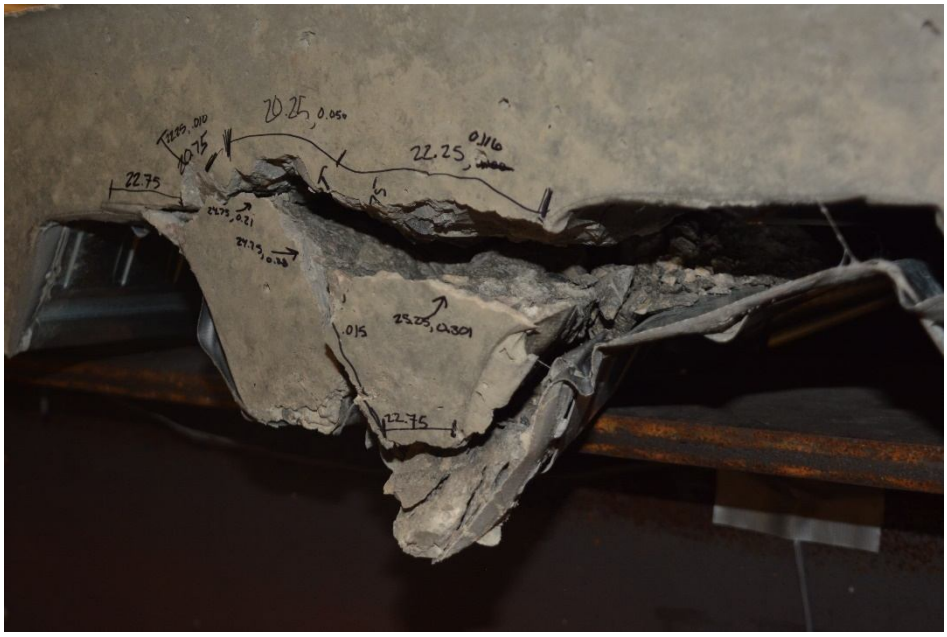

Figure 3-56. Damage at End of Test (Stud L1) Specimen 3/7.5-4-N-NF-P (Point F in Figure 3-50)

3.8 Specimen 3/6.25-4-L-RS-DT

The test specimen before and after concrete placement is shown in Figure 3-57. The deformation behavior of the specimen during early loading cycles used to calculate initial stiffness is shown in Figure 3-58.

Figure 3-57. Specimen 3/6.25-4-L-RS-DT Before and After Concrete Placement

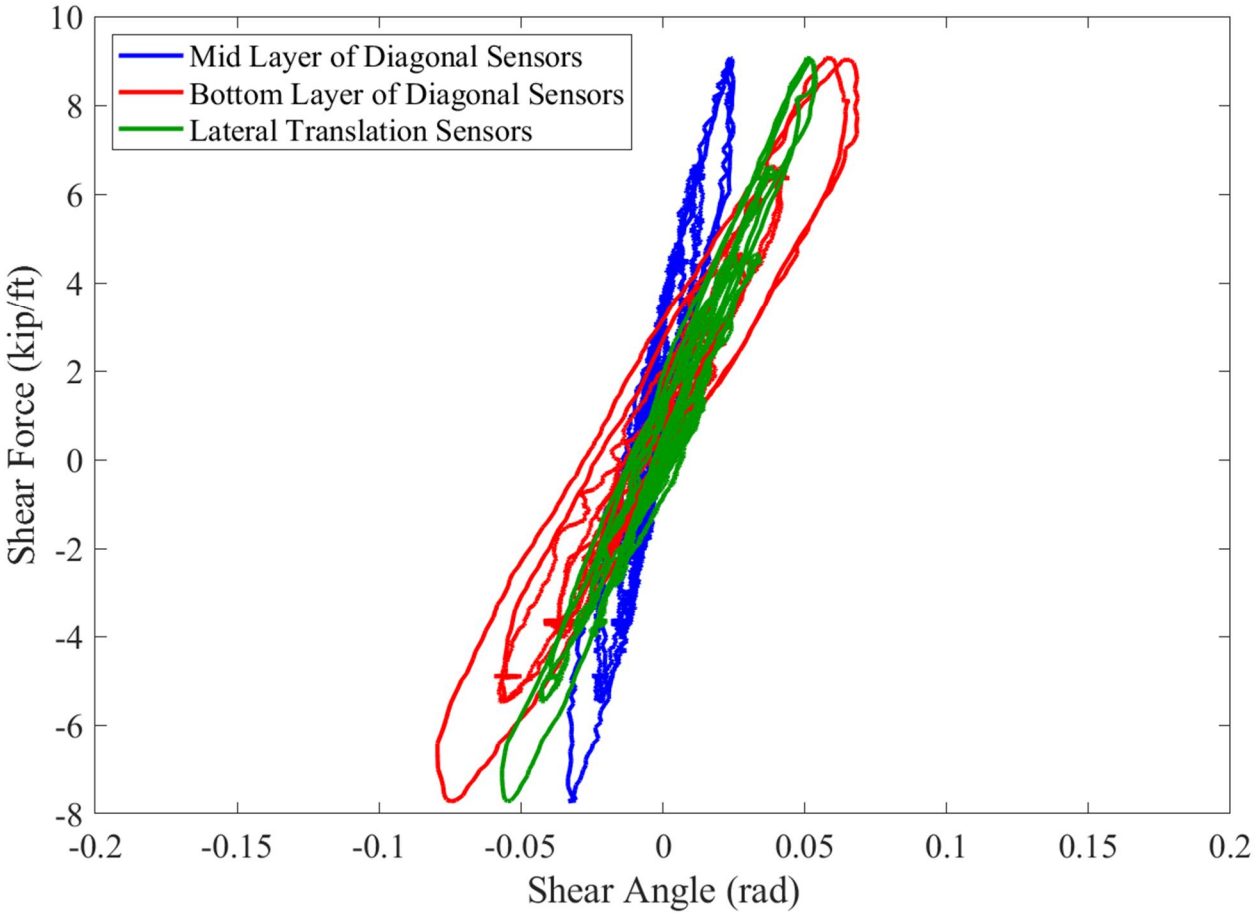

Figure 3-58. Comparison of Initial Load-Deformation Cycles Using Different Displacement Sensors for Specimen 3/6.25-4-L-RS-DT

A load deformation plot used to describe the progression of failure for this specimen is shown in Figure 3-59. The peak strength was 13.3 kip per foot of diaphragm, with a shear angle at peak strength of 0.0024 radians. The shear angle at 80% of peak strength was 0.0055 radians and the residual strength measured at 0.02 radians of 4.2 kips per foot of diaphragm. Before the test started (Figure 3-59 Point A), the specimen was searched for existing cracks, but none were found (Figure 3-60). The first occurrence of diagonal tension cracking in both directions of loading was observed at Point B in Figure 3-59, as shown in Figure 3-61.

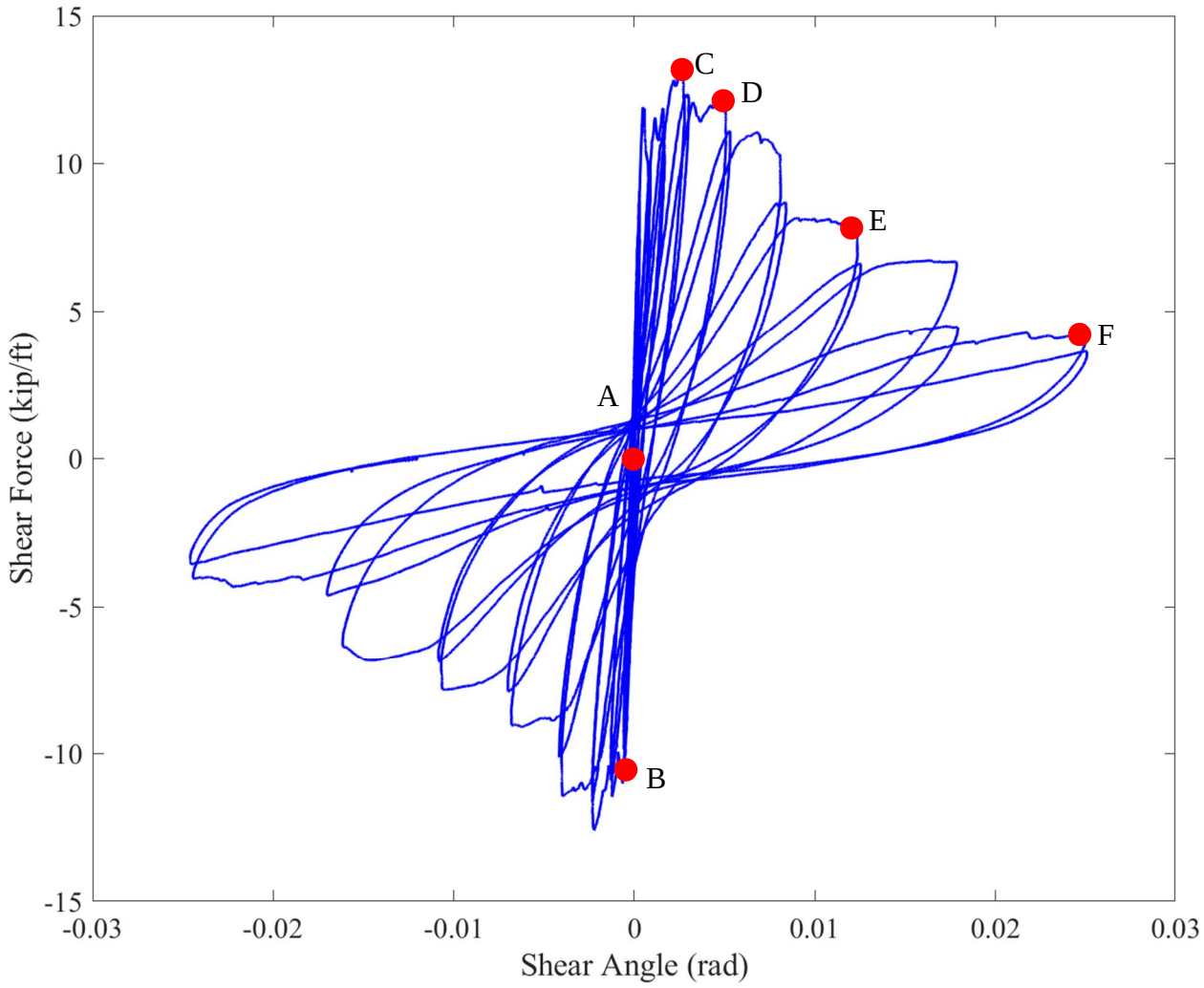

Figure 3-59. Load-Deformation Plot for Specimen 3/6.25-4-L-RS-DT

Figure 3-60. Crack Distribution of Specimen 3/6.25-4-L-RS-DT Before Testing (Point A in Figure 3-59)

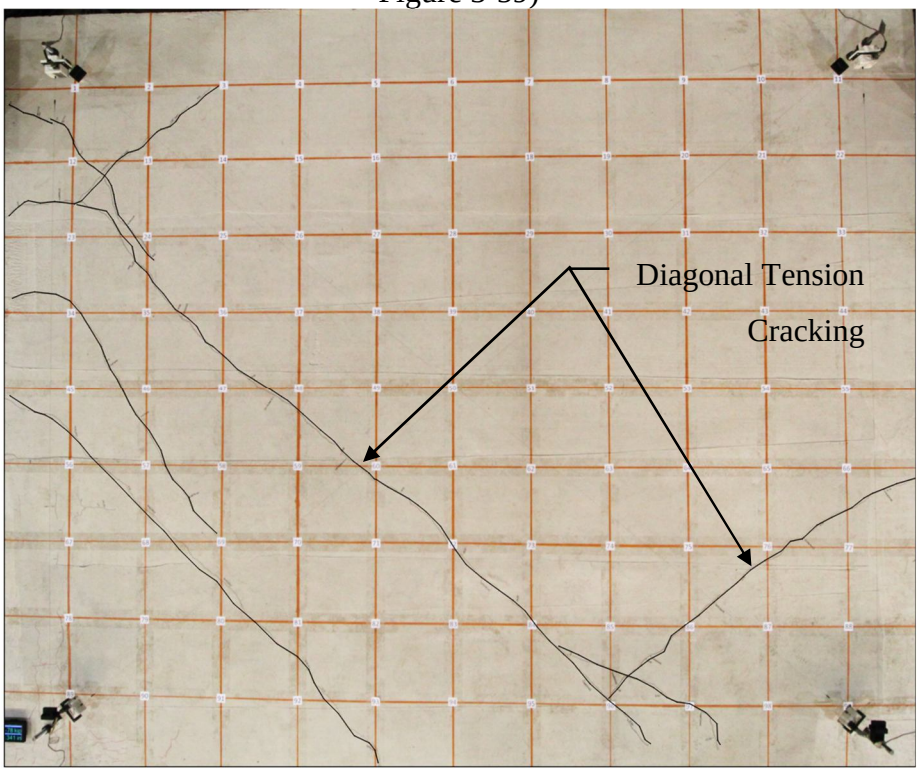

Figure 3-61. Crack Distribution of Specimen 3/6.25-4-L-RS-DT First Occurrence of Diagonal Tension Cracking (Point B in Figure 3-59)

At Point C of Figure 3-59, additional diagonal tension cracks appeared on the specimen, extending nearly across the full width of the specimen, as shown in Figure 3-62. This additional crack formation occurred at the same time as “popping” noises at regular short intervals were heard. These noises are believed to correspond to reinforcement bars rupturing, since broken bars could be observed in the cracks that opened.

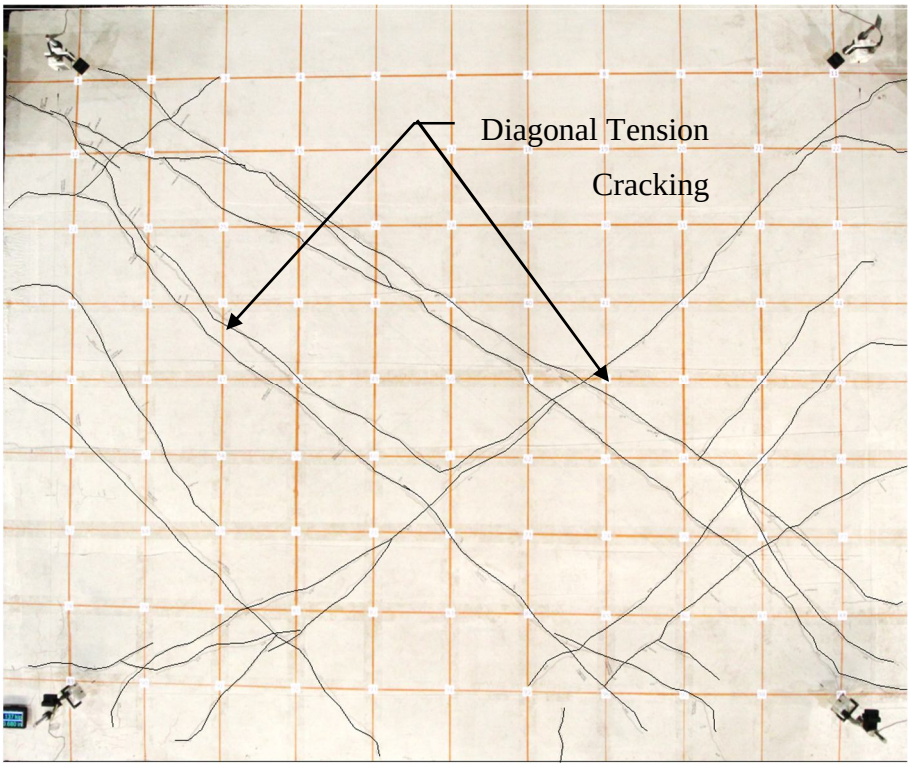

Figure 3-62. Crack Distribution of Specimen 3/6.25-4-L-RS-DT: Further Diagonal Tension Cracking at Peak Load (Point C in Figure 3-59)

After peak loading near Point D of Figure 3-59, some prominent cracks were opening more than other parallel cracks (Figure 3-63), and crack formation continued. Near Point E of Figure 3-59, the main diagonal cracks were opening up (Figure 3-64) without much additional crack formation. Broken bars could be seen crossing these cracks confirming that the reinforcement had yielded and ruptured, as shown in Figure 3-65. The state of the specimen at the end of the test is shown in Figure 3-66.

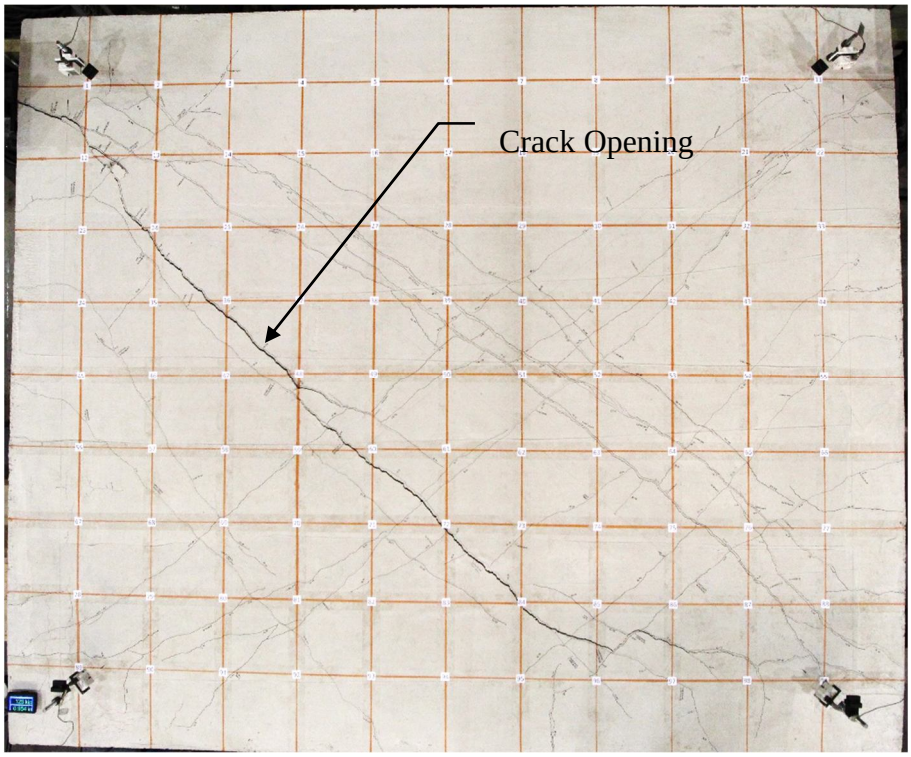

Figure 3-63. Crack Distribution of Specimen 3/6.25-4-L-RS-DT: Crack Opening Post Peak (Point D in Figure 3-59)

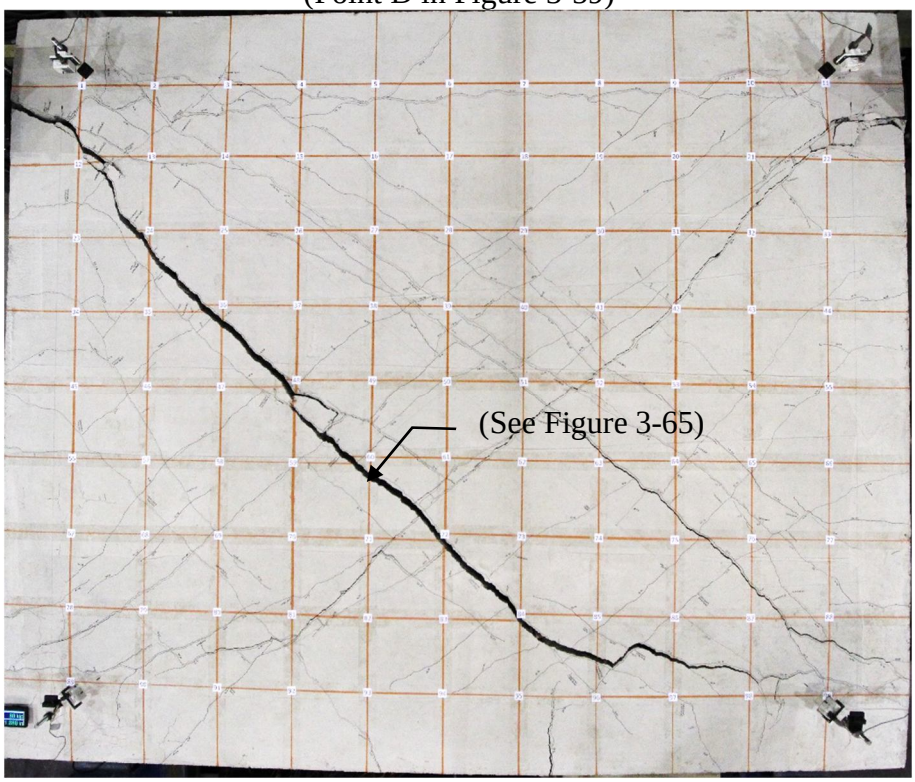

Figure 3-64. Crack Distribution of Specimen 3/6.25-4-L-RS-DT: After Drop in Strength (Point E in Figure 3-59)

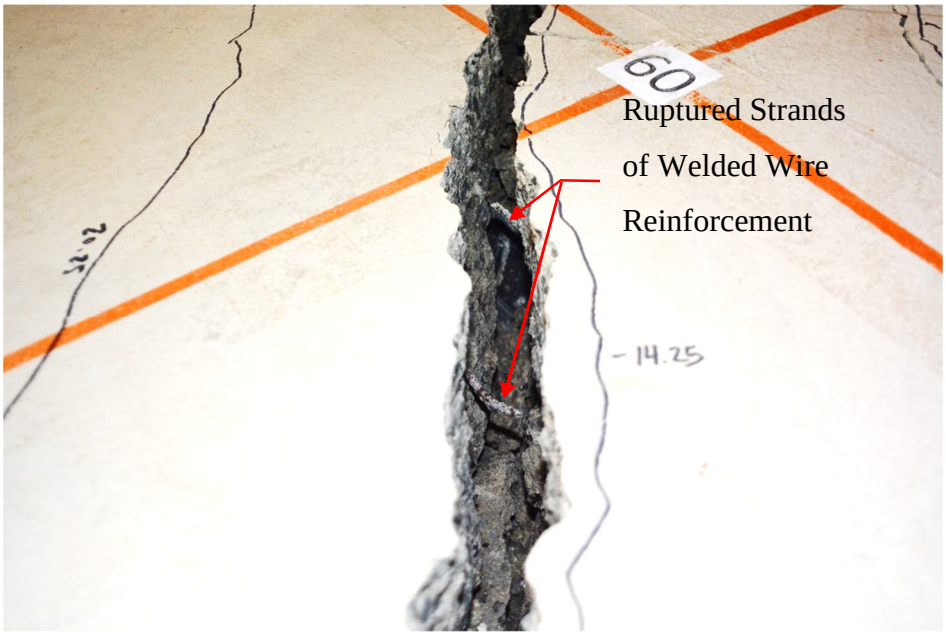

Figure 3-65. Crack Opening and Reinforcement Rupture

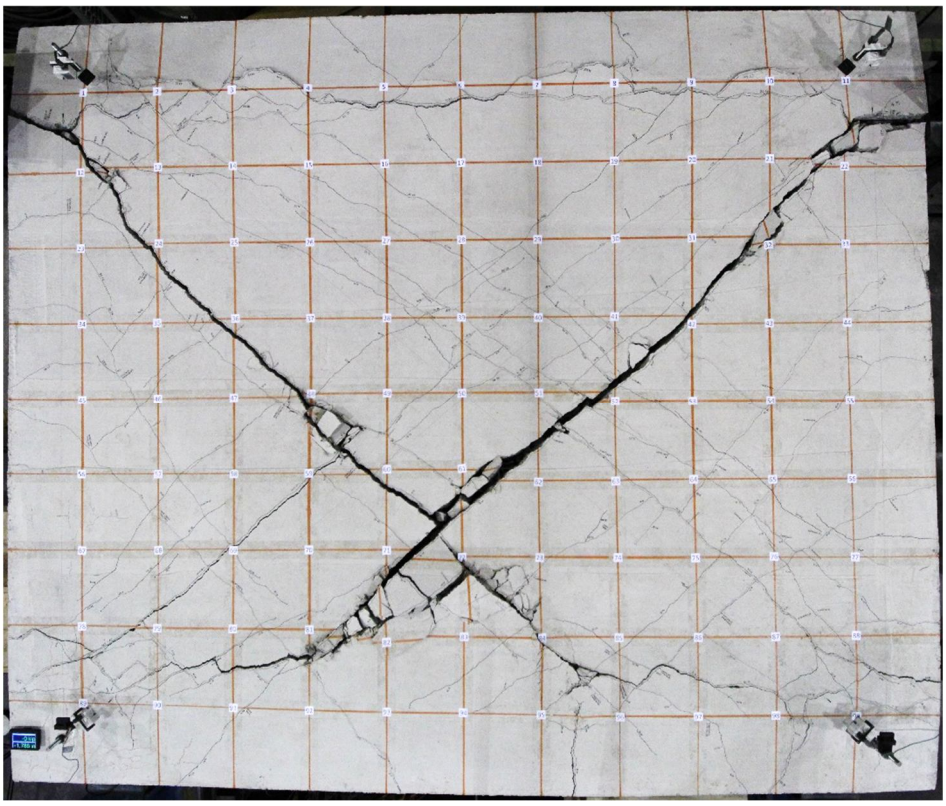

Figure 3-66. Cracking Pattern of Specimen 3/6.25-4-L-RS-DT: After Testing (Point F in Figure 3-59)

3.9 Specimen 3/7.5-NW-NF-RS

The test specimen before and after concrete placement is shown in Figure 3-68. The deformation behavior of the specimen during early loading cycles used to calculate initial stiffness is shown in Figure 3-68.

Figure 3-67. Specimen 3/7.5-4-N-NF-RS Before and After Concrete Placement

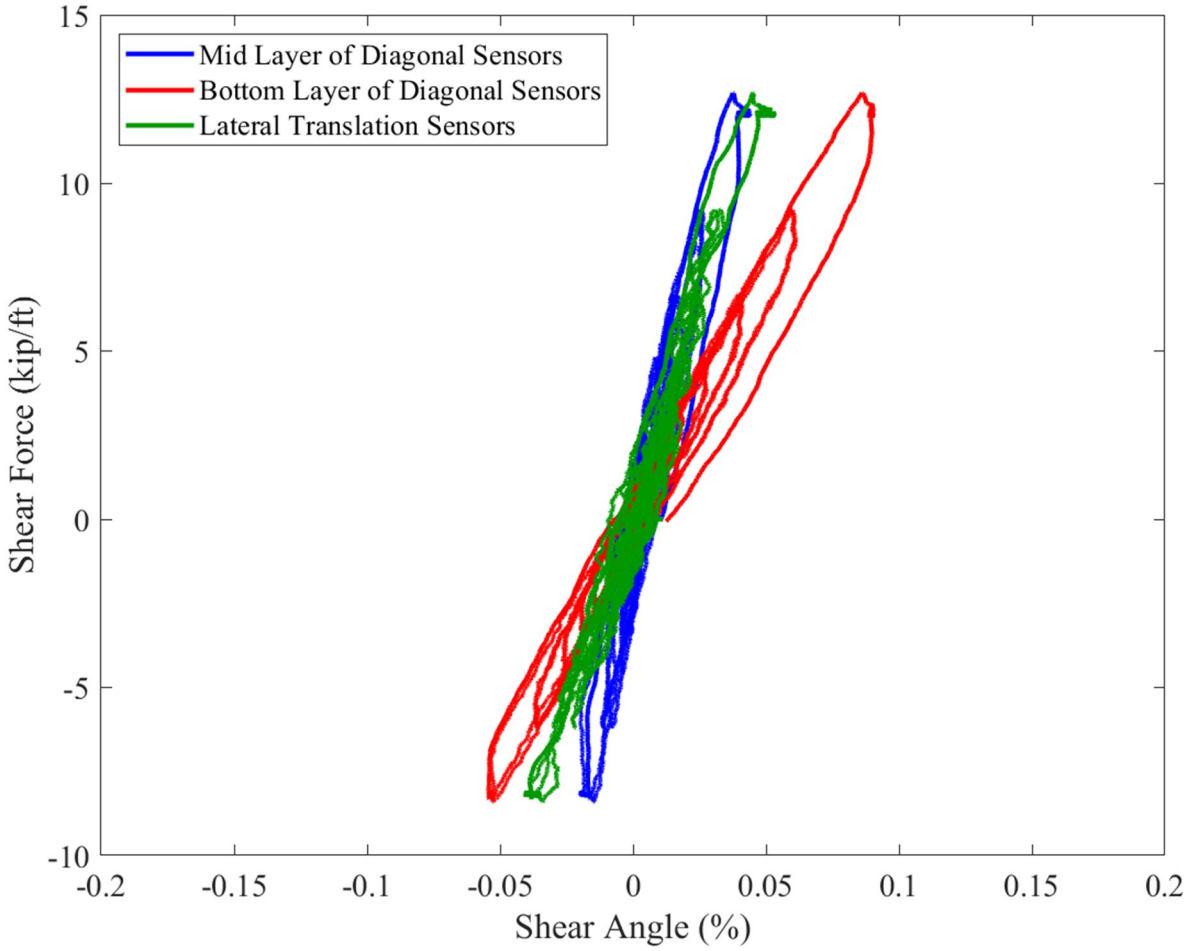

Figure 3-68. Comparison of Initial Load-Deformation Cycles Using Different Displacement Sensors for Specimen 3/7.5-4-N-NF-RS

A load deformation plot used to describe the progression of failure for this specimen is shown in Figure 3-69. The peak strength was 21.6 kip per foot of diaphragm, with a shear angle at peak strength of 0.0012 radians. The shear angle at 80% of peak strength was 0.0030 radians and the residual strength measured at 0.02 radians of 4.2 kips per foot of diaphragm. Before the test started (Figure 3-69 Point A), the specimen was searched for existing cracks, but none were found (Figure 3-70). The first occurrence of diagonal tension cracking in both directions of loading was observed at Point B in Figure 3-69, as shown in Figure 3-71. More significant cracking occurred on the second cycle of the same displacement amplitude step. During the next displacement step, which coincides with Point C of Figure 3-69, the diagonal tension cracking extended the whole width of the specimen, as shown in Figure 3-72.

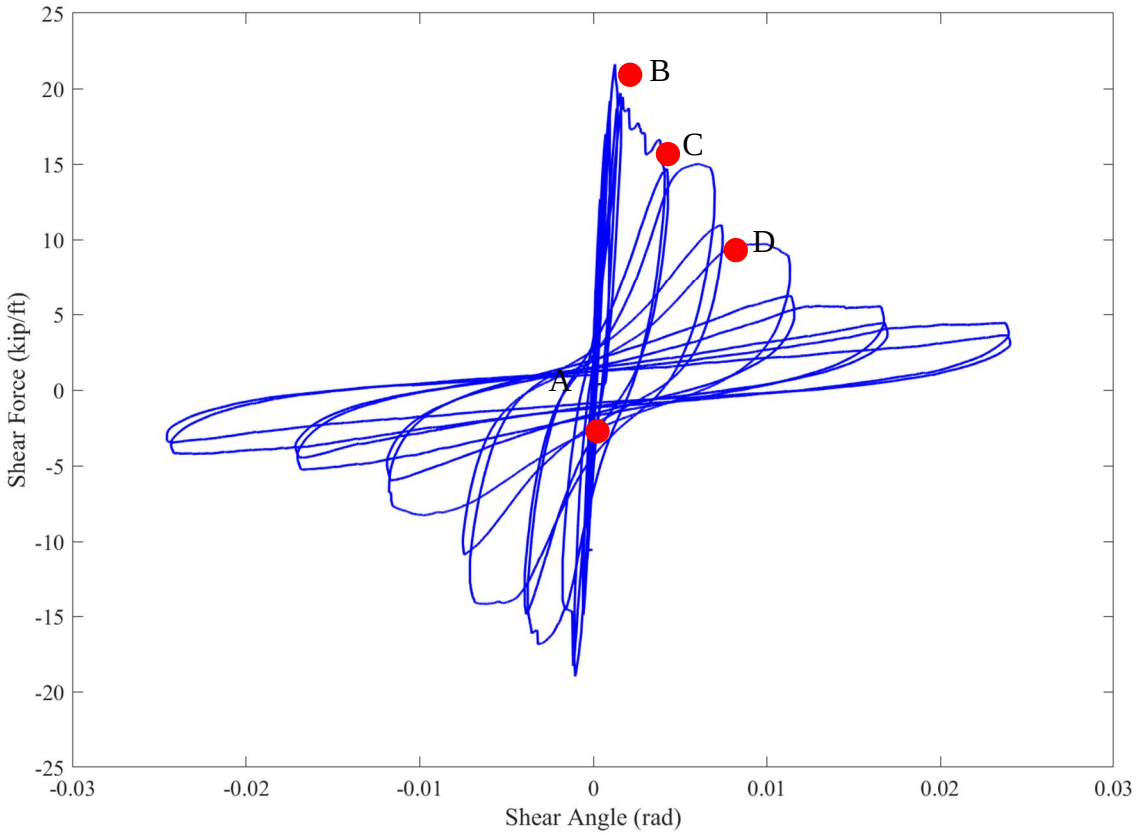

Figure 3-69. Load-Deformation Plot for Specimen 3/7.5-4-N-NF-RS

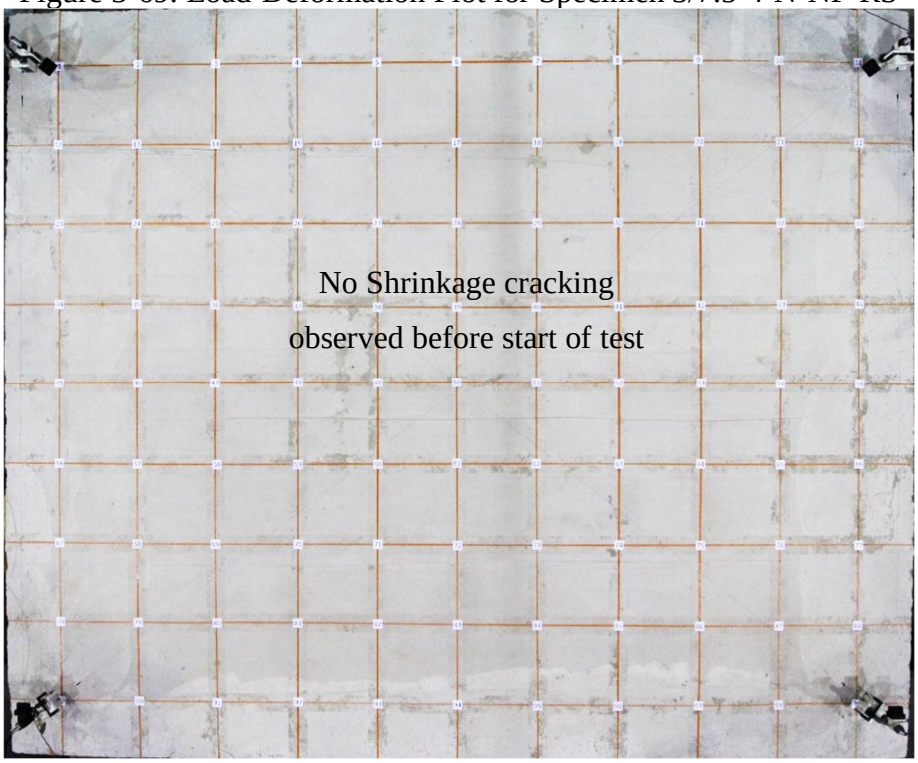

Figure 3-70. Crack Distribution of Specimen 3/7.5-4-N-NF-RS Before Testing (Point A in Figure 3-59)

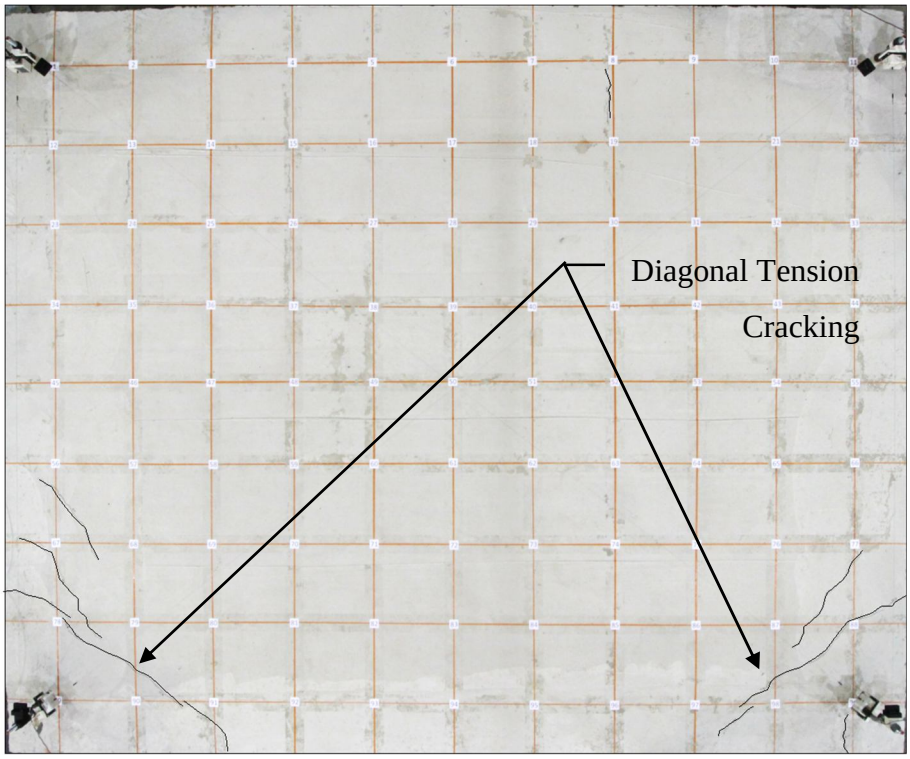

Figure 3-71. Crack Distribution of Specimen 3/7.5-4-N-NF-RS First Occurrence of Diagonal Tension Cracking (Point B in Figure 3-59)

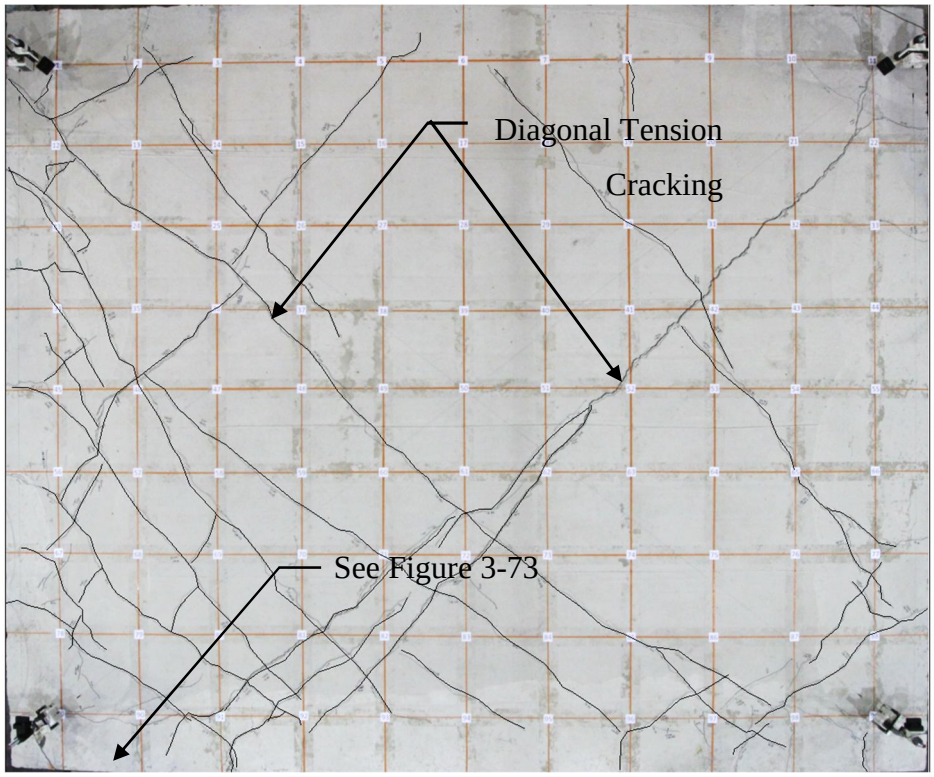

Figure 3-72. Crack Distribution of Specimen 3/7.5-4-N-NF-RS: Further Diagonal Tension Cracking Past Peak Load (Point C in Figure 3-59)

At Point C of Figure 3-69, evidence of rib shear damage was observed on the ribs of the fixed beam on either edge of the slab, as shown on Figure 3-73. The rib shear cracks extended to the surface where they seemed to join the diagonal tension cracks.

Figure 3-73. Evidence of Rib Shear Failure on Perimeter Fasteners of Fixed Beam

After considerable loss in strength (Point D in Figure 3-69), evidence of shear damage became apparent on all the ribs of the fixed beam. While 6 of the ribs (three on each edge of the specimen) exhibited evidence of rib shear, the remaining ribs located on the center of the beam exhibited failures more consistent with a concrete pullout failure mode.

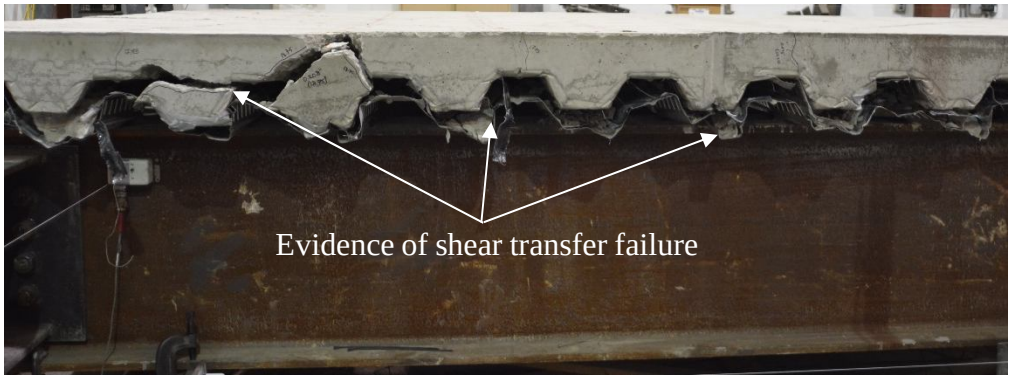

Figure 3-74. Shear Transfer Failure (Point D in Figure 3-59)

4 REFERENCES

[1] Rodriguez, M.E., Restrepo, J.L., and Blandon, J.J. (2007). Seismic Design Forces for Rigid Floor Diaphragms in Precast Concrete Building Structures, Journal of Structural Engineering, 133(11) 1604-1615.

[2] ASCE / SEI 7-16 (2016). Minimum Design Loads for Buildings and Other Structures Published by the American Society of Civil Engineers (ASCE).

[3] O'Brien, P. (2017). "Characterizing the Load-Deformation Behavior of Steel Deck Diaphragms Using Past Test Data." Virginia Tech, Blacksburg, VA, USA

[4] Luttrell, L. (1971). Shear diaphragms with lightweight concrete fill. Presented at the 1st International Specialty Conference on Cold Formed Steel Structures, pp. 111–117.

[5] Davies, J., and Fisher, J. (1979). The diaphragm action of composite slabs. Proceedings of the Institute of Civil Engineers, 67(4), pp. 891–906.

[6] ABK, A Joint Venture. (1981). Methodology for mitigation of seismic hazards in existing unreinforced masonry buildings: diaphragm testing. Report No. ABK-TR-03.

[7] Porter, M., and Greimann, L. (1980). Seismic resistance of composite floor diaphragms. Report No. ISU-ERI-AMES-80133, Iowa State University.

[8] Porter, M., and Greimann, L. (1982). Composite steel deck diaphragm slabs - design modes. 6th International Specialty Conference on Cold-Formed Steel Structures, pp. 467–484.

[9] Neilsen, M. (1984). Effects of gravity load on composite floor diaphragm behavior. Master's thesis, Iowa State University.

[10] Easterling, W. S. (1987). Analysis and design of steel-deck-reinforced concrete diaphragms. Dissertation, Iowa State University.

[11] Easterling, W. S., and Porter, M. (1988). Composite diaphragm behavior and strength. 9th International Specialty Conference on Cold-Formed Steel Structures, pp. 387–404

[12] Porter, M., and Easterling, W. (1988). Behavior, analysis, and design of steel-deck-reinforced concrete diaphragms. Report No. ISU-ERI-Ames-88305 Project 1636, Iowa State University.

[13] Easterling, W. S., and Porter, M. (1994a). Steel-deck-reinforced concrete diaphragms. I. Journal of Structural Engineering, 120(2), pp. 560–576.

[14] Easterling, W. S., and Porter, M. (1994b). Steel-Deck-Reinforced Concrete Diaphragms. II. Journal of Structural Engineering, 120(2), pp. 577–596.

[15] Prins, M. D. (1985). Elemental tests for the seismic resistance of composite floor diaphragms. Master's thesis, Iowa State University.

[16] FEMA. (2007). Interim Testing Protocols for Determining the Seismic Performance Characteristics of Structural and Nonstructural Components, (FEMA 461). Applied Technology Council, Federal Emergency Management Agency.

[17] AISI. (2013). Test standard for cantilever test method for cold-formed steel diaphragms, (AISI S907-13). American Iron and Steel Institute

[18] ICC. (2016) Acceptance Criteria for Steel Deck Roof and Floor Systems (AC43-16). ICC Evaluation Service.

[19] AISI. (2016). North American Standard for the Design of Profiled Steel Diaphragms, (AISI S310-16). American Iron and Steel Institute.

[20] AISC (2016). Specification for Structural Steel Buildings. (ANSI/AISC 360-16). American Institute of Steel Construction.

[21] RCSC (2014). Specification for Structural Joints Using High-Strength Bolts. Research Council on Structural Connections
[22] ACI (2019). Building Code Requirements for Structural Concrete, (ACI 318-19). American Concrete Institute

APPENDIX A: PROCEDURE USED TO CORRECT SHEAR ANGLE OF SPECIMEN 3/7.5-4-N-NF-P

. The data acquisition system malfunctioned during testing of specimen 3/7.5-4-N-NF-P, resulting in the loss of data including displacement sensors. As a result, the load deformation plot for this specimen is obtained from the data recorded by the actuator controller and modified to account for flexibility of the testing rig. This was done by obtaining a relationship between applied load and the difference between shear angle calculated using the mid layer and shear angle calculated using the displacement of the actuators for the specimens tested to date. The relationship between applied load and the difference in shear angle measurements from the actuator and mid layer of diagonal string potentiometers is shown in Figures A1, A2, and A3 for specimens 2/4.5-4-N-RS-DT, 3/6.25-4-L-RS-DT, and 3/7.5-4-N-NF-RS, respectively. This relationship was found to be linear and relatively consistent across the specimens. The slopes of the linear relationship that was obtained for each specimen are summarized in Table A 1.

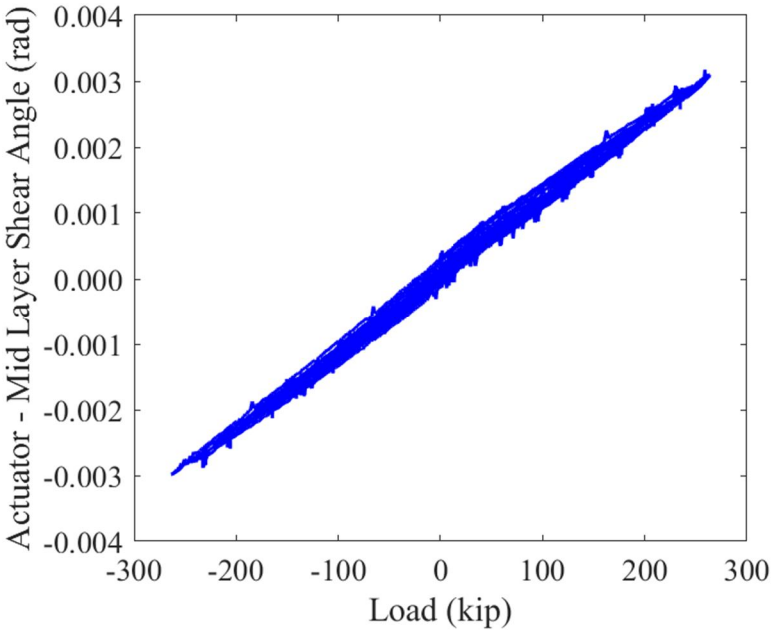

Figure A 1. Relationship between Applied Load and the Difference in Shear Angle Measurements from the Actuator and Mid Layer of Diagonal Sensors for Specimen 2/4.5-4-N-RS-DT

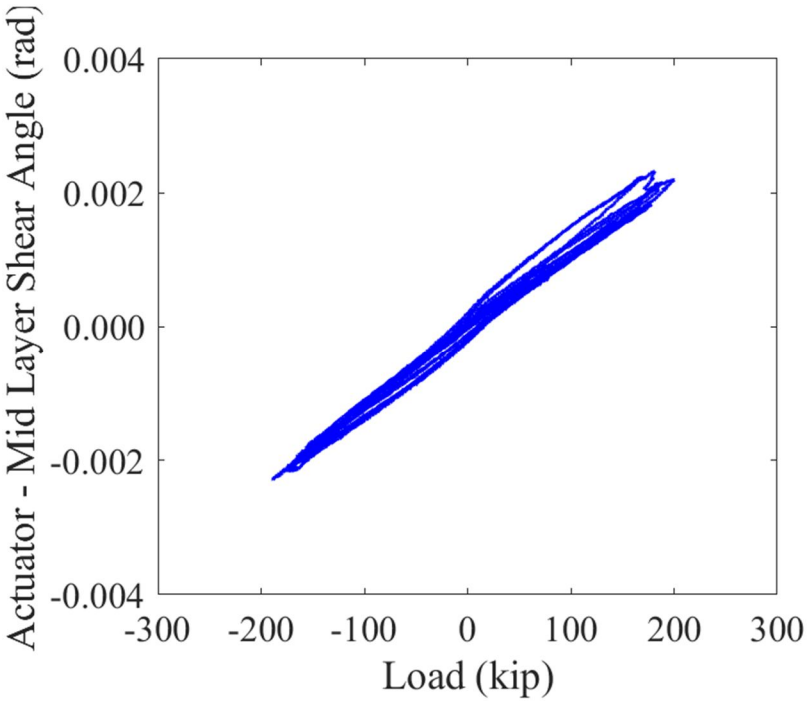

Figure A 2. Relationship between Applied Load and the Difference in Shear Angle Measurements from the Actuator and Mid Layer of Diagonal Sensors for Specimen 3/6.25-4-L-RS-DT

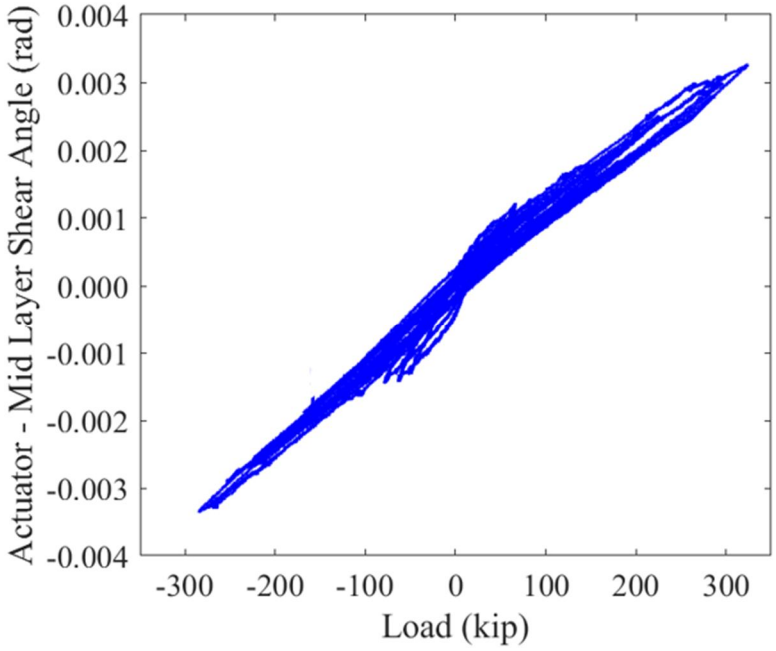

Figure A 3. Relationship between Applied Load and the Difference in Shear Angle Measurements from the Actuator and Mid Layer of Diagonal Sensors for Specimen 3/7.5-4-N-NF-RS

Table A 1. Summary of Slopes Obtained from Relationship between Applied Load and the Difference in Shear Angle Measurements from the Actuator and Mid Layer of Diagonal Sensors

Specimen	Slope (rad/kip)
4.5-2-4-LW-NF-RS	0.0000116
3/6.25-4-L-RS-DT	0.0000115
3/7.5-4-N-NF-RS	0.0000112
Average	0.0000115

The average slope was from Table A1 was to modify the actuator shear angle of specimen 3/7.5-4-N-NF-P using Equation A1 to obtain a load-deformation plot that could be assumed to provide a reasonable estimate on the behavior of the specimen. The resulting load-deformation plot is compared to the original plot obtained from actuator data in Figure A 4.

$$\gamma_{mod} = \gamma_{act} - m_{avg} \cdot P \quad \text{(A1)}$$

Where,

γ_{mod}= Corrected shear angle

γ_{act} = Shear angle calculated from actuator displacement

m_{avg} = Average slope obtained from relationship between load and applied load and the difference in shear angle measurements from the actuator and mid layer of diagonal sensors (Table A.1)

P = Applied Load

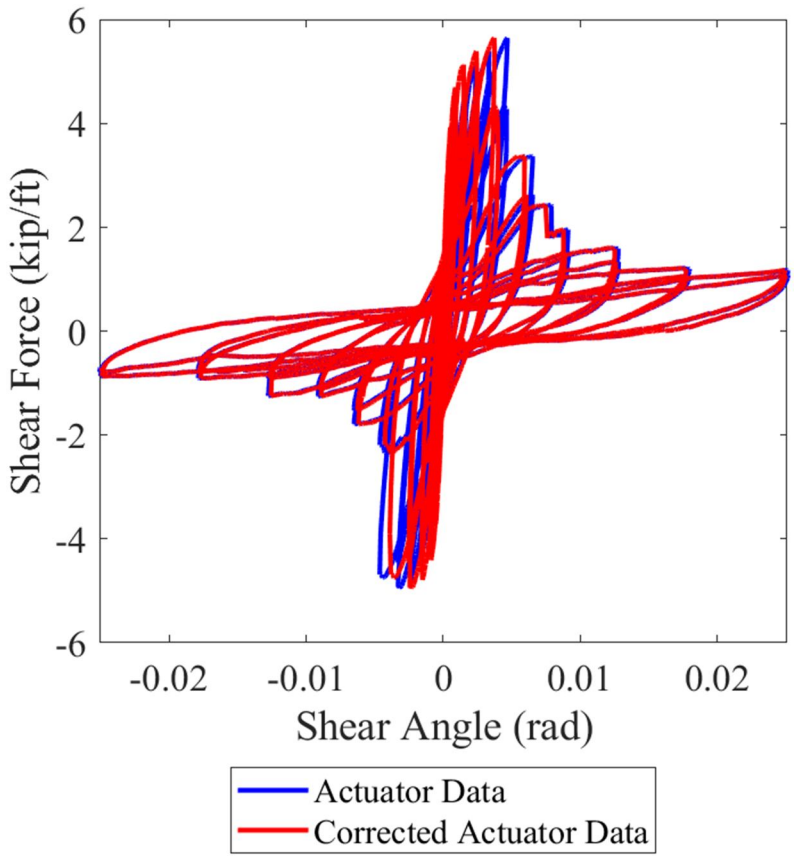

Figure A 4. Resulting Load Deformation Plot from Correction Procedure for Specimen 3/7.5-4-N-NF-P

APPENDIX B: BAREFRAME TEST RESULTS

Per AISI S907 [2], a bare frame test was performed to show that a negligible amount of shear was being resisted by the testing frame. This test was performed with additional weight on the loading beam to simulate the maximum weight that the beam carried for the heaviest specimen tested. Three 18 ft. long W44x230 beams (roughly 12,400 lbs.) were placed on top of the loading beam to simulate the worst-case tributary weight on that beam during testing. The bare frame was subjected to a maximum displacement of 4.0 in. AISI S907 [2] states that if the load from a bare frame test is less than 2% of the maximum load from the diaphragm test (measured at the same displacement), then the shear load from the diaphragm test need not be corrected for bare frame resistance. For all specimens, the bare frame resistance was less than 0.02 times the ultimate shear strength of the specimen, as summarized in Table B 1 and therefore bare frame resistance was neglected.

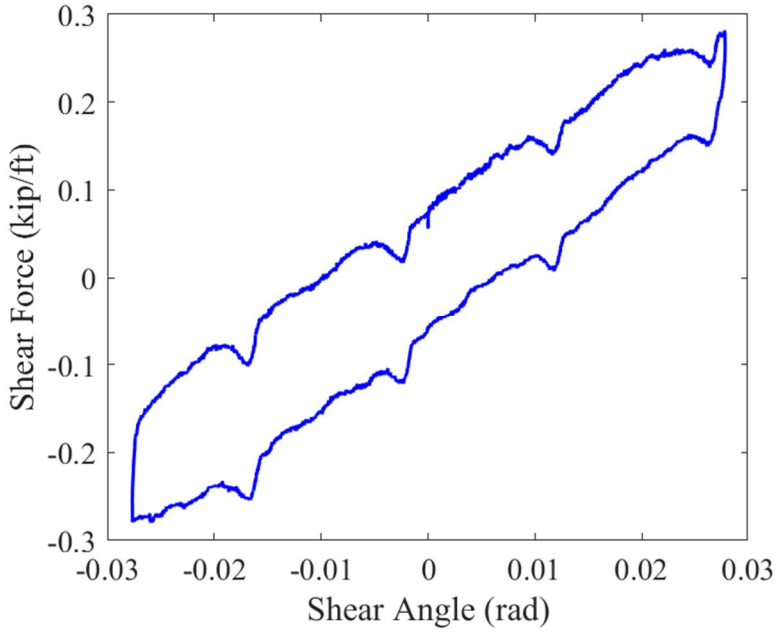

Figure B 1. Load-Deformation Plot for Bare-Frame Test

Table B 1. Summary of Bare Frame Resistance

Specimen	Bare Frame Resistance at Shear Angle Corresponding to Ultimate Strength of Specimen (kip/ft)	2% of Ultimate Strength of Specimen (kip/ft)
3/6.25-4-L-NF-DT	0.095	0.192
3/7.5-4-N-NF-DT	0.093	0.307
2/4-4-L-NF-DT	0.108	0.179
3/6.25-4-L-NF-P	0.072	0.081
2/4.5-4-L-RS-DT	0.116	0.352
3/7.5-4-N-NF-P	0.101	0.113
3/6.25-4-L-RS-DT	0.098	0.267
3/7.5-4-N-RS-DT	0.091	0.432

APPENDIX C: TESTING FRAME DRAWINGS AND DETAILS

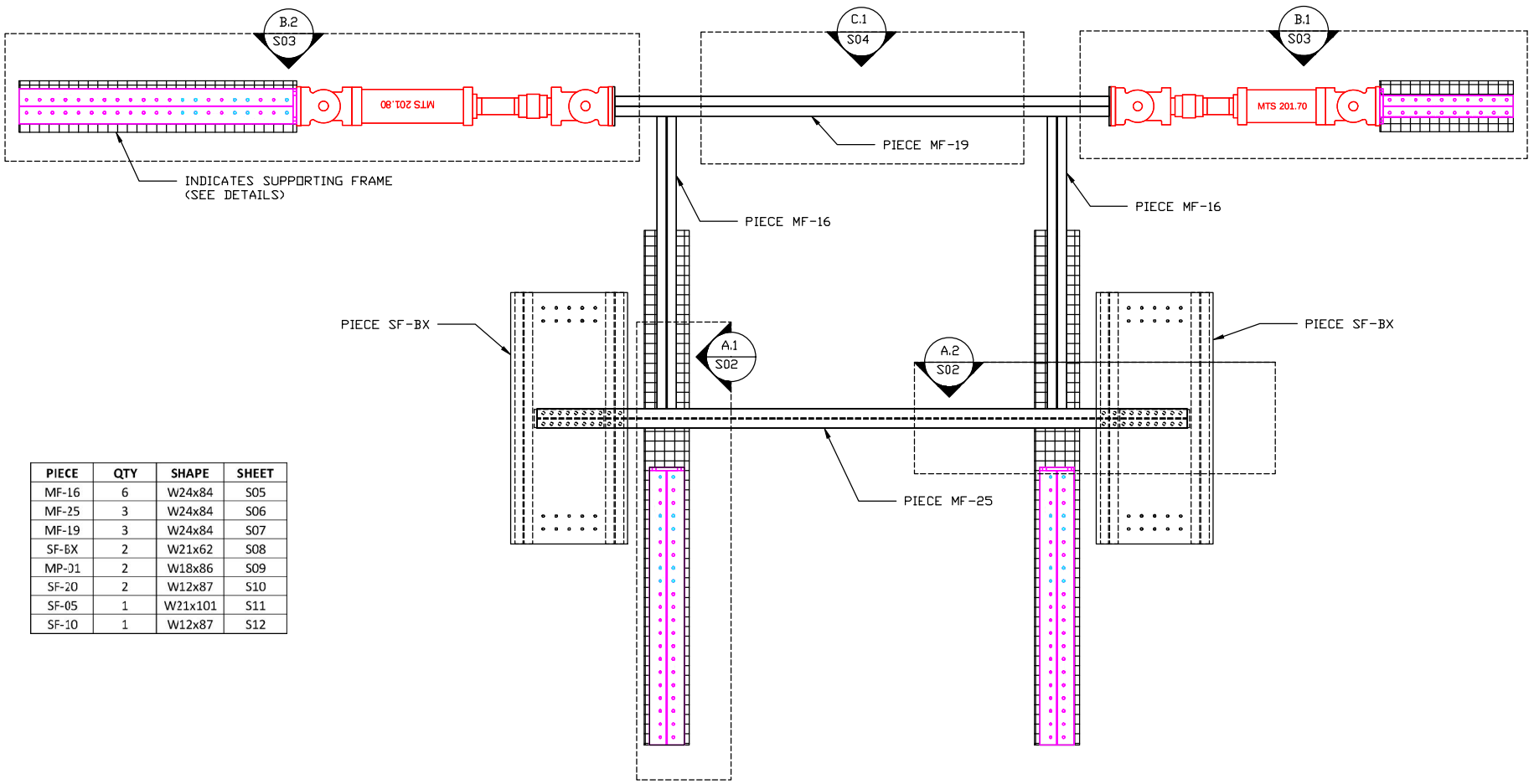

PIECE	QTY	SHAPE	SHEET
MF-16	6	W24x84	S05
MF-25	3	W24x84	S06
MF-19	3	W24x84	S07
SF-BX	2	W21x62	S08
MP-01	2	W18x86	S09
SF-20	2	W12x87	S10
SF-05	1	W21x101	S11
SF-10	1	W12x87	S12

VIRGINIA TECH	COMPOSITE DIAPHRAGM CANTILEVER TEST FRAME	NOV 9, 2017	S01
	TESTING SETUP LAYOUT	R. AVELLANEDA	

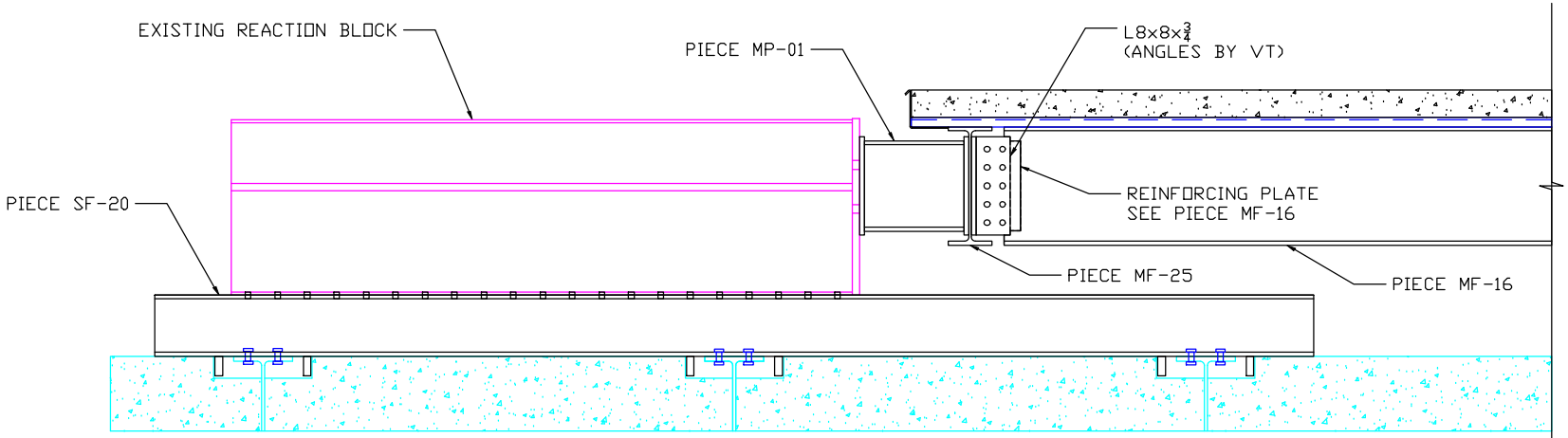

DETAIL A.1

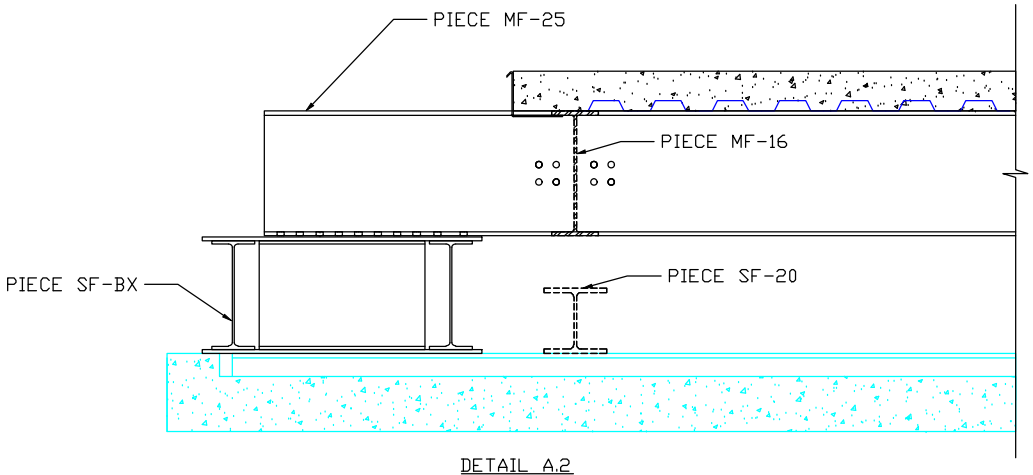

DETAIL A.2

VIRGINIA TECH	COMPOSITE DIAPHRAGM CANTILEVER TEST FRAME	NOV 9, 2017	S02
	REACTION BLOCK DETAILS	R. AVELLANEDA	

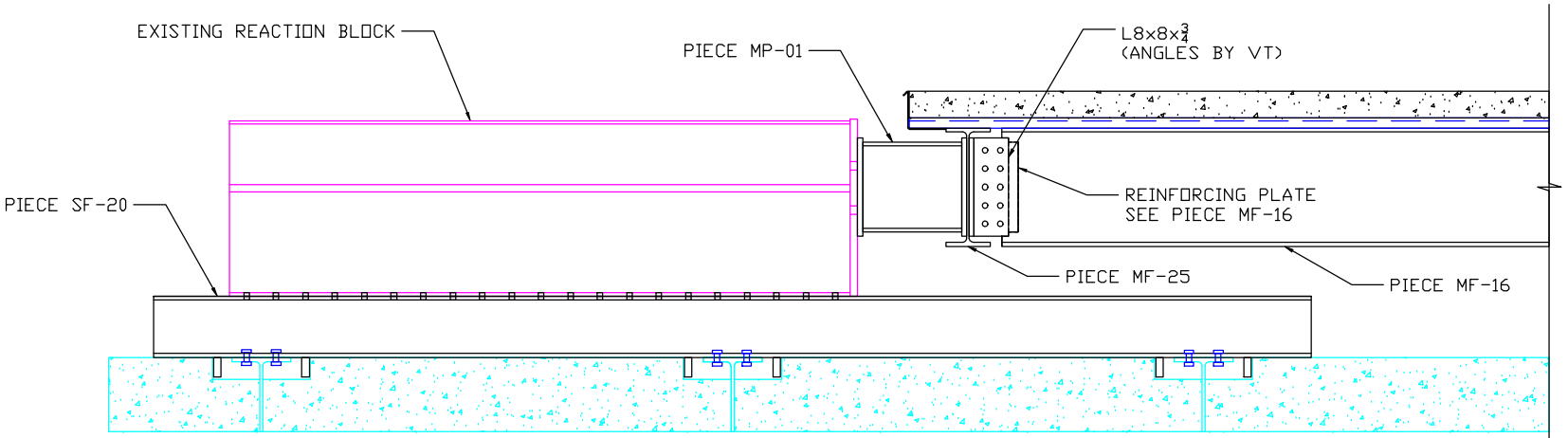

DETAIL A.1

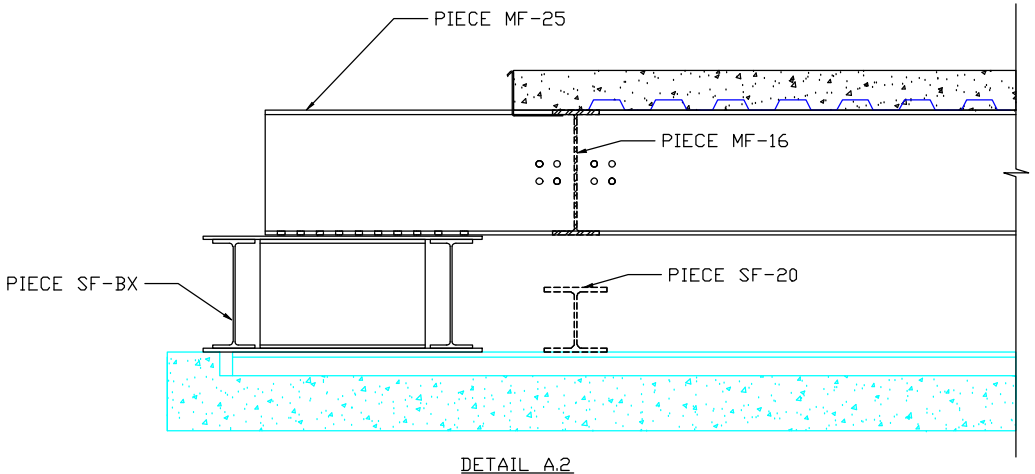

DETAIL A.2

VIRGINIA TECH	COMPOSITE DIAPHRAGM CANTILEVER TEST FRAME	NOV 9, 2017	S03
	REACTION BLOCK DETAILS	R. AVELLANEDA	

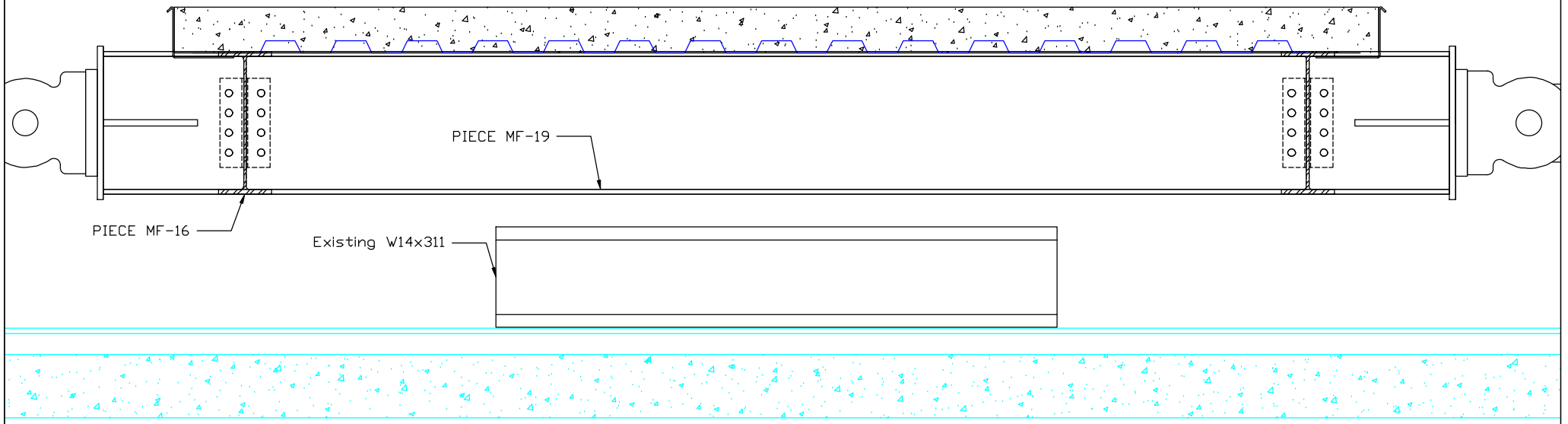

DETAIL C.1

VIRGINIA TECH	COMPOSITE DIAPHRAGM CANTILEVER TEST FRAME	NOV 9, 2017	S04
	ROLLER DETAILS	R. AVELLANEDA	

PIECE = MF-16 ; QTY = 6 ; SHAPE = W24x84

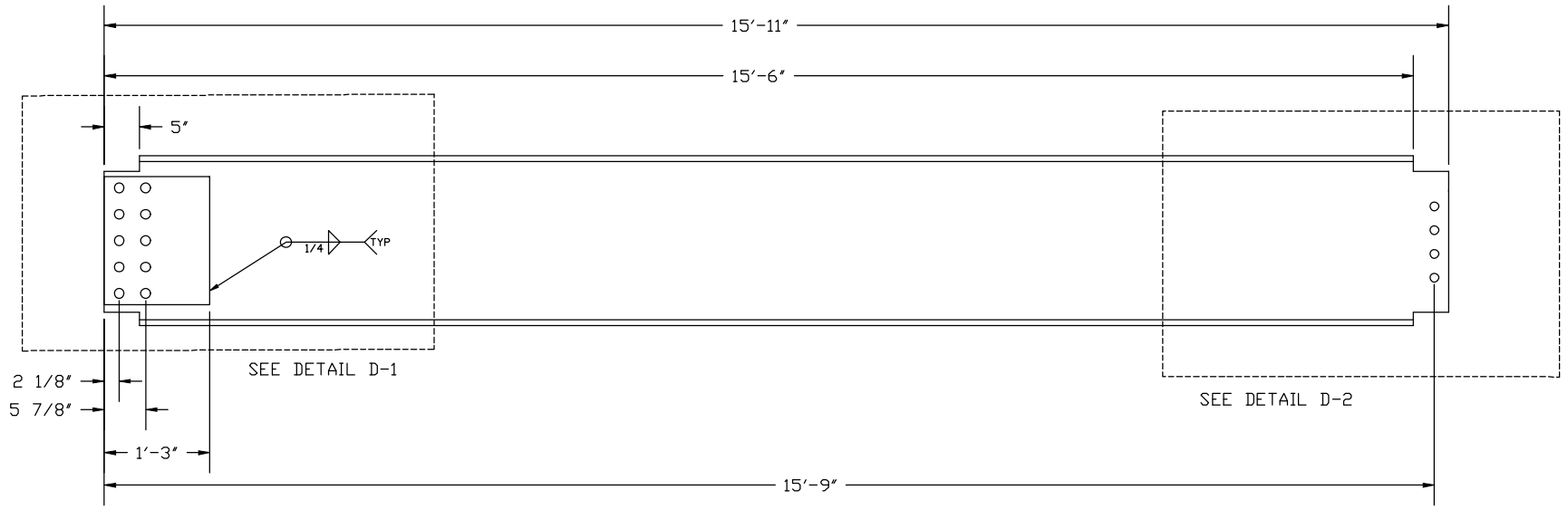

DETAIL D-1

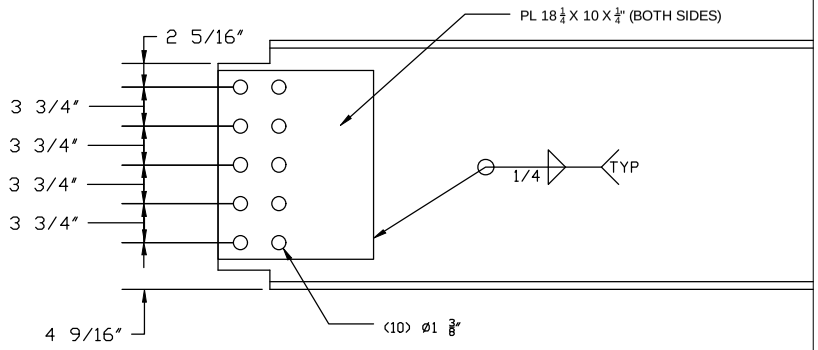

DETAIL D-2

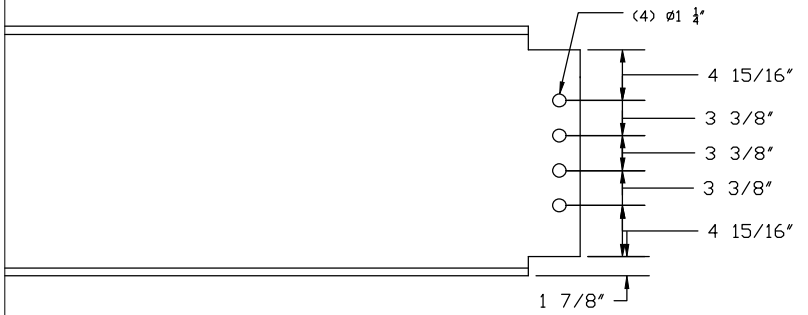

VIRGINIA TECH	COMPOSITE DIAPHRAGM CANTILEVER TEST FRAME	NOV 9, 2017	S05
	PIECE MF-16	R. AVELLANEDA	

PIECE = MF-25 ; QTY = 3 ; SHAPE = W24x84

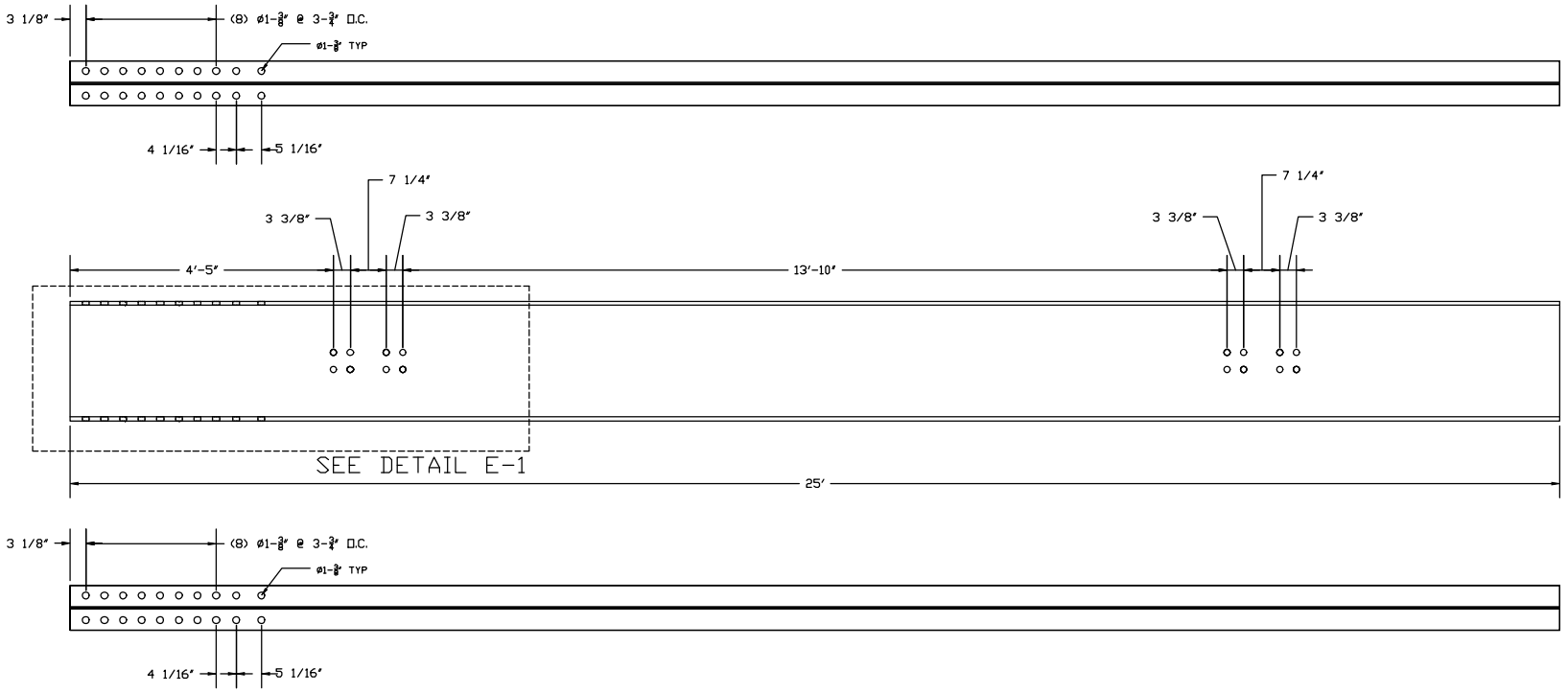

DETAIL E-1

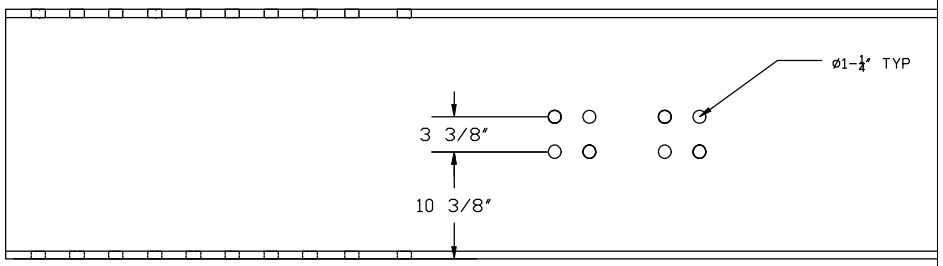

VIRGINIA TECH	COMPOSITE DIAPHRAGM CANTILEVER TEST FRAME	NOV 9, 2017	S06
	PIECE MF-25	R. AVELLANEDA	

PIECE = MF-19 ; QTY = 3 ; SHAPE = W24x84

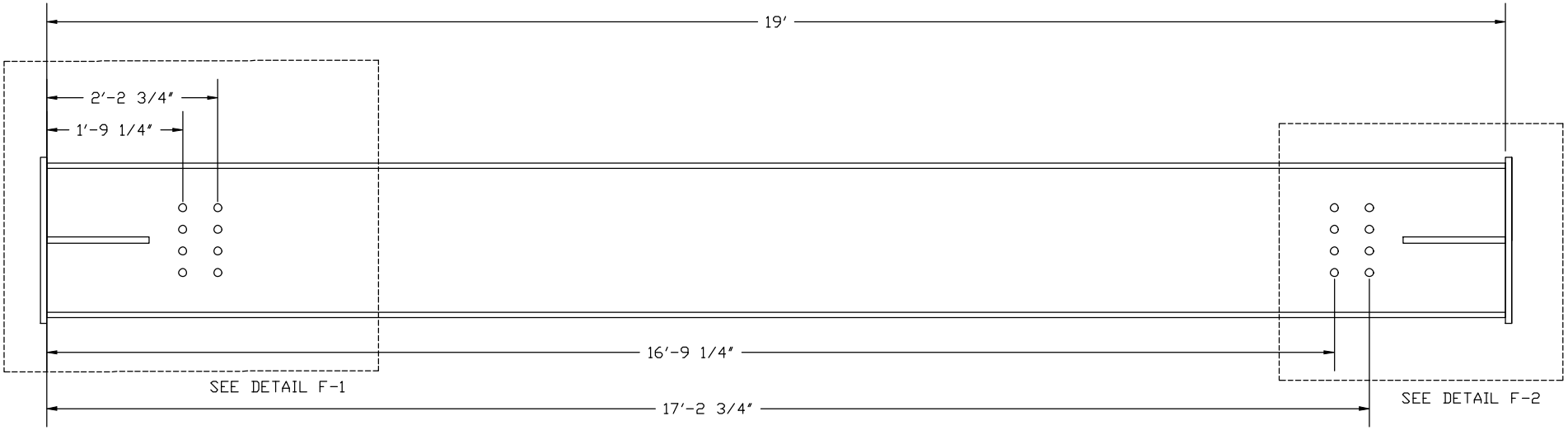

DETAIL F-1

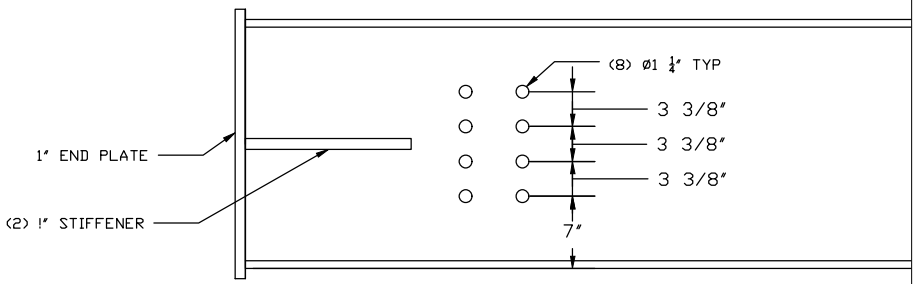

DETAIL F-2

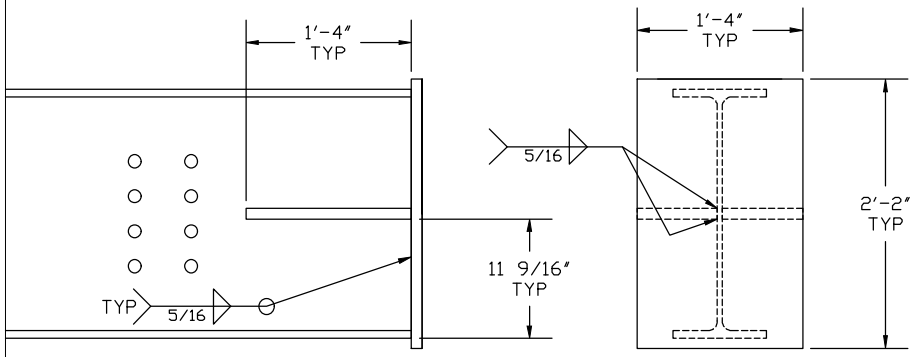

VIRGINIA TECH	COMPOSITE DIAPHRAGM CANTILEVER TEST FRAME	NOV 9, 2017	S07
	PIECE MF-19	R. AVELLANEDA	

PIECE = SF-BX ; QTY = 2 ; SHAPE = W21x62

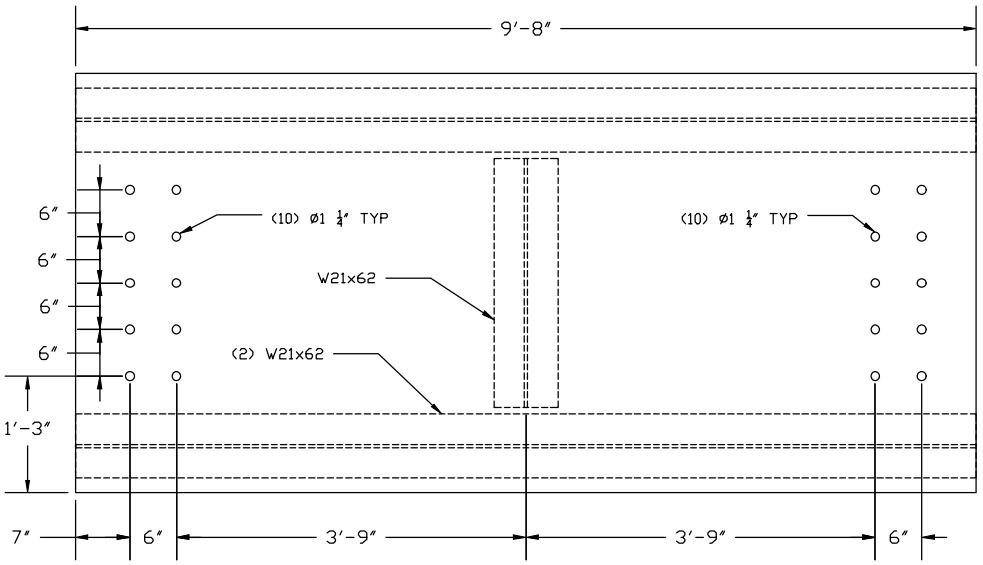

BOTTOM

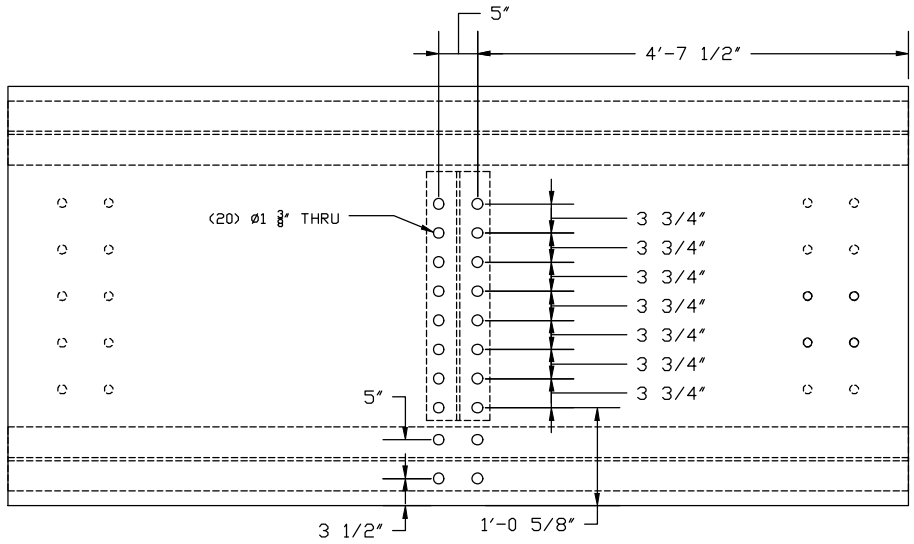

TOP

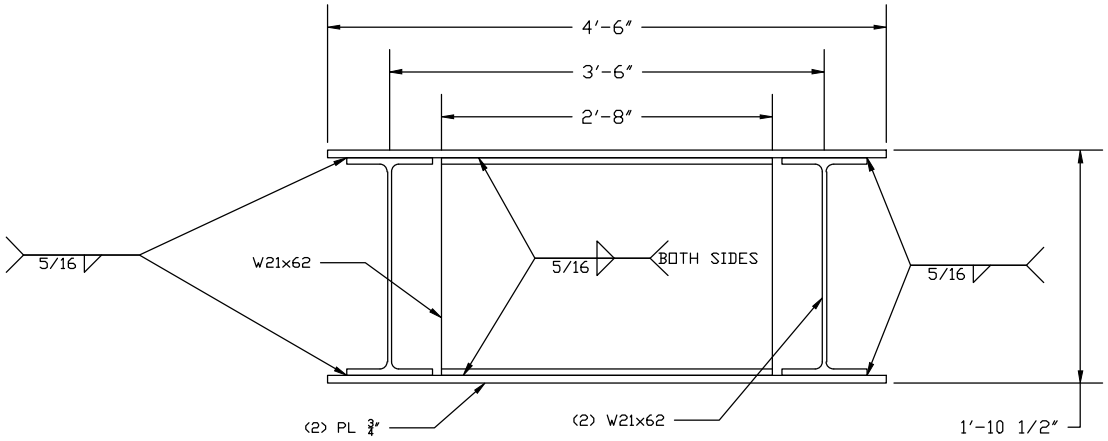

VIRGINIA TECH	COMPOSITE DIAPHRAGM CANTILEVER TEST FRAME	NOV 9, 2017	S08
	PIECE SF-BX	R. AVELLANEDA	

PIECE = MP-01 ; QTY = 2 ; SHAPE = W18x86

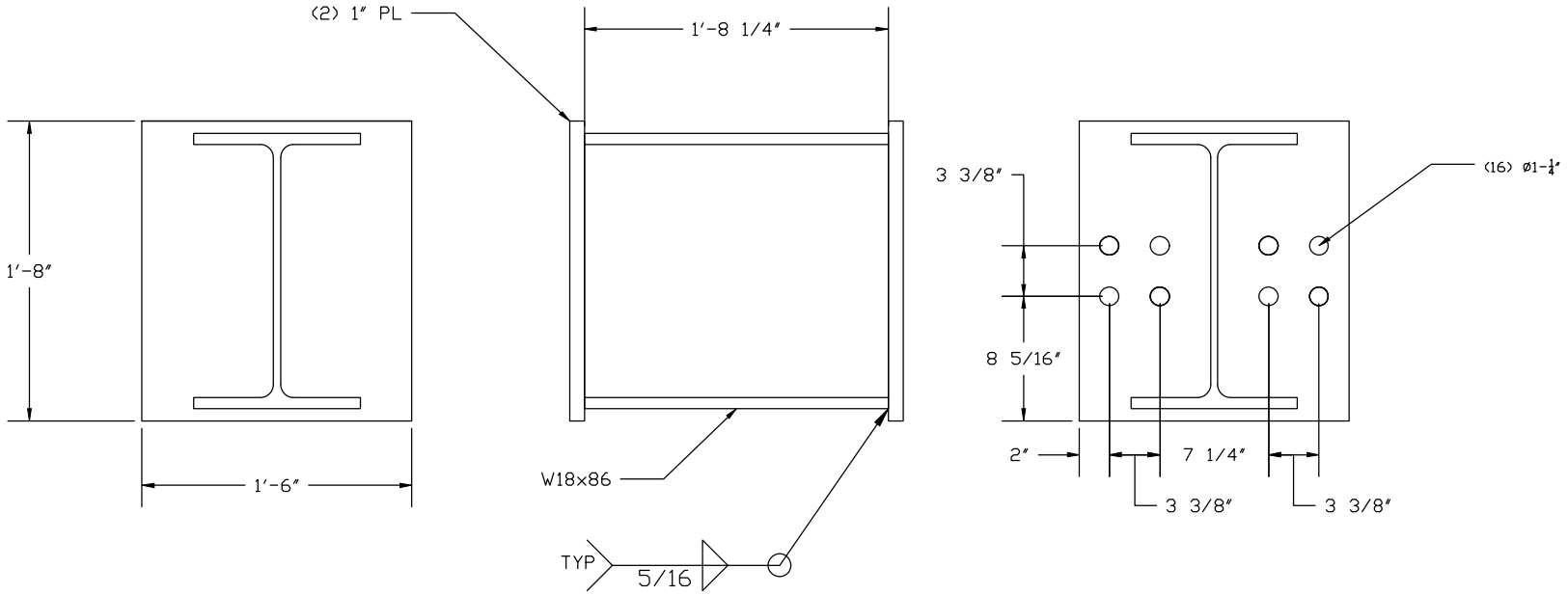

VIRGINIA TECH	COMPOSITE DIAPHRAGM CANTILEVER TEST FRAME	NOV 9, 2017	S09
	PIECE MP-01	R. AVELLANEDA	

PIECE = SF-20 ; QTY = 2 ; SHAPE = W12x87

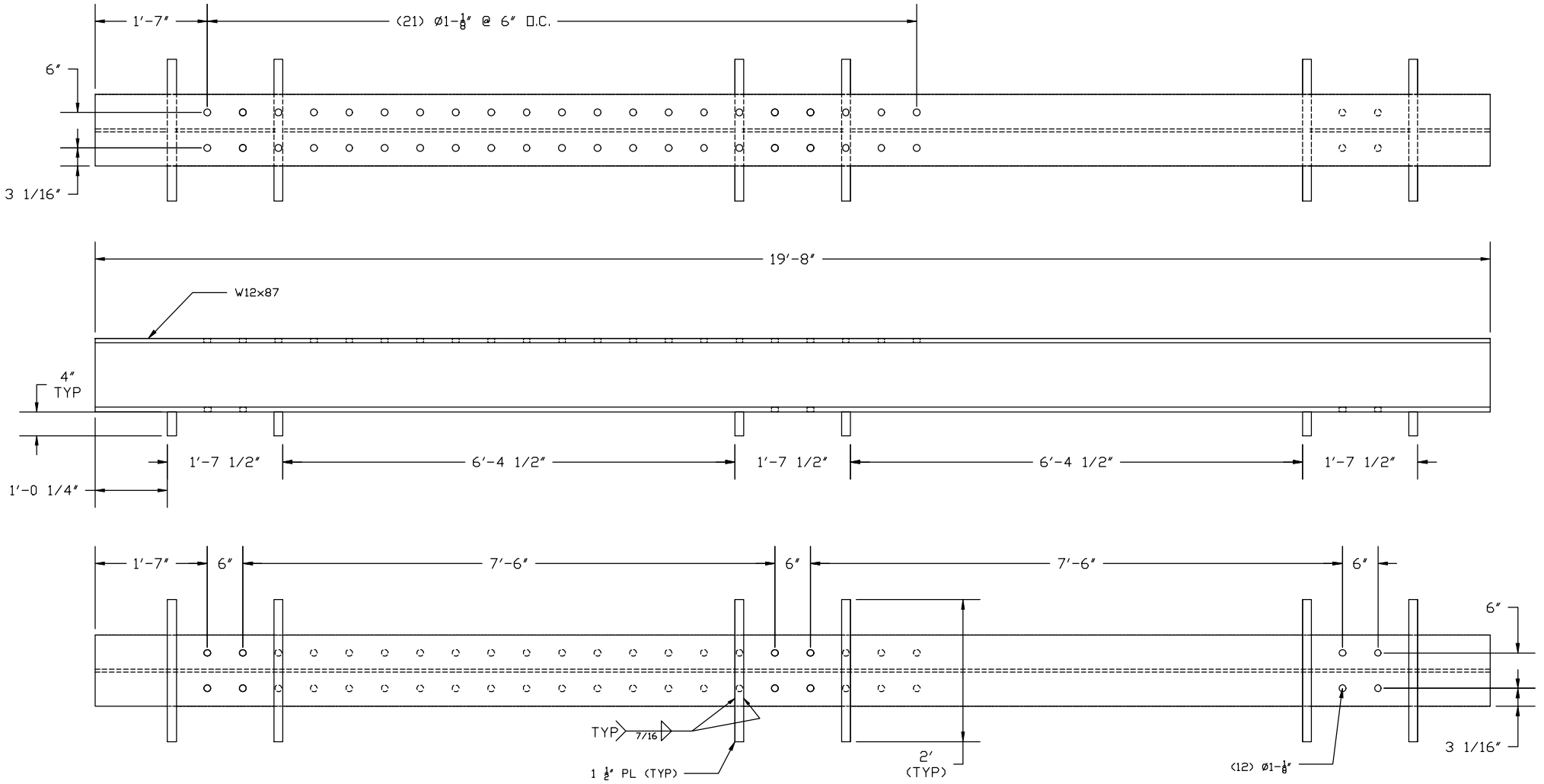

VIRGINIA TECH	COMPOSITE DIAPHRAGM CANTILEVER TEST FRAME	NOV 9, 2017	S10
	PIECE SF-20	R. AVELLANEDA	

PIECE = SF-05 ; QTY = 1 ; SHAPE = W21x101

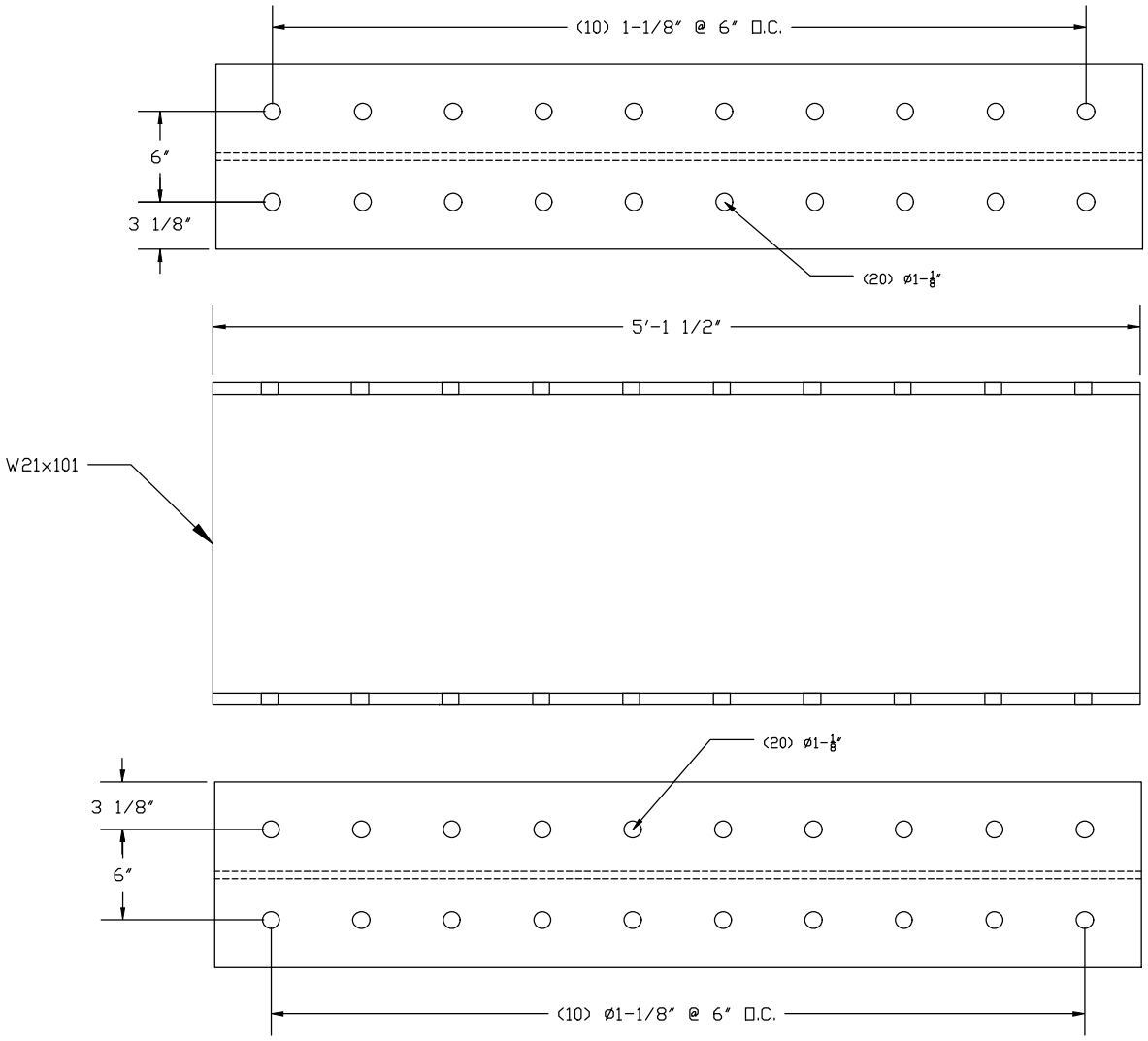

VIRGINIA TECH	COMPOSITE DIAPHRAGM CANTILEVER TEST FRAME	NOV 9, 2017	S11
	PIECE SF-05	R. AVELLANEDA	

PIECE = SF-10 ; QTY = 1 ; SHAPE = W12x87

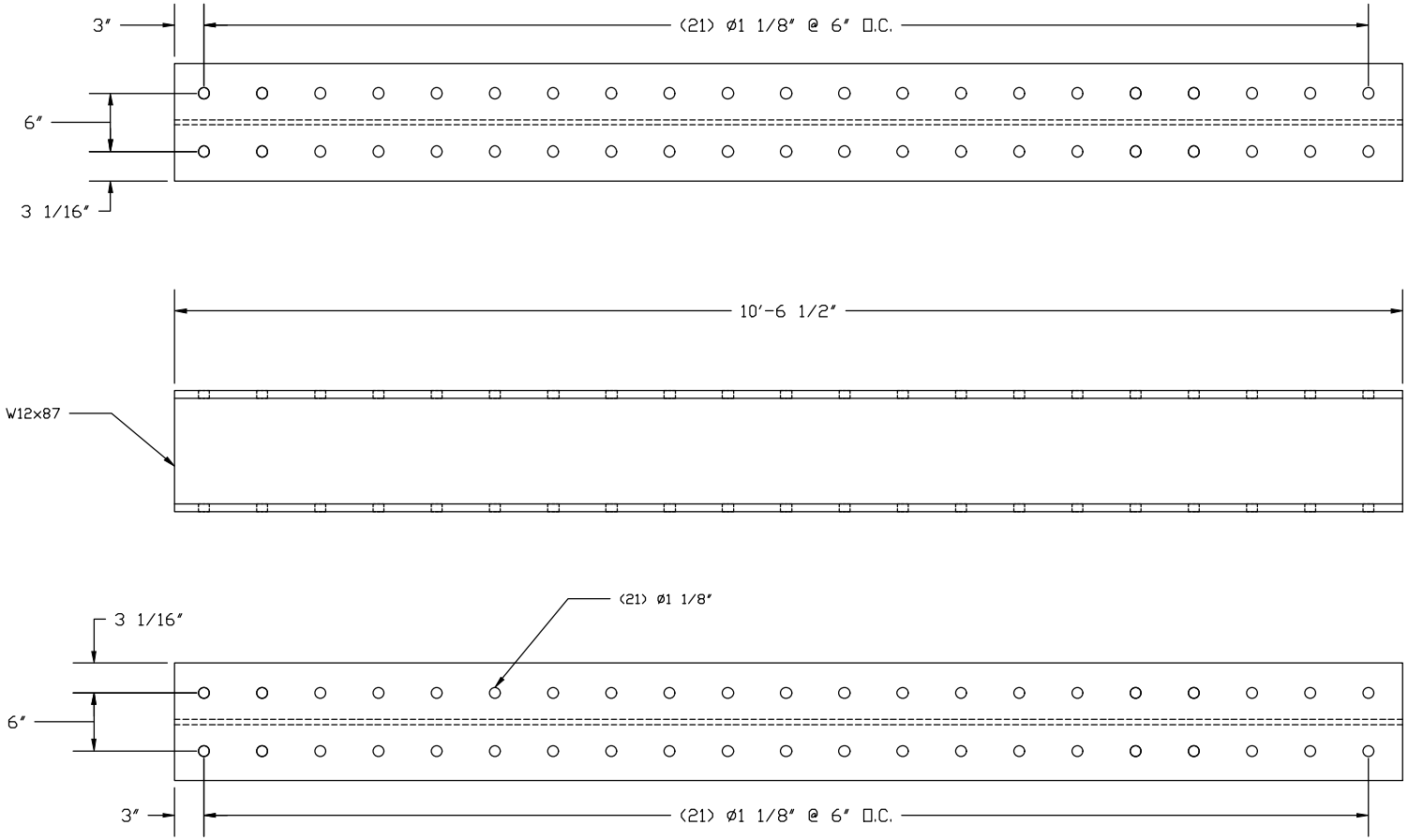

VIRGINIA TECH	COMPOSITE DIAPHRAGM CANTILEVER TEST FRAME	NOV 9, 2017	S12
	PIECE SF-10	R. AVELLANEDA	

APPENDIX D: SPECIMEN DETAILS

The purpose of this appendix is to detail the aspects of each specimen which deviated from the setup summarized in Section 2.

D.1 Specimen 3/6.25-4-L-NF-DT

During construction of this specimen, the stud welder malfunctioned during the welding of one of the headed studs in the fixed beam, as seen in Figure D-1. As a result, the studs in that rib were staggered differently from the rest of studs, as seen in Figure D-2.

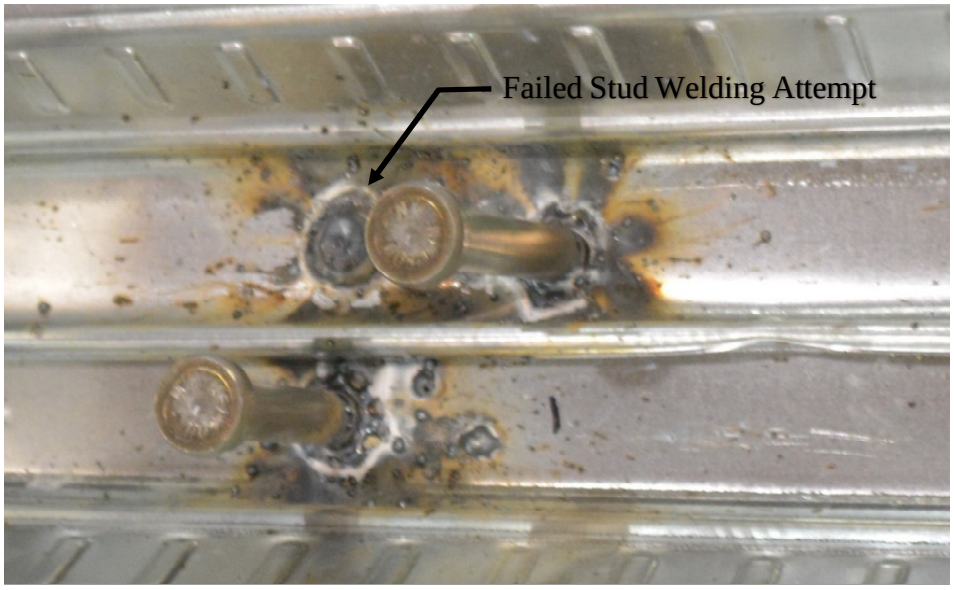

Figure D-1. Failed Stud Welding Attempt in Specimen 3/6.25-4-L-NF-DT

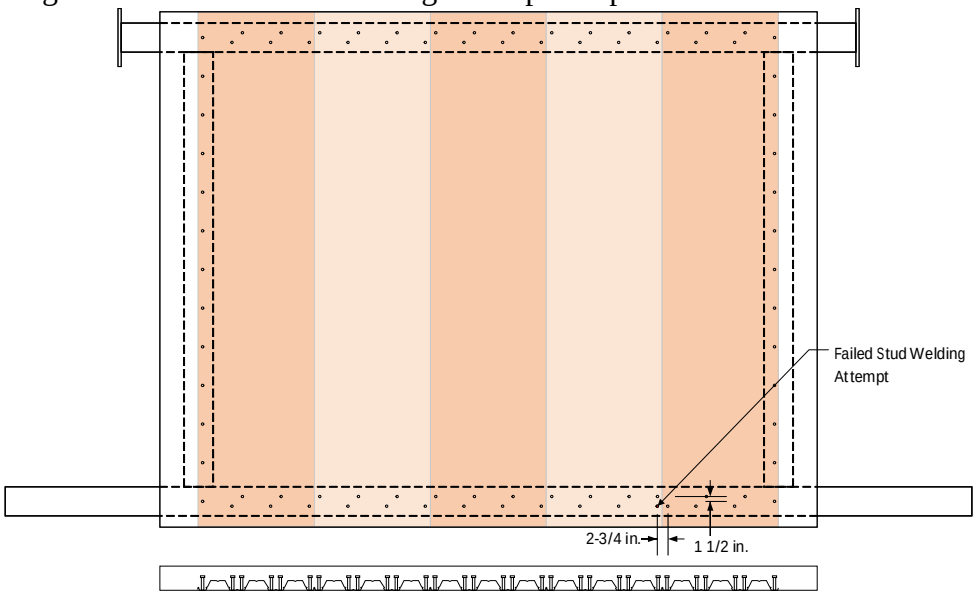

Figure D-2. Location of Failed Stud Welding Attempt in Specimen 3/6.25-4-L-NF-DT

D.2 Specimen 3/7.5-4-N-NF-DT

During the construction of this specimen, the stud welder malfunctioned during the welding of one of the headed studs in the fixed beam, as seen in Figure D-3. As a result, the studs in that rib were staggered differently from the rest of studs, as seen in Figure D-4.

Figure D-3. Failed Stud Welding Attempt in Specimen 3/7.5-4-N-NF-DT

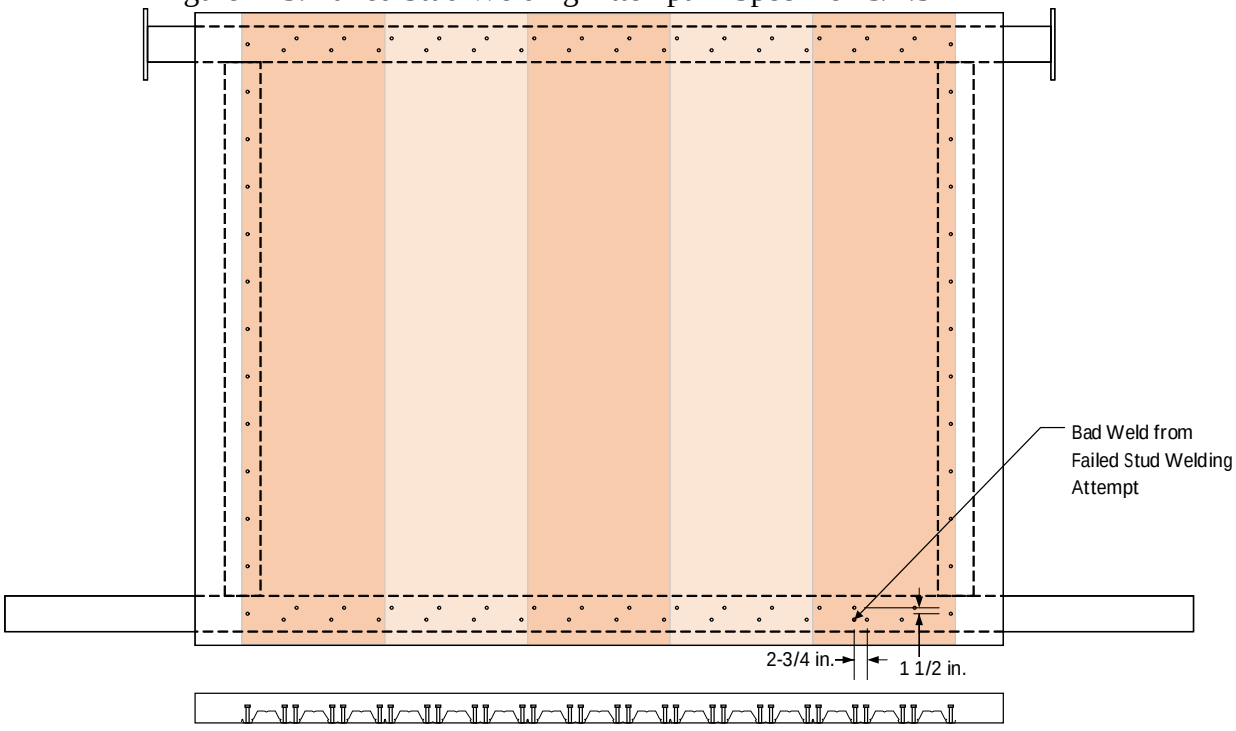

Figure D-4. Location of Failed Stud Welding Attempt in Specimen 3/7.5-4-N-NF-DT

D.3 Specimen 3/7.5-NW-NF-RS

During the construction of this specimen, poor contact between the steel deck and the top flange of the beam, prior to welding of one of the studs in one of the side beams, resulted in poor fusion of the weld at the base of the stud, the steel deck, and the top flange, as shown in Figure D-5. An additional stud was welded six inches away from the affected stud to compensate. The location of the issue is shown in Figure D-6.

Figure D-5. Poor Fusion Between Weld at Base of Stud, Steel Deck, and Top Flange of Beam for Specimen 3/7.5-NW-NF-RS

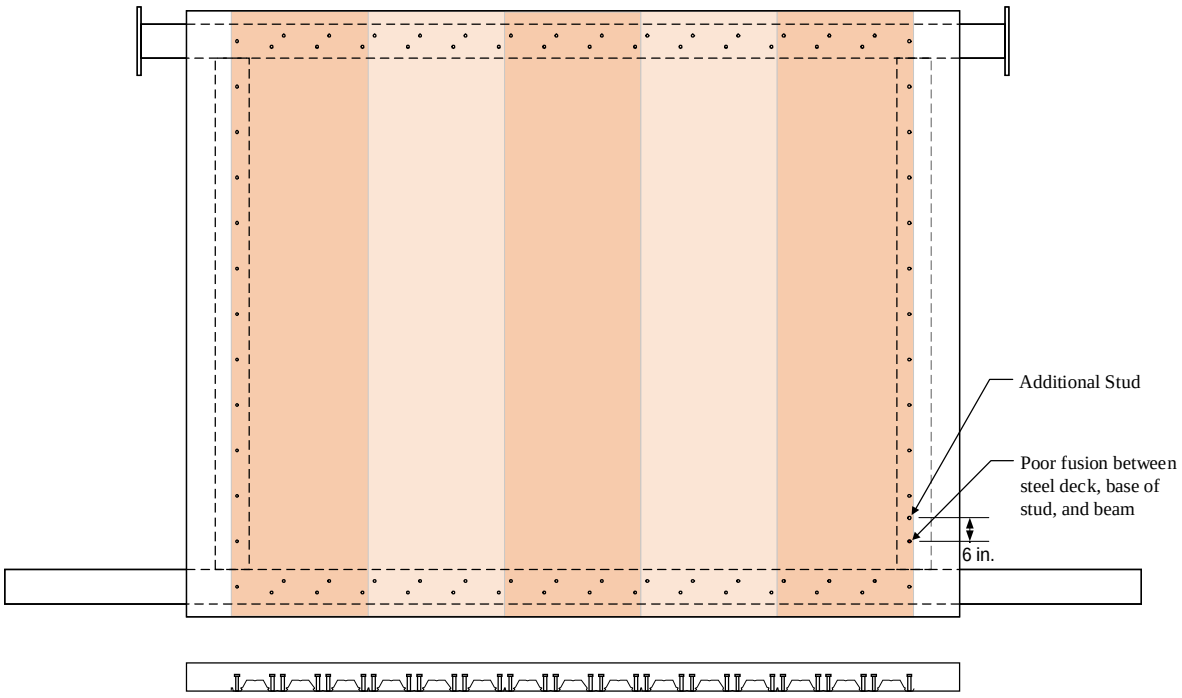

Figure D-6. Location of Poor Fusion Between Weld at Base of Stud, Steel Deck, and Top Flange of Beam for Specimen 3/7.5-NW-NF-RS